

Direct Enantioselective HPLC Monitoring of Lipase-Catalyzed Kinetic Resolution of Tiaprofenic Acid in Nonstandard HPLC Organic Solvents

ASHRAF GHANEM,^{1*} MOHAMMED NABIL ABOUL-ENEIN,² AIDA EL-AZZOUNY,² MOHAMMED F. EL-BEHAIRY,^{1,2} EBTESAM AL-HUMAIID,¹ ALWALEED A. ALAIDAN,¹ KAMILIA AMIN,³ AND MOHAMMED N. AL-AHDAL¹

¹*Biomedical Chemistry Unit, Biological and Medical Research Department, King Faisal Specialist Hospital and Research Centre, Riyadh, Saudi Arabia*

²*Medicinal and Pharmaceutical Chemistry Department, Pharmaceutical and Drug Industries Research Division, National Research Centre (NRC), Dokki-Cairo, Egypt*

³*Pharmaceutical Chemistry Department, Faculty of Pharmacy, Cairo University, Cairo, Egypt*

ABSTRACT The first straightforward lipase-catalyzed enantioselective access to enantiomerically enriched tiaprofenic acid as a versatile method in chiral separation of racemates is demonstrated. The latter was directly monitored by enantioselective HPLC using a 3,5-dimethylphenylcarbamate derivative of cellulose-based chiral stationary phase namely Chiralpak IB (the immobilized version of Chiralcel OD). Non-standard HPLC organic solvents were used as diluent to dissolve the “difficult to dissolve” enzyme substrate (the acid) and as eluent for the simultaneous enantioselective HPLC baseline separation of both substrate and product in one run without any further derivatization. The existence of a non-standard HPLC organic solvent (e.g., methyl *tert*-butyl ether) in the mobile phase composition is mandatory to accomplish the simultaneous enantioselective HPLC baseline separation of both substrate and product. *Chirality* 20:871–877, 2008. © 2008 Wiley-Liss, Inc.

KEY WORDS: Chiralpak IB; direct monitoring; enantioselective separation; HPLC; kinetic resolution; lipases; tiaprofenic acid

INTRODUCTION

Nonsteroidal anti-inflammatory drugs (NSAIDs) of the 2-arylpropionic acid (2-APA) class represent one of the most commercially successful and important classes of analgesic anti-inflammatory drugs. A common structural feature of 2-APA NSAIDs is a sp³-hybridized tetrahedral chiral carbon heteroatom within the propionic acid side chain moiety, with the *S*-enantiomer possessing most of the beneficial anti-inflammatory activity. In vivo, however, some of this class of compounds, namely, profens undergoes, to a limited degree, inversion from the (*R*) to the (*S*) form. Examples include the (*R*)-(–)-enantiomers of ibuprofen and naproxen which were converted in blood into the corresponding (*S*)-(+)-enantiomers.¹ However, only naproxen and flunaxaprofen are administered as the pure (*S*)-(+)-enantiomer.

Tiaprofenic acid (5-benzoyl- α -methyl-2-thiopheneacetic acid) belongs to this class of compounds having potent anti-inflammatory and analgesic properties.² Several studies in healthy and arthritic subjects have involved the administration of the racemate. However, tiaprofenic acid has been suggested to exhibit limited pharmacokinetic stereoselectivity.³ In view of the increasing legislative concern regarding the development and use of single enantiomeric drug in studying the pharmacokinetics and pharmacodynamics of each separate enantiomer, an enan-

tioselective straightforward route to access to separate enantiomers is required. The enantioselective resolution of tiaprofenic acid was reported using gas chromatography GC, high performance liquid chromatography HPLC and capillary electrochromatography (CEC).^{4–10} Most of these assays are indirect which involve the formation of diastereomers through reaction of the carboxylic acid moiety in tiaprofenic acid with a coupling reagent, 2,2,2-trichloroethyl chloroformate, to form a mixed anhydride. The latter is followed by the formation of an amide using *L*-leucinamide. However, in addition to racemization, partial or complete chiral conversion might occur.⁴ In fact, none of the reported procedure used to access to enantiomerically pure/enriched tiaprofenic acid did include a straightforward enzymatic resolution of the racemates. This is prob-

Dedicated to Professor Nina Berova on the occasion of her receiving the Chirality medal 2007.

Contract grant sponsor: King Abdul-Aziz City for Science and Technology; Contract grant number: KACST 25/08.

*Correspondence to: Ashraf Ghanem, Biomedical Chemistry Unit, Biological & Medical Research Department, King Faisal Specialist Hospital & Research Centre, MBC-03-95, P.O. Box 3354, Riyadh 11211, Kingdom of Saudi Arabia. E-mail: ghanem@kfshrc.edu.sa

Received for publication 12 September 2007; Accepted 29 November 2007
DOI: 10.1002/chir.20533

Published online 1 February 2008 in Wiley InterScience
(www.interscience.wiley.com).

ably due to solubility problems of the substrate in conventional standard HPLC organic solvents and the difficulty associated with the simultaneous resolution of the free acid (enzyme substrate) and its corresponding ester (product) in one run without derivatization. A mandatory highly required step for the monitoring of the enantiomeric excesses of substrates and product during the enzymatic reaction.

The enantioselective transformations catalyzed by enzymes in non-standard HPLC organic solvents,^{11–13} such as dichloromethane (DCM), ethyl acetate (EtOAc), methyl *tert*-butyl ether (MtBE), and tetrahydrofuran (THF) might be the method of choice to overcome solubility problem of the substrate. However, reactions in non-standard HPLC organic solvents are usually monitored off-line, since such harmful solvents might cause irreversible damage of the CSP by dissolving or swelling of the chiral selector.¹⁴ In a typical offline HPLC monitoring of an enzymatic reaction, an aliquot of the supernatant reaction mixture is withdrawn at several time intervals during the course of a biotransformation; solvent is evaporated, the residue is dissolved in mobile phase eluent, and analyzed by HPLC equipped with appropriate chiral stationary phase and UV detector.¹⁵

Yet, a new technology has been introduced by making the HPLC CSPs with a silica support onto which the polymer chiral selector (polysaccharide derivative) has been bonded/immobilized.^{16–19} Thus, Chiralpak IA, a 3,5-dimethylphenylcarbamate derivative of amylose, immobilized onto silica (the immobilized version of Chiralpak AD) was the first launched in this series followed by Chiralpak IB, a 3,5-dimethylphenylcarbamate derivative of cellulose (the immobilized version of Chiralcel OD).^{11,20} Such immobilization of the polymeric chiral selectors on the silica support is considered as an efficient approach to confer a universal solvent compatibility to this kind of CSP, thereby broadening the choice of solvents able to be used as mobile phase eluent or diluent. This is of particular interest in monitoring reactions performed in non-standard HPLC organic solvents.

Here, we report on the first straightforward lipase-catalyzed enantioselective access to enantiomerically enriched tiaprofenic acid directly monitored by enantioselective HPLC using non-standard HPLC organic solvents as diluent to dissolve the enzyme substrate and eluent to analyze both substrate and product in one run without further derivatization.

EXPERIMENTAL PROCEDURES

Instrumentation

The mobile phase for HPLC was filtered through a Millipore membrane filter (0.45 μ m) from Nihon Millipore (Yonezawa, Japan) and degassed via Waters in-line degasser AF. The HPLC system consisted of a Waters binary pump, Model 1525, (Milford, MA), equipped with a dual λ absorbance detector model 2487, an autosampler model 717plus and an optical rotation detector (Ibz Messtechnik GmbH, Hannover, Germany) operating at room temperature. DOI 10.1002/chir

The UV-detector was set at 300 nm. Chiralcel OD (4.6 mm \times 250 mm ID coated on 5 μ m silica-gel) and Chiralpak IB (4.6 mm \times 250 mm ID immobilized on 5 μ m silica-gel) column was purchased from Chiral Technologies Europe (Illkirch, France). The enantiomeric excess *ee* of the substrate (*ee*_s) and the product (*ee*_p) as well as the conversion (Conv.) and enantioselectivity (*E*) were calculated as previously described.^{21–23}

Materials

All solvents used as mobile phase in HPLC including 2-propanol were HPLC-grade and purchased from Fisher Scientific (Fair Lawn, NJ). *n*-butanol used in the synthesis of ester was Analar grade and purchased from BDH chemicals (Poole, England). Lipases from *Aspergillus niger* (lipase AS), *Burkholderia cepacia* (formerly *Pseudomonas cepacia*) free (lipase PS) and immobilized on ceramic particles (lipase PS-C) together with *Candida rugosa* (lipase AYS) were gifts from Amano (Nagoya, Japan). Immobilized *Candida antarctica* lipase B (Novozym 435), its free form (Novozyme 525), and immobilized *Rhizomucor miehei* lipase (lipozyme RM IM) were from Novo Nordisk (Bagsvaerd, Denmark). Lipase type VII from *Candida rugosa* (CRL) was from Sigma (Steinheim, Germany). Lipase from *Candida cylindracea* (CCL) and lipase immobilized in sol-gel-Ak on sintered glass from *Mucor miehei* (MML) were purchased from Fluka (Buchs, Switzerland). Tiaprofenic acid was extracted from the readily marketed tablets SURGAM[®] according to literature procedure.²⁴

Chromatographic Conditions

The mobile phase was consisted of *n*-hexane/methyl *tert*-butyl ether/2-propanol/trifluoroacetic acid (90:10:1:0.2 v/v/v/v) and the flow rate was 1 ml/min. The column was operated at room temperature (24°C). UV detection was set at 300 nm.

Chemical Synthesis of Racemic Butyl Ester of Tiaprofenic Acid (2)

Few drops of conc. sulfuric acid were added to 0.77 M racemic tiaprofenic acid (**1**) in benzene followed by the addition of 1 ml of *n*-butanol (0.01 mol, 3 M equiv.). The mixture was stirred under reflux over night, solvent was evaporated under vacuum and the residue was neutralized with 10% sodium hydrogen carbonate. The ester was extracted twice using 30 ml diethyl ether. The ether was dried over sodium sulfate anhydrous, filtered, and evaporated under vacuum to afford 1 g pale yellowish oil (73% chemical yield).

Lipase-Catalyzed Esterification of Tiaprofenic Acid (1)

Twenty milligrams (0.077 mmol) racemic tiaprofenic acid **1**, *n*-butanol (0.21 mmol, 3 equiv.), molecular sieves, and 2.0 ml either standard (acetonitrile) or non-standard HPLC organic solvent (such as toluene, MTBE, EtOAc, THF or DCM) were added and stirred in a 4 ml reaction vial. The reaction mixture was thermostated at 40°C. Sample (100 μ l) was withdrawn and injected at zero time (control). Lipase (100 mg) was added and 50 μ l sample was

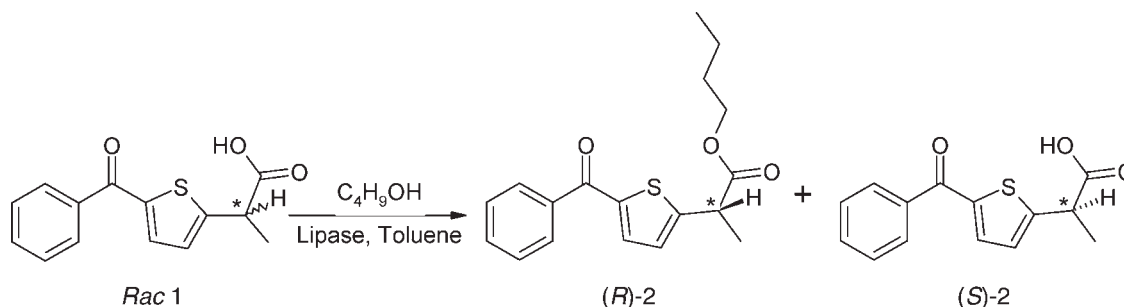


Fig. 1. Lipase-catalyzed enantioselective esterification of racemic tiaprofenic acid (1) using *n*-butanol in non-standard HPLC organic solvents.

withdrawn and directly injected to HPLC without dilution or workup at several time intervals.

Lipase-Catalyzed Hydrolysis of Tiaprofenic Acid Butyl Ester (2)

Tiaprofenic acid butyl ester (24.3 mg; 0.077 mmol), 1.0 of ml solvent, and 1.0 ml of 0.1 M phosphate buffer (pH 7) were added to 4 ml reaction vial. The reaction mixture was thermostated at 40°C and 50 μ l sample of the non-standard HPLC organic solvent aliquot was withdrawn and injected at zero time (control). Lipase was (100 mg) added and 50 μ l samples of the non-standard HPLC organic solvent aliquot were withdrawn at several time intervals. The samples were filtered and used directly without dilution for direct enantioselective HPLC analysis.

RESULTS AND DISCUSSION

The precise determination of the enantiomeric excess of substrates and products is an important prerequisite for the detailed investigation of the enzyme-catalyzed enantioselective resolution of racemates. For an efficient monitoring of the lipase-catalyzed enantioselective resolution of tiaprofenic acid **1** (cf. Fig. 1), the acid itself (**1**) and its cor-

responding ester (**2**) should be simultaneously baseline separated in their racemic synthesized form. This should be ultimately done in one run without further derivatization. Thus, the enantioselective HPLC separation of both synthesized racemic acid (**1**) and its corresponding butyl ester (**2**) was investigated using either coated 3,5-dimethylphenylcarbamate derivative of cellulose-based chiral stationary phase namely Chiralcel OD or its immobilized version namely Chiralpak IB using standard organic solvents consisting of *n*-hexane/2-propanol with different volume ratios. Only the acid (**1**) was baseline separated using the above mentioned mobile phase composition with volume ratio 90/10 *v/v* and the ester itself has never been separated simultaneously in the same run on both columns. Because of the limited solvent choice restricted to standard organic solvents in coated Chiralcel OD, this phase was excluded from our investigation which has been continued on its immobilized version, namely, Chiralpak IB having broader choice of solvents used as mobile phases. The latter include nonstandard HPLC solvents like ethyl acetate (AcOEt), dichloromethane (DCM), tetrahydrofuran (THF), and other solvents in which the polysaccharide derivatives themselves are dissolved or swollen. Indeed, these solvents can not be used as mobile phase eluents in conventionally coated HPLC columns (e.g., Chiralcel OD). The above mentioned non-standard solvents have been investigated solely or in combination with

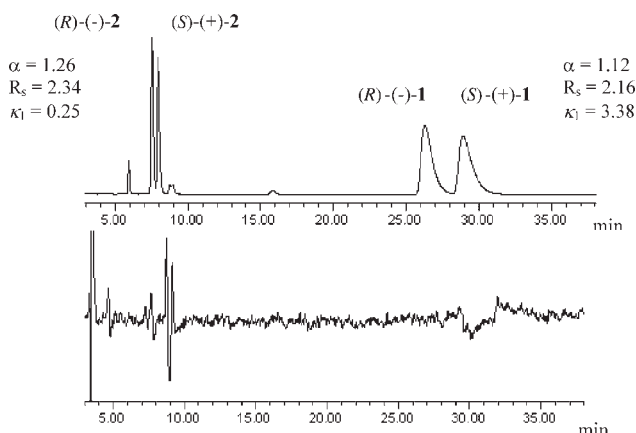


Fig. 2. Baseline separation and traces of the polarimetric detection of racemic tiaprofenic acid (**1**) and its corresponding butyl ester (**2**) on Chiralpak IB. Chromatographic conditions: mobile phase: *n*-hexane/MTBE/2-propanol/trifluoro acetic acid (90:10:1:0.2 *v/v/v/v*) at 1 ml flow rate and UV 300 nm. Chromatographic parameters including the retention factor of the first peak (k_1), separation factor (α) and the resolution (R_s) are shown.

TABLE 1. Enzymatic parameters including enantiomeric excesses of both substrate (**1**) and product (**2**) ee_s and ee_p , respectively, conversion and enantioselectivity (E) of different lipases screened for the enantioselective esterification of tiaprofenic acid (**1**) using 1-butanol in acetonitrile as standard organic solvent

Lipase	Time (h)	ee_s (%)	ee_p (%)	Conversion %	E
Novozyme435	48	47.2	49.6	48.7	4.6
Novozyme525	48	4.8	14.8	24.5	1.4
Lipozyme	120	7.2	12.6	36.6	1.3
Lipase AS	120	5.6	27.2	17.2	1.8
Lipase PS	120	4.9	1.6	75.0	1.0
Lipase AYS	120	4.6	3.5	56.4	1.1
CRL	120	4.5	1.9	69.7	1.0
Lipase PS-C	120	4.2	12.6	25.3	1.3
CCL	120	4.5	1.7	72.0	1.0
MML	120	4.1	6.1	40.2	1.1

TABLE 2. Enzymatic parameters including enantiomeric excesses of both substrate (**1**) and product (**2**) ee_s and ee_p , respectively, conversion and enantioselectivity (E) of some selected lipases screened for the enantioselective esterification of tiaprofenic acid (**1**) using 1-butanol in several non-standard HPLC organic solvents

Lipase	Solvent	Log P	Time (h)	ee_s (%)	ee_p (%)	Conv. (%)	E
Novozyme435	Toluene	2.50	0.66	70.9	59.6	54.3	8.1
	MTBE	1.30	5	46.0	64.0	41.8	7.1
	Ethylacetate	0.68	72	10.8	75.6	12.5	8.0
	THF	0.49	72	0.9	71.5	1.2	6.0
	DCM	1.30	48	41.9	70.6	37.2	8.7
Novozyme525	Toluene	2.50	8	47.4	62.7	43.0	6.9
	MTBE	1.30	24	25.2	44.4	36.1	3.3
	Ethylacetate	0.68	72	15.9	56.0	22.1	4.1
	THF	0.49	72	2.2	67.0	3.1	5.1
	DCM	1.30	16	16.3	85.2	16.0	14.7

n-hexane in mobile phase composition using different ratios for the simultaneous separation of **1** and **2** in one run on Chiralpak IB. A simultaneous baseline separation of both racemic tiaprofenic acid (**1**) and its corresponding butyl ester (**2**) was achieved in one run using *n*-hexane associated with MTBE as a non-standard HPLC organic solvent, 2-propanol and trifluoroacetic acid in mobile phase

composition (n-Hex/MTBE/2-PrOH/trifluoroacetic acid (90:10:1:0.2 v/v/v/v) (see Fig. 2). Once the enantioselective baseline separation of the enzyme substrate (**1**) and the expected product (**2**) is settled, the enzymatic reaction can be easily and directly HPLC monitored in either standard or non-standard HPLC organic solvents. Thus, the screening of different lipases for the enantioselective

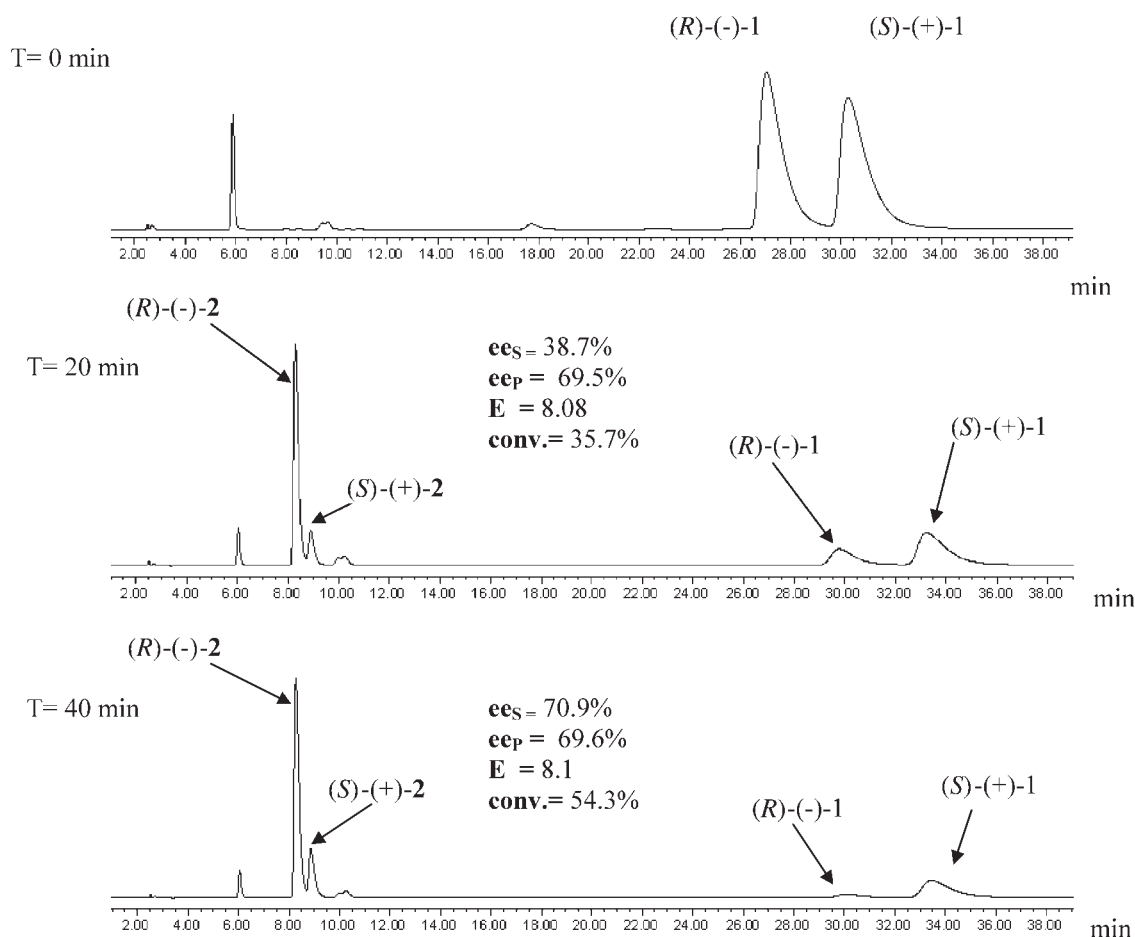


Fig. 3. HPLC chromatograms (from $t = 0$ to $t = 40$ min) showing the UV traces of both substrate (**1**) and product (**2**) during the direct HPLC monitoring of the reaction progress of the Novozyme435-catalyzed enantioselective esterification of **1** using 1-butanol in toluene as non-standard HPLC organic solvent.

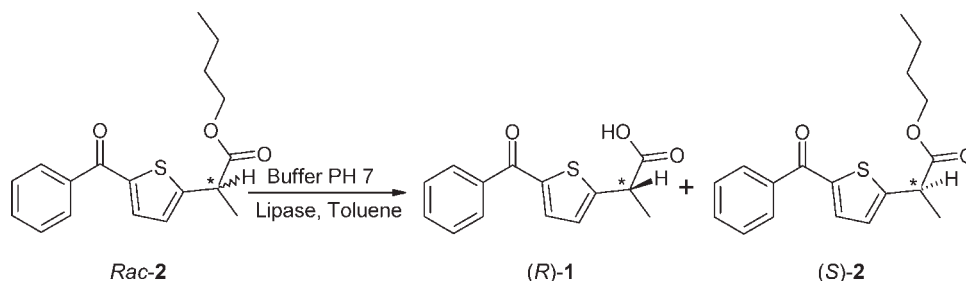


Fig. 4. Lipase-catalyzed enantioselective hydrolysis of butyl ester (**2**) in a biphasic system consisting of non-standard HPLC organic solvent and phosphate buffer (pH 7).

esterification of tiaprofenic acid (see Fig. 1) was first performed in acetonitril (log P -0.34) as standard organic solvent. Of all 10 tested lipases, only immobilized lipase from *Candida antarctica* lipase B CAL-B (Novozyme 435) showed better enantioselectivity (also called enantiomeric ratio) *E* in shorter time (up to 48 h). The rest did not show any promising results even after 120 h. Results are shown in Table 1. In most cases of the enantioselective esterification of racemic **1** [(*RS*)-**1**], (*R*)-**1** was the faster reacting enantiomer which was selectively esterified to afford its corresponding butyl ester (*R*)-**2** leaving the second enantiomer of the substrate (*S*)-**1** in enantiomerically enriched form. This was achieved when using different lipases in presence of *n*-butanol in acetonitril as standard organic solvent (cf. Table 1).

On the basis of the above-mentioned results, two lipases were selected for further investigation in nonstandard solvents. Thus, lipase from *Candida antarctica* lipase B CAL-B (Novozyme 435) and its free form (Novozyme 525) were used for the enantioselective esterification of racemic tiaprofenic acid **1** in nonstandard HPLC solvents such as toluene, methyl *tert*-butyl ether (MTBE), ethyl acetate (EtOAc), tetrahydrofuran (THF), and dichloromethane (DCM); results are summarized in Table 2. The reactions were directly monitored by enantioselective HPLC using Chiralpak IB without further workup or removal of the nonstandard solvent. In comparison with the lipase-catalyzed kinetic resolution of (**1**) in acetonitril as standard organic solvent, better enantioselectivity *E*, enantiomeric excesses of both substrate (**1**) and product (**2**) and faster reaction rate were observed when using non-standard HPLC organic solvents.

In terms of enantioselectivity (*E*), enantiomeric excesses of unreacted substrate (ee_s), enantiomeric excess of the resulting product (ee_p), and the reaction time at maximum conversion (54.3%), lipase from *Candida antarctica* B (CAL-B) known as Novozyme 435 showed the best performance in toluene having log P 2.50 (ee_s = 70.9%, ee_p = 59.6%, E = 8.16 after 40 min). Log P in Table 2 is defined as the ratio of concentration of a substance in two immiscible phases at equilibrium namely octanol and water and used to describe the correlation of hydrophobicity and the enantioselectivity *E* of lipases (cf. Fig. 3).

Compared with the esterification experiments in the nonaqueous medium consisting of standard and non-standard HPLC organic solvents described above, the enzymatic hydrolysis of the butyl ester (*RS*)-**2** in aqueous medium proceeded slowly (2 days) (cf. Fig. 4). Only two lipases, namely, Novozyme 435 and 525, were able to conduct poor enantioselective resolution when toluene was used in combination with sodium phosphate buffer (pH 7) in a biphasic system (ee_s 29.3%, ee_p 19.8, Conv. 59.6%, E = 1.9 for Novozyme 435 and ee_s 33.4%, ee_p 26.7, Conv. 55.5%, E = 2.3 for Novozyme 525). These results promote us to study the screening of both enzymes for the enantioselective hydrolysis of racemic (**2**) in other nonstandard HPLC organic solvents, namely, MTBE, EtOAc, and DCM. Results are summarized in Table 3. In terms of the enantioselectivity (*E*), enantiomeric excesses of unreacted substrate (ee_s of the ester (*S*)-**2**), enantiomeric excess of the resulting product (ee_p of the acid (*R*)-**1**) and the reaction time at maximum conversion (56.1%), lipase from *Candida antarctica* B (CAL-B) known as Novozyme 435 showed the best performance when used in a biphasic solvents

TABLE 3. Enzymatic parameters including enantiomeric excesses of both substrate (**2**) and product (**1**) ee_s and ee_p , respectively, conversion and enantioselectivity (*E*) of selected lipases screened for the enantioselective hydrolysis of racemic tiaprofenic acid butyl ester (**2**) in a biphasic system consisting of a nonstandard HPLC organic solvent and a phosphate buffer pH 7

Lipase	Solvent	Log P	Time (h)	ee_s (%)	ee_p (%)	Conv. (%)	<i>E</i>
Novozyme435	MTBE	1.30	2	61.6	47.1	56.6	5.0
	Ethylacetate	0.68	120	16.8	1.3	1.4	0.2
	DCM	1.30	120	31.7	12.0	2.0	4.3
Novozyme525	MTBE	1.30	2	24.3	54.3	30.9	4.2
	Ethylacetate	0.68	120	0.1	28.3	0.4	1.7
	DCM	1.30	120	13.7	39.6	2.5	2.6

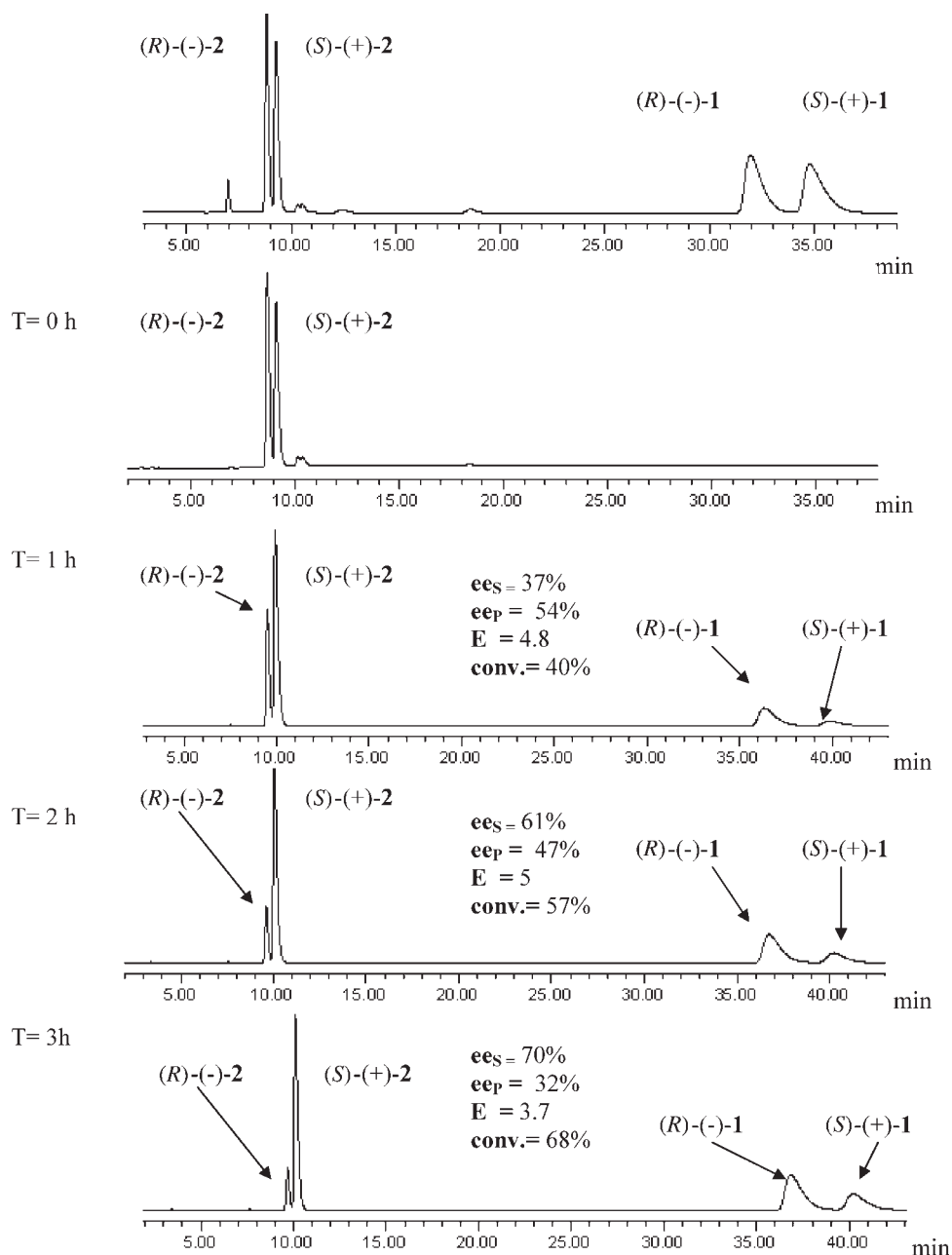


Fig. 5. Selected HPLC chromatograms (from $t = 0$ to $t = 3$ h) showing UV traces of both substrate (2) and product (1) during the direct HPLC monitoring of the reaction progress of the enantioselective hydrolysis of tiaprofenic acid butyl ester (2) in a biphasic system consisting of a non-standard HPLC organic solvent and a phosphate buffer (pH 7).

consisting of MTBE and buffer (pH 7) ($ee_s = 61.6\%$, $ee_p = 47.1\%$, $E = 5.0$ after 2 h (cf. Fig. 5).

CONCLUSION

The lipase-catalyzed biotransformation of tiaprofenic acid in non-standard HPLC solvents can be easily monitored by direct enantioselective HPLC equipped with UV, optical detector, and immobilized chiral stationary phase, namely, Chiralpak IB. A part from what has been previously reported,^{25–27} the current method allows direct and continuous monitoring of the biocatalyzed reaction conducted in

non-standard HPLC organic solvents without any workup. This could offer unique capabilities to allow the exploration of the enantioselectivity of lipases toward “difficult to dissolve” substrates in non-standard HPLC organic solvents. To the best of our knowledge, this is the first report on the lipase-catalyzed kinetic resolution of tiaprofenic acid.

LITERATURE CITED

1. Ferretti R, Gallinella B, La Torre F, Villan C. Direct high-performance liquid chromatography resolution on chiral columns of tiaprofenic acid and related compounds in bulk powder and pharmaceutical formulations. *J Chromatogr A* 1995;704:217–223.

2. Sorkin EM, Brogden RN. Tiaprofenic acid. A review of its pharmacological properties and therapeutic efficacy in rheumatic diseases and pain states. *Drugs* 1985;29:208–235.
3. Singh NN, Jamali F, Pasutto FM, Russel AS, Coutts RT, Drader KS. Pharmacokinetics of the enantiomers of tiaprofenic acid in humans. *J Pharm Sci* 1986;75:439–442.
4. Vakily M, Jamali F. Pharmacokinetics of tiaprofenic acid in humans: lack of stereoselectivity in plasma using both direct and precolumn derivatization methods. *J Pharm Sci* 1996;85:638–642.
5. Davies NM. Clinical pharmacokinetics of tiaprofenic acid and its enantiomers. *Clin Pharmacokinet* 1996;31:331–347.
6. Geisslinger G, Menzel S, Brune K. Stereospecific determination of tiaprofenic acid in plasma: problems with drug degradation. *J Chromatogr B* 1996;675:77–81.
7. Aturki Z, Camera E, La Torre F, Fanali S. Direct chiral resolution of tiaprofenic acid in pharmaceutical formulations by capillary zone electrophoresis using cyclodextrins as chiral selector. *J Capillary Electrophor* 1995;2:213–217.
8. Fradi I, Servais A, Pedrini M, Chiap P, Ivanyi R, Crommen J, Fillet M. Enantiomeric separation of acidic compounds using single-isomer amino cyclodextrin derivatives in nonaqueous capillary electrophoresis. *Electrophoresis* 2006;27:3434–3442.
9. Jiang Z, Bertazzo M, Suessmuth RD, Yang Z, Smith NW, Schurig V. Highlighting the role of the chlorine substituents in the glycopeptide antibiotic balhimycin for chiral recognition in capillary electrophoresis. *Electrophoresis* 2006;27:1154–1162.
10. Shinozuka T, Nakajima R. *Drugs and poisons in humans: a handbook of practical analysis*. Suzuki O, Watanabe K, editors. Berlin and Heidelberg: Springer-Verlag; 2005. p 325.
11. Zhang T, Nguyen D, Franco P, Murakami T, Ohnishi A, Kurosawa H. Cellulose 3,5-dimethylphenylcarbamate immobilized on silica: a new chiral stationary phase for the analysis of enantiomers. *Anal Chim Acta* 2006;557:221–228.
12. Zhang T, Kientzy C, Franco P, Ohnishi A, Kagamihara Y, Kurosawa H. Solvent versatility of immobilized 3,5-dimethylphenylcarbamate of amylose in enantiomeric separations by HPLC. *J Chromatogr A* 2005;1075:65–75.
13. Ghanem A, Naim L. Immobilized versus coated amylose tris(3,5-dimethylphenylcarbamate)chiral stationary phases for the enantioselective separation of cyclopropane derivatives by liquid chromatography. *J Chromatogr A* 2006;1101:171–178.
14. Ghanem A. True and false reversal of the elution order of barbiturates on a bonded cellulose-based chiral stationary phase. *J Chromatogr A* 2006;1132:329–332.
15. Kamal A, Sanbhor M, Shaik AA, Sravanthi V. One-pot synthesis and resolution of chiral allylic alcohols. *Tetrahedron: Asymmetry* 2003;14:2839–2844.
16. Francotte ER. Enantioselective chromatography as a powerful alternative for the preparation of drug enantiomers. *J Chromatogr A* 2001;906:379–397.
17. Chankvetadze B, Ikai T, Yamamoto C, Okamoto Y. High-performance liquid chromatographic enantioseparations on monolithic silica columns containing a covalently attached 3,5-dimethylphenylcarbamate derivative of cellulose. *J Chromatogr A* 2004;1042:55–60.
18. Chen X, Liu Y, Qin F, Kong L, Zou H. Synthesis of covalently bonded cellulose derivative chiral stationary phases with a bifunctional reagent of 3-(triethoxysilyl)propyl isocyanate. *J Chromatogr A* 2003;1010:185–194.
19. Cirilli R, Simoneli A, Ferretti R, Bolasco A, Chimenti P, Secci D, Macconi E, La Torre F. Analytical and semipreparative high performance liquid chromatography enantioseparation of new substituted 1-thiocarbamoyl-3,5-diaryl-4,5-dihydro-(1H)-pyrazoles on polysaccharide-based chiral stationary phases in normal-phase, polar organic and reversed-phase conditions. *J Chromatogr A* 2006;1101:198–203.
20. Zhang T, Schaeffer M, Franco P. Optimization of the chiral separation of a Ca-sensitizing drug on an immobilized polysaccharide-based chiral stationary phase: case study with a preparative perspective. *J Chromatogr A* 2005;1083:96–101.
21. Ghanem A. Trends in lipase-catalyzed asymmetric access to enantiomerically pure/enriched compounds. *Tetrahedron* 2007;63:1721–1754.
22. Ghanem A, Schurig V. Lipase-catalyzed irreversible transesterification of 1-(2-Furyl)-ethanol using isopropenyl acetate. *Chirality* 2001;13:118–123.
23. Chen CS, Fujimoto Y, Girdaukas G, Sih CJ. Quantitative analyses of biochemical kinetic resolutions of enantiomers. *J Am Chem Soc* 1982;104:7294–7299.
24. Ali AMM, Emara KM, Khodari M. Quantification of tiaprofenic acid using voltammetric and spectrophotometric techniques. *Analyst (London)* 1994;119:1071–1074.
25. CHIRAL TECHNOLOGIES EUROPE. Application Guide Software, 2006. CHIRAL TECHNOLOGIES EUROPE, Illkirch, France, 2006.
26. Okamoto Y, Aburatani R, Kaida Y, Hatada K, Inotsume N, Nakano M. Direct chromatographic separation of 2-arylpropionic acid enantiomers using tris(3,5-dimethylphenylcarbamate)s of cellulose and amylose as chiral stationary phases. *Chirality* 1989;1:239–242.
27. Mutsaers JHGM, Kooreman HJ. Preparation of optically pure 2-aryl- and 2-aryloxy-propionates by selective enzymic hydrolysis. *Recl Trav Chim Pays-Bas* 1991;110:185–188.

Chiral Molecules with Polyhedral T, O, or I Symmetry: Theoretical Solution to a Difficult Problem in Stereochemistry

SRI KAMESH NARASIMHAN,¹ XIAOYING LU,¹ AND YAN-YEUNG LUK^{1,2*}

¹Department of Chemistry, Syracuse University, Syracuse, New York

²Department of Biomedical and Chemical Engineering, Syracuse University, Syracuse, New York

ABSTRACT Ever since point groups of symmetry have been used to describe molecules after Van't Hoff and Le Bel proposed tetrahedral structures for carbon atoms in 1874, it remains difficult to design chiral molecules with polyhedral symmetry **T**, **O**, or **I**. Past theoretical and experimental studies have mainly accomplished molecular structures that have the conformations for satisfying the **T** symmetry. In this work, we present a general theoretical approach to construct rigid molecular structures that have permanently the symmetry of **T**, **O**, and **I**. This approach involves desymmetrization of the vertices or the edges of Platonic solid-shaped molecules with dissymmetric moieties. Using density functional theory (DFT) and assisted model building and energy refinement (AMBER) computational methods, the structure, the rigidity, and the symmetry of the molecule are confirmed by assessing the lowest energy conformation of the molecule, which is initially presented in a planar graph. This method successfully builds molecular structures that have the symmetry of **T**, **O**, and **I**. Interestingly, desymmetrization of the edges has a more stringent requirement of rigidity than desymmetrization of the vertices for affording the **T**, **O**, or **I** symmetry. *Chirality* 20:878–884, 2008. © 2008 Wiley-Liss, Inc.

KEY WORDS: chiral polyhedral symmetry; dissymmetry; stereochemistry; trioxatricornan; T, O, I symmetry

INTRODUCTION

After the tremendous discovery of the three dimensional tetrahedral configuration of carbon center in 1874 by Van't Hoff (and Le Bel), who proposed “the extension into space of the structural formula,”¹ symmetry elements used for describing macroscopic objects such as plants, animals, and crystals have been judiciously applied to describe molecular structures.² Interestingly, there exists a set of three high symmetry point groups (**T**, **O**, and **I**) theoretically, but it has been difficult to conceive molecular structures that satisfy rigorously the symmetry requirements of any one of these symmetry point groups. Over the past century, this problem has fascinated among the most prominent chemists to design and synthesize structures that possess these symmetries.^{3–9} These symmetries belong to a class of chiral point groups that bear all the rotational symmetry elements belonging to the polyhedral shapes of platonic solids, and thus are referred to as **T**, **O**, and **I**, without having the subscript d or h. In these point groups, symmetry elements of the first kind (identity, **E**; rotation, **C_n**) are preserved and the symmetry elements of the second kind (reflection, σ ; inversion, **i**; rotation and reflection, **S_n**) are prohibited.^{10,11} While the theoretical framework for this class of symmetry is well established, the actual structure as molecules or objects have long been sought after. A few textbooks that choose to disclose this problem describe the issue by statements such as “**T**

symmetry is very rarely, if ever, encountered in real molecule”⁵; “Molecules belonging to **T** and **O** are unknown”⁶; “**I** symmetry is mentioned purely for the sake of completeness, since no example of its occurrence in Nature is known”;⁵ “No optically active molecules with **T**, **O**, **I** symmetry has ever been studied.”⁴ In this work, we describe the challenges involved in imagining or designing these molecules, and present a general theoretical method for designing rigid molecules with **T**, **O**, and **I** symmetry.

While the design and imagination for molecules with **T**, **O**, and **I** symmetry has been difficult, there has been significant developments in noncovalent assemblies that are reported to have a **T** symmetry.^{12–22} Notably, Stang and coworkers have synthesized several high symmetry assemblies including three-dimensional metallacyclic poly-

This article contains supplementary material available via the Internet at <http://www.interscience.wiley.com/jpages/0899-0042/suppmat>. Contract grant sponsors: Syracuse University; Stereochemical Society of Greater New York (Administered at Columbia University, NY); Syracuse Center of Excellence CARTI award funded by U.S. Environmental Protection Agency; Contract grant number: X-8323501-0; National Science Foundation-CMMI; Contract grant number: 0727491.

*Correspondence to: Yan-Yeung Luk, Department of Chemistry, Department of Biomedical and Chemical Engineering, Syracuse University 1-014 CST, 111 College Place, Syracuse, NY 13244. E-mail: yluk@syr.edu
Received for publication 5 September 2007; Accepted 5 January 2008
DOI: 10.1002/chir.20545
Published online 11 February 2008 in Wiley InterScience (www.interscience.wiley.com).

gons and polyhedra via spontaneous self-assembly using coordination as a driving force.^{23–27} A **T**-symmetric species is accomplished by employing tridentate ligand 1,3,5-tris[(4-pyridyl) ethynyl] benzene and [(*R*)-(+)-BINAP] Pd^{II} and -Pt^{II} bis (triflates) to form noncovalent self-assembly.²⁸

MOLECULAR CONFORMATIONS WITH **T** SYMMETRY

Theoretically, molecules (or objects in general) with **T**, **O**, or **I** symmetry are chiral, and possess multiple rotational axes. A **T**-molecule has the symmetry elements of identity (**E**), 3 two-fold rotational axes (**C**₂), and 4 three-fold rotational axes (**C**₃), which gives a symmetry number (*s*) of 12.^{2,5,10} An **O**-molecule has the symmetry elements of **E**, 6**C**₂, 4**C**₃, and 3**C**₄, which affords *s* = 24.^{2,5,10} An **I**-molecule has the symmetry elements of **E**, 15**C**₂, 10**C**₃, and 6**C**₅, which affords *s* = 60.^{2,5,10} Because of the high symmetry numbers and the multiple rotational axes, chiral molecules with **T**, **O**, or **I** symmetry are considered highly symmetric.⁹ Nature, on the other hand, has long provided some assembled materials with these highly symmetric chiral symmetries. For example, amphibian red-cell L ferritin proteins are of **O** symmetry²⁹ and supramolecular assemblies of many viruses are of **I** symmetry.^{30–35} Furthermore, a sculpture named “Sphere with Fish” presenting carvings of 12 identical fish by artist Maurits Cornelis Escher has demonstrated the **T** symmetry. To this date, it remains a challenge for chemists to come up with, let alone to synthesize, structures that rigorously satisfy the **T**, **O**, and **I** symmetry. However, a few studies have achieved molecules with transient conformations that are of **T** symmetry.

Design of covalent single structure that fulfills chiral polyhedral symmetry can be traced back to Pierre Curie’s proposition about the relation between physical property and symmetry, which was first noted in 1894 that symmetry is a subtractive property: “... it is merely necessary to combine an achiral skeleton of the appropriate symmetry with a set of ligands which preserves all symmetry elements of the first kind while destroying all those of the second.”^{9,36} This statement became an important guideline for many who later attempted designing molecules with **T** symmetry.⁹ Gerhard Herzberg in 1945 noted that **T** symmetry is attainable simply by twisting all four methyl groups of neopentane (C(CH₃)₄) in the same direction and to the same extent (but by less than 60°).^{37,38} This design does fulfill all requirements for **T** symmetry, but such a **T** molecule requires synchronized rotations of all the σ bonds or a frozen conformation with all bond angles fixed at a certain value. Note that a molecule such as C(*R**)₄, where *R**) groups are homochiral moieties with **C**₁ symmetry, has the symmetry point group of **D**₂, not of **T**.^{8,9} Cahn et al. proposed a hypothetical structure for a **T** molecule in 1966 by stating that “it is possible to build a molecule of **T** symmetry round a tetrahedral atom by bridging in pairs with six like bridges four like tetrahedral atoms directly bound to it, each bridge containing a plane of chirality which destroys planes of symmetry, but preserves a two-fold rotational axis between the atoms bridged. The bridges might, for example,

be *trans*-olefinic, of the form —(CH₂)_{*n*}CR=CR—(CH₂)_{*n*}—. The chiralities of the chiral planes being alike, the 4 three-fold axes of rotation will be preserved, and hence the overall symmetry will be **T**.”³⁹ Because the conformation of this molecule is flexible, this molecular design will depend on the conformation of minimum energy to afford a **T** symmetry.

Caldwell and Eyring in 1971 proposed to construct **T**, **O**, or **I** molecules from “... placing an irregular protrusion anywhere on one of the faces of the original figure (platonic solids) except on a plane or axis of symmetry. Additionally, identical protrusions at the positions attainable by the first under all combinations of the original group’s proper rotations will lead to the desired lower symmetry.”⁴ There is no explicit documentation of structures or objects that are designed based on this guideline. Farina and Morandi in 1974 published a hypothetical structure for **T** molecule, of which we believe is consistent with Caldwell and Eyring’s suggestion. This design consisted of “adamantane as an achiral simplex with spiranic or twistane type ring attachments on the vertices.”⁹ This molecule also requires a synchronized ring puckering or the same ring puckering for all of its cyclic substituents to avoid different local conformations in the molecule, which can result in a **C**₁ symmetry (or possibly other symmetries that are not a **T**) for the molecule.^{8,9} Interestingly, Cotton et al. described a revision of this hypothetical structure in one of his recent paper that presented a cage assembly that has the **T** symmetry.¹⁹ The revised structure replaces the cyclopentyl group in the Farina’s design with cyclopropyl groups on the adamantane core, which appears to offer a rigid molecule with **T** symmetry.¹⁹ Neither of these two adamantane molecules has been synthesized.

The early experimental evidence of molecules with **T** symmetry include the study of tetrakis(trimethylsilyl)silane by Bartell et al. in 1970⁴³ and the synthesis of tert-butyltetrahedrane by Maier and Pfromm in 1978.⁴⁴ Calculations by Mislow and coworkers show that both of the molecules assume a **T** symmetry in its ground state in gas phase with a low energy barrier between the enantiomers, which render the system necessarily racemic at ambient temperature.^{45,46} Later, Nakazaki and Naemura attempted the first synthesis of enantiomerically pure molecules with **T** symmetry by substituting adamantane (symmetry: **T**_d) with four enantiomerically pure trishomocubane (symmetry: **D**₃) with known absolute stereochemistry using a linker of —CH₂OC(O)CH₂—. ^{47,48} However, Mislow soon noted that “the interposition of the acetoxymethyl (CH₂OC(O)CH₂) groups destroys all three fold symmetry inherent in the four 2-*D*₃-trishomocubanyl groups and in the adamantane skeleton, and **T** symmetry is ipso facto unattainable for any conceivable conformation.”⁴⁹ Responding to this criticism, Nakazaki and coworkers later synthesized a similar molecule by replacing the linker with a linear and rigid buta-1,3-diynyl groups.^{50–52} Recently, a surprisingly stable tetrakis(trimethylsilyl)tetrahedrane has also been accomplished.⁵³ For all of these studies, the **T** symmetry exists in a specific transient conformation or via a presumed synchronized motion of the conformation of the molecule. A molecular structure that exhibits permanent

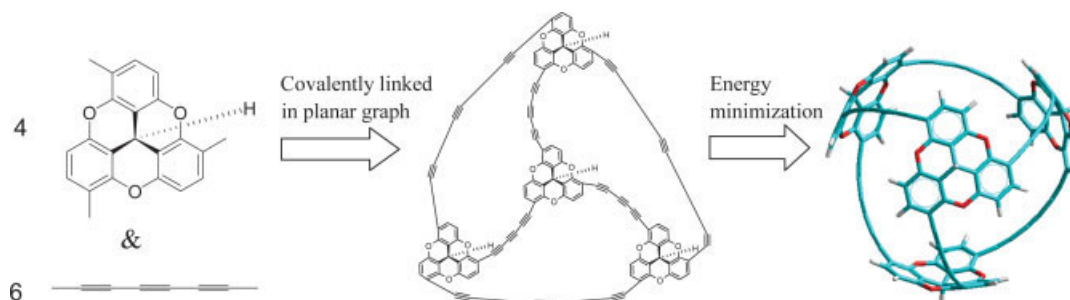


Fig. 1. The bowl-shaped trioxatricornan core has three flanking substituents giving rise to a C_3 -dissymmetric moiety that can occupy the vertices of a tetrahedron to afford a chiral molecule with **T** symmetry. [Color figure can be viewed in the online issue, which is available at www.interscience.wiley.com.].

T, **O**, or **I** symmetry is still unknown. Apart from the molecules discussed above, a flexible molecule with **T** symmetry has been synthesized not with the intention to achieve **T** symmetry. Fritz Vögtle et al. have reported the synthesis of a cage molecule with four benzene rings at the vertices of a tetrahedron connected by flexible methylene units. This molecule racemizes with a fairly low barrier and is at the fast exchange limit at temperatures above -90°C .⁵⁴

APPROACH, RESULTS, AND DISCUSSION

Consistent with the guideline given by Pierre Curie,^{9,36} we present here a general desymmetrization method for constructing not only chiral molecules that rigorously satisfy **T** symmetry, but also chiral molecules that satisfy **O** and **I** symmetries. In this article, we have used the assisted model building and energy refinement (AMBER) force field^{40,41} and density functional theory (DFT) with the B3LYP hybrid functional and 6-31G(d) basis set to calculate the energies of the proposed structures. DFT computations were preformed using GAUSSIAN-03.⁴² Optimized structures were verified to be at true minima in the potential energy surface by harmonic vibrational analyses which revealed no imaginary vibrational frequencies.

Desymmetrization of the Vertices

Our approach to construct molecules with **T**, **O**, or **I** symmetry involves the following four steps: First, choose a Platonic solid-like skeleton^{2,55} that has **T_d**, **O_h**, or **I_d** symmetry, and present the structure in a planar graph.⁵⁶ Second, replace each of the vertices of the skeleton with a C_3 -dissymmetric structural moiety of the same chirality. Third, replace “edges” and connections with functional groups that maintain the rigidity of the whole molecule. Finally, use a computation method to obtain the atom configuration (conformation) of minimum energy for the molecule and to examine its symmetry. As an example for designing molecules with **T**-symmetry, we use the Platonic solid, tetrahedron (symmetry: **T_d**), and replace each vertex with a C_3 -dissymmetric trioxatricornan^{57–61} and each “edge” with three acetylene groups. Here, we used DFT to obtain the minimum energy structure and the prescribed symmetry of the proposed molecule. This approach results in a rigid,

strained chiral molecule that appears to be highly symmetric (see Fig. 1). To support that the obtained structure is of a global energy minimum, we also used AMBER⁴² to obtain the energy minimum structure by starting with many grossly different planar graphs of the designed molecule. The results show that the same structure as that obtained by DFT, which prescribes a **T** symmetry, was obtained with all the sampled planar graphs. Examining the symmetry elements of this molecule reveals that there exists a two-fold rotational (C_2) axis that passes through each pair of the opposite edges, and a three-fold rotational (C_3) axis that passes through the center of each trioxatricornan vertex and the center of the opposite face. As the tetrahedron consists of four edges and four faces, there are three C_2 and four C_3 rotational axes. Overall, the symmetry elements consist of identity **E**, $3C_2$, and $4C_3$ rotational axes, and has a symmetry number of 12.^{2,10} Because the molecule is rigid, these symmetry elements gives rise to a permanent **T** symmetry for the molecule.

Using the same method, we also designed molecules with **O** and **I** symmetry. Constructing the structure and sampling the conformations using AMBER from their planar graphs, we obtained molecules with **O** and **I** symmetry (see Fig. 2). Examining the symmetry of molecules with **O** and **I** symmetry reveals that there is a slight difference in the nature of the rotational axes between **T** and **O** (or **I**) molecules designed in this method. Whereas the C_3 axis in the **T** molecule passes through a vertex and its opposite face, all of the rotational axes in **O** and **I** pass through the same structural moieties (vertex-to-vertex, edge-to-edge and face-to-face of the polyhedron). The **O** molecule has the elements identity **E**, and rotational axes of $6C_2$ (passing through the edges), $4C_3$ (passing through the vertices), and $3C_4$ (passing through the faces), and has a symmetry number of 24.^{2,10} The **I** molecule has the elements identity **E**, rotational axes of $15C_2$ (passing through the edges), $10C_3$ (passing through the vertices), and $6C_5$ (passing through the faces), and has a symmetry number of 60.^{2,10} Details of the symmetry analysis with different orientations of the **T**, **O**, or **I** molecule is shown in the supporting information. We note that this desymmetrization method is general in that other C_3 -dissymmetric molecules may also be used on the vertices of the molecule. For example, perhydrotriquinacene can be used to con-

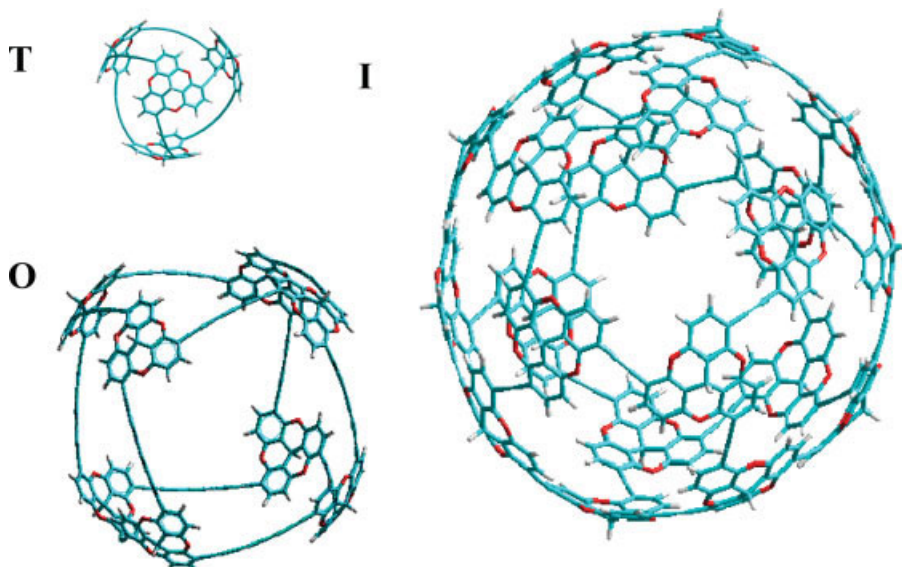


Fig. 2. Proposed molecules with the symmetry of **T** (symmetry elements: **E**, $3C_2$, $4C_3$), **O** (symmetry elements: **E**, $6C_2$, $4C_3$, $3C_4$) and **I** (symmetry elements: **E**, $15C_2$, $10C_3$, $6C_5$). All three molecules consist of C_3 -dissymmetric trioxatricornans at the vertices. [Color figure can be viewed in the online issue, which is available at www.interscience.wiley.com.].

struct molecules with **T**, **O** or **I** symmetry (See supporting information).

Desymmetrization of the Edges

Modifying Cahn et al.'s suggestion³⁹ molecules with **T**, **O**, or **I** symmetry are also constructed by desymmetrizing the edges with C_2 -dissymmetric biphenyl moieties (see Fig. 3) instead of desymmetrization of the vertices. Detailed analysis of the symmetry of these two molecules is shown in the Supporting Information.

Interestingly, we find that the requirement of the rigidity for desymmetrization of the edges appears to be more stringent than for desymmetrization of vertices. For example, if a single sp^3 carbon is used in place of the benzene ring, the **O** molecule collapses from a cube shape to a crumpled conformation during the calculation by AMBER (see Fig. 4). We checked this instability of the structure by other computational methods including DFT, Hartree-Fork Theory and AM1. All methods showed that this structure collapsed while searching for the conformation of the minimum energy. From the crumpled conformation,

it appears that the bond angle (109.5°) of the sp^3 carbon is not rigid enough to support the caged skeleton, and thus the strain in the molecule and/or π -stacking of the aromatic ring is causing the two bridging methylene carbon to twist, leading to an eventual total collapse of the molecule.

We note that designing the optimal packing of tetrahedron that gives the maximum density is still unachieved—an unsolved problem of considerable importance.⁶² Because the molecules with **T**, **O**, and **I** symmetry proposed in this work (see Fig. 2) have the rigid shapes of Platonic solids, the assembly of the molecules with **T** symmetry (see Fig. 1) to form crystals or liquid crystals will be particularly interesting and important as it may shed light on how tetrahedron will pack.

In addition, highly symmetric and strained molecules are of fundamental and application interests for their reactivities and propensity to rearrange.⁶³ In particular, acetylene-based, but achiral polyhedranes has been synthesized

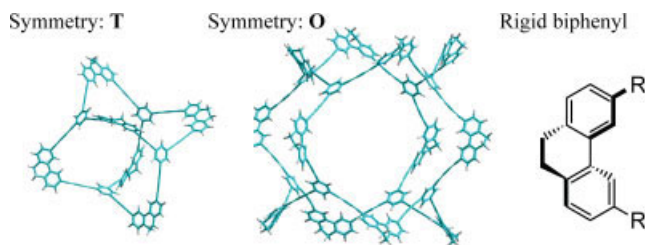


Fig. 3. Proposed molecules with **T** and **O** symmetry by desymmetrization of the edges with C_2 -dissymmetric biphenyls connected with two buta-1, 3-diyne. The rigidity of the molecules is confirmed by energy minimization of the conformations. [Color figure can be viewed in the online issue, which is available at www.interscience.wiley.com.].

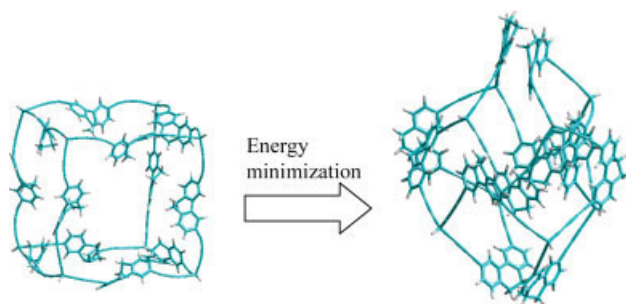


Fig. 4. Desymmetrization of the edges with C_2 -dissymmetric biphenyls and sp^3 vertices leads to collapse of the molecule destroying the **O** symmetry. [Color figure can be viewed in the online issue, which is available at www.interscience.wiley.com.].

and proposed for electrooptical^{64,65} and biological applications.⁶⁶ Because of the considerable interests, several theoretical studies using both quantum and molecular mechanics have been carried on for the stability and strain analysis of both hypothetical and synthetic acetylene-based polyhedranes.^{67,68} Past synthesis of highly symmetric achiral molecules, such as cubane⁶⁹ and dodecahedrane^{70,71} has resulted in advances in fundamental understanding^{72–76} and application development.^{77–81} There are, however, much less similar studies on highly strained, symmetric, and yet chiral molecules. Their kinetics for rearrangement,⁸² whether racemization or new stereogenic centers will arise during their rearrangement⁸³ and reactions (such as polymerization)^{84,85} is of interest for a wide range of potential applications.⁸⁶ As such, we are currently focusing on the synthesis of the resolved chiral molecule with **T** symmetry via schemes that are less than eight steps from a known structure of trioxatricornan.⁶¹ Examining the strained part of the **T** molecule, the bond angles between the acetylene and phenyl ring and among the acetylene groups range from 167.4° to 173.1° (see supporting materials), which is about 10° from an unstrained 180°. Other reportedly synthesized strained molecule bearing acetylene units show bond angles for sp carbon in the range 151.8°–178.7°.⁸⁷ We believe that this particular design of molecule with **T** symmetry is an attainable structure.

CONCLUSIONS

In this work, we present a general desymmetrization method for constructing rigid molecules that rigorously and permanently satisfy the symmetry of **T**, **O**, and **I**, which exist theoretically but were never “visualized” before. This method involves replacing the vertices on a Platonic solid-shaped molecule with **C**₃-dissymmetric moieties or the edges with **C**₂-dissymmetric moieties while maintaining the rigidity of the molecule. It is important to note that the design rigid shape for these cage-like molecules should be confirmed to be the conformation of minimum energy by using computational methods even though the molecules are designed *a priori* with rigid components. This class of designed molecules with chiral polyhedral symmetry appears to be strained, and does not require a synchronized conformation to maintain the **T**, **O** or **I** symmetry.

ACKNOWLEDGMENTS

We thank Professor Timothy M. Korter (SU) for all the Quantum Mechanics-based computations. We also thank Professor Michael B. Sponsler and Jerry Goodisman (SU) for helpful discussions.

LITERATURE CITED

- Ramsay OB, editor. ACS symposium series, Vol. 12: Van't Hoff-Le Bel Centennial. Washington, DC: ACS; 1975. 194 p.
- Jaeger FM. Lectures on the principle of symmetry and its practical application in all natural sciences. Amsterdam: Elsevier; 1917. 305 p.
- Schulman JM, Disch RL. Theoretical studies of dodecahedrane. 2. Dodecahedrane, inclusion compounds, and fluorine derivatives. *J Am Chem Soc* 1978;100:5677–5681.
- Caldwell DJ, Eyring H. The theory of optical activity. New York: Interscience; 1971. p 90–92.
- Cotton FA, Wilkinson G. Advanced inorganic chemistry. New York: Wiley; 1999. p 1321–1324.
- Donaldson JD, Ross SD. Symmetry and stereochemistry. New York: Halsted; 1972. p 36–37.
- Rassat A. Chirality and symmetry aspects of spheroarenes, including fullerenes. *Chirality* 2001;13:395–402.
- Fujita S. Systematic design of chiral molecules of high symmetry. Achiral skeletons substituted with chiral ligands. *Bull Chem Soc Jpn* 2000;73:2679–2685.
- Farina M, Morandi C. High symmetry chiral molecules. *Tetrahedron* 1974;30:1819–1831.
- Eliel EL, Wilen SH, Mander LN. Stereochemistry of organic compounds. New York: Wiley; 1994. 1267 p.
- Kettle SFA. Symmetry and structure. New York: Wiley; 1985. 10 p.
- Cotton FADL, Lin C, Murillo CA. The designed “self-assembly” of a three-dimensional molecule containing six quadruply-bonded Mo24+ units. *Chem Commun* 1999;841–841.
- James SL, Mingos DMP, White AJP, Williams DJ. Anion-templated formation of a unique inorganic “super-adamantoid” cage [Ag6(triphos)4(O3SCF3)4]2+ [triphos = (PPh2CH2)3CMe]. *Chem Commun* 1998;2323–2324.
- Raptis RG, Georgakaki IP, Hockless DCR. A FeIII/oxo cubane contained in an octanuclear complex of **T** symmetry that is stable over five oxidation states. *Angew Chem Int Ed* 1999;38:1632–1634.
- Sander J, Hegetschweiler K, Morgenstern B, Keller A, Amrein W, Weyhermuller T, Muller I. Metal binding of polyalcohols. Part 7. T-symmetrical icosahedra: a new type of chirality in metal complexes. *Angew Chem Int Ed* 2001;40:4180–4182.
- Seidel SR, Stang PJ. High-symmetry coordination cages via self-assembly. *Acc Chem Res* 2002;35:972–983.
- Terpin AJ, Ziegler M, Johnson DW, Raymond KN. Coordination number incommensurate cluster formation. Part 18. Resolution and kinetic stability of a chiral supramolecular assembly made of labile components. *Angew Chem Int Ed* 2001;40:157–160.
- Yang H-B, Ghosh K, Northrop BH, Stang PJ. Self-recognition in the coordination-driven self-assembly of three-dimensional M3L2 polyhedra. *Org Lett* 2007;9:1561–1564.
- Cotton FA, Murillo CA, Yu R. Deliberate synthesis of the preselected enantiomer of an enantiorigid molecule with pure rotational symmetry **T**. *Dalton Trans* 2005;19:3161–3165.
- Zimmer A, Kuppert D, Weyhermuller T, Muller I, Hegetschweiler K. Linear primary polyamines as building blocks for coordination polymers. Part 3. Complex formation of NiII, CuII, PdII, and CoIII with 1,2,3,4-tetraaminobutane. *Chem Eur J* 2001;7:917–931.
- Saalfraank RW, Stark A, Bremer M, Hummel HU. Adamantanoid chelate complexes. 2. Tetranuclear chelate(4-) ions of divalent metals (manganese, cobalt, nickel) with idealized T-symmetry from spontaneous self-organization. *Angew Chem* 1990;102:292–295.
- Saalfraank RW, Stark A, Peters K, Von Schnering HG. Adamantanoid chelate complexes. 1. The first adamantanoid alkaline earth metal chelate complex: synthesis, structure and reactivity. *Angew Chem* 1988;100:878–880.
- Olenyuk B, Levin MD, Whiteford JA, Shield JE, Stang PJ. Self-assembly of nanoscopic dodecahedra from 50 pre-designed components. *J Am Chem Soc* 1999;121:10434–10435.
- Stang PJ. Molecular architecture: coordination as the motif in the rational design and assembly of discrete supramolecular species—self-assembly of metallacyclic polygons and polyhedra. *Chem Eur J* 1998;4:19–27.
- Stang PJ, Olenyuk B. Self-assembly, symmetry, and molecular architecture: coordination as the motif in the rational design of supramolecular metallacyclic polygons and polyhedra. *Acc Chem Res* 1997;30:502–518.
- Stang PJ, Olenyuk B. Transition-metal-mediated self-assembly of discrete nanoscopic species with well-defined shapes and geometries. *Handbook Nanostruct Mater Nanotechnol* 2000;5:167–224.

27. Kuehl CJ, Kryschenko YK, Radhakrishnan U, Seidel SR, Huang SD, Stang PJ. Self-assembly of nanoscopic coordination cages of D3h symmetry. *Proc Natl Acad Sci USA* 2002;99:4932–4936.
28. Stang PJ, Olenyuk B, Muddiman DC, Wunschel DS, Smith RD. Transition-metal-mediated rational design and self-assembly of chiral, nanoscale supramolecular polyhedra with unique T symmetry. *Organometallics* 1997;16:3094–3096.
29. Trikha J, Theil EC, Allewell NM. High resolution crystal structures of amphibian red-cell L ferritin: potential roles for structural plasticity and solvation in function. *J Mol Biol* 1995;248:949–967.
30. Bruinsma RF, Gelbart WM, Reguera D, Rudnick J, Zandi R. Viral self-assembly as a thermodynamic process. *Phys Rev Lett* 2003;90:248101–248104.
31. Glaser RMC. Escher's drawings as an educational tool for general and special positions of symmetry in crystals and molecules. *Enantiomer* 1996;1:233–247.
32. Zandi R, Reguera D, Bruinsma RF, Gelbart WM, Rudnick J. Origin of icosahedral symmetry in viruses. *Proc Natl Acad Sci USA* 2004;101:15556–15560.
33. Arnold E, Rossmann MG. The use of molecular-replacement phases for the refinement of the human rhinovirus 14 structure. *Acta Crystallogr Sect A Found Crystallogr* 1988;A44:270–282.
34. Fisher AJ, Johnson JE. Ordered duplex RNA controls capsid architecture in an icosahedral animal virus. *Nature* 1993;361:176–179.
35. Rossmann MG, Arnold E, Erickson JW, Frankenberger EA, Griffith JP, Hecht HJ, Johnson JE, Kamer G, Luo M, Mosser AG, Rueckert RR, Sherry B, Vriend G. Structure of a human common cold virus and functional relationship to other picornaviruses. *Nature* 1985;317:145–153.
36. Curie P. Sur la symétrie dans les phénomènes physiques. Symétrie d'un champ électrique et d'un champ magnétique. *J Phys III* 1894;3:394–417.
37. Herzberg G. Atomic spectra and atomic structure, 2nd ed. New York: Dover; 1945. 271 p.
38. Herzberg G. Infrared and raman spectra of polyatomic molecules. New York: D. Van Nostrand Co; 1945.
39. Cahn RS, Ingold C, Prelog V. Specification of molecular chirality. *Angew Chem Int Ed Engl* 1966;5:385–415.
40. Hyperchem. Professional release 7.0. Gainesville, Florida: AMBER force field optimized by Polak-Ribiere; Hypercube, Inc.
41. Weiner PK, Kollman PA. AMBER: assisted model building with energy refinement. A general program for modeling molecules and their interactions. *J Comput Chem* 1981;2:287–303.
42. Frisch MJ, Trucks GW, Schlegel HB, Scuseria GE, Robb MA, Cheeseman JR, Montgomery JJA, Vreven T, Kudin KN, Burant JC, Millam JM, Iyengar SS, Tomasi J, Barone V, Mennucci B, Cossi M, Scalmani G, Rega N, Petersson GA, Nakatsuji H, Hada M, Ehara M, Toyota K, Fukuda R, Hasegawa J, Ishida M, Nakajima T, Honda Y, Kitao O, Nakai H, Klene M, Li X, Knox JE, Hratchian HP, Cross JB, Bakken V, Adamo C, Jaramillo J, Gomperts R, Stratmann RE, Yazyev O, Austin AJ, Cammi R, Pomelli C, Ochterski JW, Ayala PY, Morokuma K, Voth GA, Salvador P, Dannenberg JJ, Zakrzewski VG, Dapprich S, Daniels AD, Strain MC, Farkas O, Malick DK, Rabuck AD, Raghavachari K, Foresman JB, Ortiz JV, Cui Q, Baboul AG, Clifford S, Cioslowski J, Stefanov BB, Liu G, Liashenko A, Piskorz P, Komaromi I, Martin RL, Fox DJ, Keith T, Al-Laham MA, Peng CY, Nanayakkara A, Challacombe M, Gill PMW, Johnson B, Chen W, Wong MW, Gonzalez C, Pople JA. Gaussian 03, Revision C. 02. Wallingford, CT: Gaussian, Inc.; 2004.
43. Bartell LS, Clippard FB Jr, Boates TL. Electron diffraction study of the molecular structure of tetrakis(trimethylsilyl)silane. *Inorg Chem* 1970;9:2436–2439.
44. Maier G, Pfriem S. Small rings. 24. Tetra-tert-butylcyclopentadienone. *Angew Chem* 1978;90:551–552.
45. Hounshell WD, Mislow K. Tetra-tert-butyltetrahedrane has T symmetry. *Tetrahedron Lett* 1979;19:1205–1208.
46. Iroff LD, Mislow K. Molecules with T symmetry. Conformational analysis of systems of type M[C(CH₃)₃]₄ and M[Si(CH₃)₃]₄ by the empirical force field method. *J Am Chem Soc* 1978;100:2121–2126.
47. Nakazaki M, Naemura K. Synthesis and absolute configuration of the first optically active organic molecule with T symmetry. (-)-1,3,5,7-Tetrakis[2-(1S,3S,5R,6S,8R,10R)-D3-trishomocubanylacetoxymethyl]adamantane. *J Chem Soc Chem Commun* 1980;911–912.
48. Nakazaki M, Naemura K. Synthesis and absolute configuration of the first optically active organic molecule with T symmetry: (-)-1,3,5,7-tetrakis[(2-(1S,3S,5R,6S,8R,10R)-D3-trishomocubanyl)acetoxy]methyl]adamantane. *J Org Chem* 1981;46:106–111.
49. Mislow K. On the symmetry of (-)-1,3,5,7-tetrakis[2-(1S,3S,5R,6S,8R,10R)-D3-trishomocubanylacetoxymethyl]adamantane. *J Chem Soc Chem Commun* 1981;234.
50. Nakazaki M, Naemura K, Hokura Y. Synthesis of (+)-1,3,5,7-tetrakis[2-(1S,3S,5R,6S,8R,10R)-D3-trishomocubanylbuta-1,3-diynyl]adamantane. An optically active organic molecule with T symmetry of known absolute configuration. *J Chem Soc Chem Commun* 1982;1245–1246.
51. Nakazaki M. The synthesis and stereochemistry of chiral organic molecules with high symmetry. *Top Stereochem* 1984;15:199–251.
52. Naemura K, Hokura Y, Nakazaki M. Synthesis of (+)-1,3,5,7-tetrakis[2-(1S,3S,5R,6S,8R,10R)-D3-trishomocubanylbuta-1,3-diynyl]adamantane, the first optically active organic molecule with T symmetry and of known absolute configuration. *Tetrahedron* 1986;42:1763–1768.
53. Maier G, Neudert J, Wolf O, Pappusch D, Sekiguchi A, Tanaka M, Matsuo T. Tetrakis(trimethylsilyl)tetrahedrane. *J Am Chem Soc* 2002;124:13819–13826.
54. Voegtli F, Gross J, Seel C, Nieger M. C₃₆H₃₆, a tetrahedral enclosure of four benzene rings in a globular hydrocarbon framework. *Angew Chem* 1992;104:1112–1114 (See also *Angew Chem Int Ed Engl* 1992;31:1069–1071).
55. Hargittai I, Hargittai M. Symmetry through the eyes of a chemist. 1986. 458 p.
56. Simon JA. Topological Approach to the stereochemistry of nonrigid molecules. In: King RB, Rouvray DH, editors. *Graph theory and topology in chemistry*. Amsterdam: Elsevier; 1987. p 43–75.
57. Faldt A, Krebs FC, Thorup N. Synthesis, structure and properties of various molecules based on the 4,8,12-trioxa-4,8,12,12c-tetrahydrodibenzoc[cd,mn]pyrene system with an evaluation of the effect of differing molecular substitution patterns on the space group symmetry. *J Chem Soc Perkin Trans* 1997;2:2219–2227.
58. Martin JC, Smith RG. Factors influencing the basicities of triarylcarbinols. The synthesis of sesquixanthidrol. *J Am Chem Soc* 1964;86:2252–2256.
59. Krebs FC, Laursen BW, Johannsen I, Faldt A, Bechgaard K, Jacobsen CS, Thorup N, Boubekeur K. The geometry and structural properties of the 4,8,12-trioxa-4,8,12,12c-tetrahydrodibenzoc[cd,mn]pyrene system in the cationic state. Structures of a planar organic cation with various monovalent and divalent anions. *Acta Crystallogr Sect B* 1999; B55:410–413.
60. Laursen BW, Krebs FC, Nielsen MF, Bechgaard K, Christensen JB, Harrit N. 2,6,10-Tris(dialkylamino)trioxatriangulenium Ions. *J Am Chem Soc* 1998;120:12255–12263.
61. Lofthagen M, VernonClark R, Baldrige KK, Siegel JS. Synthesis of trioxatricornan and derivatives. Useful keystones for the construction of rigid molecular cavities. *J Org Chem* 1992;57:61–69.
62. Conway JH, Torquato S. Packing, tiling, and covering with tetrahedra. *Proc Natl Acad Sci USA* 2006;103:10612–10617.
63. Greenberg A, Liebman JF. Strained organic molecules. New York: Academic Press; 1978. 416 p.
64. Diederich F. Carbon-rich acetylenic scaffolding: rods, rings and switches. *Chem Commun* 2001;219–227.
65. Gobbi L, Seiler P, Diederich F. A novel three-way chromophoric molecular switch: pH and light controllable switching cycles. *Angew Chem Int Ed* 1999;38:674–678.
66. Siemsen P, Livingston RC, Diederich F. Acetylenic coupling: a powerful tool in molecular construction. *Angew Chem Int Ed Engl* 2000;39:2632–2657.
67. Jarowski PD, Diederich F, Houk KN. Structures and stabilities of diacetylene-expanded polyhedranes by quantum mechanics and molecular mechanics. *J Org Chem* 2005;70:1671–1678.

68. Bachrach SM, Demoin DW. Computational studies of ethynyl- and diethynyl-expanded tetrahedranes, prismanes, cubanes, and adamantanes. *J Org Chem* 2006;71:5105–5116.
69. Eaton PE, Cole TW Jr. Cubane. *J Am Chem Soc* 1964;86:3157–3158.
70. Paquette LA, Balogh DW, Usha R, Kountz D, Christoph GG. Crystal and molecular structure of a pentagonal dodecahedrane. *Science* 1981;211:575–576.
71. Paquette LA, Ternansky RJ, Balogh DW. A strategy for the synthesis of monosubstituted dodecahedrane and the isolation of an isododecahedrane. *J Am Chem Soc* 1982;104:4502–4503.
72. Griffin GW, Marchand AP. Synthesis and chemistry of cubanes. *Chem Rev* 1989;89:997–1010.
73. Hassenrueck K, Martin HD, Walsh R. Consequences of strain in (CH)₈ hydrocarbons. *Chem Rev* 1989;89:1125–1146.
74. Luh T-Y, Stock LM. Kinetic acidity of cubane. *J Am Chem Soc* 1974;96:3712–3713.
75. White MA, Wasylishen RE, Eaton PE, Xiong Y, Pramod K, Nodari N. Orientational disorder in solid cubane: a thermodynamic and carbon-13 NMR study. *J Phys Chem* 1992;96:421–425.
76. Yildirim T, Gehring PM, Neumann DA, Eaton PE, Emrick T. Unusual structure, phase transition, and dynamics of solid cubane. *Phys Rev Lett* 1997;78:4938–4941.
77. Eaton PE. Cubanes: starting materials for the chemistry of the 1990s and the next century. *Angew Chem* 1992;104:1447–1462 (See also *Angew Chem Int Ed Engl* 1992;31:1421–1436).
78. Eaton PE, Gilardi RL, Zhang M-X. Polynitrocubanes: advanced high-density, high-energy materials. *Adv Mater* 2000;12:1143–1148.
79. Eaton PE, Zhang M-X, Gilardi R, Gelber N, Iyer S, Surapaneni R. Octanitrocubane: a new nitrocarbon. *Propellants Explos Pyrotech* 2002;27:1–6.
80. Osmont A, Gokalp I, Catoire L. Evaluating missile fuels. *Propellants Explos Pyrotech* 2006;31:343–354.
81. Zhang M-X, Eaton PE, Gilardi R. Hepta- and octanitrocubanes. *Angew Chem Int Ed* 2000;39:401–404.
82. Marchand AP, Weimar WR Jr. Improved synthesis of 7-bromonorbornane. *Chem Ind* 1969;200.
83. Chance RR, Sowa JM. An examination of the thermal polymerization of a crystalline diacetylene using diffuse reflectance spectroscopy. *J Am Chem Soc* 1977;99:6703–6708.
84. Charych DH, Nagy JO, Spevak W, Bednarski MD. Direct colorimetric detection of a receptor-ligand interaction by a polymerized bilayer assembly. *Science* 1993;261:585–588.
85. Charych D, Cheng Q, Reichert A, Kuziemko G, Stroh M, Nagy JO, Spevak W, Stevens RC. A “litmus test” for molecular recognition using artificial membranes. *Chem Biol* 1996;3:113–120.
86. Diederich F, Stang PJ, Tykwinski RR, editors. *Acetylene chemistry: chemistry, biology and material science*. Weinheim: Wiley-VCH; 2005. 508 p.
87. Tobe Y, Ohki I, Sonoda M, Niino H, Sato T, Wakabayashi T. Generation and characterization of highly strained dibenzotetrakisdehydro[12]annulene. *J Am Chem Soc* 2003;125:5614–5615.

Parallel SFC/MS-MUX Screening to Assess Enantiomeric Purity

DEREK B. LASKAR, LU ZENG,* RONGDA XU, AND DANIEL B. KASSEL

Department of Analytical Chemistry and Technology, Takeda San Diego, Inc., San Diego, California

ABSTRACT Enantiomeric excess (*ee*) was evaluated for two internally synthesized compound libraries using a high-throughput automated, intelligent four-channel parallel supercritical fluid chromatography/mass spectrometry system equipped with a multiplexed ion source interface (SFC/MS-MUX). The two libraries contained compounds spanning a wide range of enantiomeric ratios with structurally diverse chemical scaffolds and stereogenic centers. The system analyzed each sample simultaneously against four chiral columns using up to six organic modifiers. Enhancements to our previously published parallel supercritical fluid chromatography/mass spectrometry system were implemented to address the challenges associated with automated trace enantiomer identification and quantitation. A reversal of enantiomer elution order was observed for several samples across multiple CSPs and modifiers. The relationship between elution order and % *ee* accuracy is presented for compounds exhibiting high, middle and low % *ee* values. Despite incidences in which the minor enantiomer eluted prior to the major enantiomer with less than baseline resolution, the overall % *ee* was in agreement with separations in which full baseline resolution was achieved. The methods presented here demonstrate the value and utility of high-throughput *ee* determinations to support drug discovery and development programs. *Chirality* 20:885–895, 2008. © 2008 Wiley-Liss, Inc.

KEY WORDS: enantioselective screening; racemate; enantiopure; supercritical fluid chromatography (SFC); high-throughput analysis; mass spectrometry; multiplexed ion source (MUX); enantioseparation; enantiomeric excess

INTRODUCTION

The value and importance of measuring enantiomeric purity of chiral drug substances during drug discovery and development is widely recognized by pharmaceutical and biotechnology industries. Since the publication of formal guidelines for the development of the stereoisomeric drugs by FDA in the early 90s, there has been a growing need to develop robust screening methods that enable scientists to rapidly identify, quantify, and evaluate enantiomeric sample mixtures to assess enantiomeric purities.¹

Chromatographic separations have been the preferred method for the characterization and purification of enantiomers in lieu of indirect methods (e.g. chemical derivatizations).^{2,3} Numerous publications have demonstrated the advantage of packed-columns coated with polysaccharide (amylose and cellulose derivatives) chiral stationary phases (CSPs) as chiral selectors to chromatographically resolve enantiomer pairs.^{4,5} Supercritical fluid chromatography (SFC) offers the advantage of lower viscosity mobile phase relative to other chromatographic techniques (e.g. CE and HPLC), thereby enabling higher flow rates to be utilized, which leads to faster analysis times and superior chromatographic peak resolutions.^{6–8} SFC has been reported to have the most extensive enantioselectivity.⁹ Typically, SFC is coupled with ultraviolet (UV) detection to identify analytes.^{10,11} However, there are significant advantages of using mass spectrometry (MS) as a means of detection: (1) MS provides higher sensitivity than UV to

detect trace enantiomer peaks that would otherwise not be detected, (2) chromophores are not required for detection, (3) Selected Ion Monitoring (SIM) ensures that nonisobaric impurities are disregarded in the sample analysis, and (4) instrument vendor data acquisition software programs can be readily modified with visual basic instrument control applications that enable automated data acquisition and data processing.¹² Moreover, coupling SFC with mass spectrometry (SFC/MS) has been demonstrated to be a powerful technique, owing to faster vaporization of solvents at the ion source—by CO₂'s nebulizing effect—resulting in a tolerance for a broader range of flow rates at the ion source interface.^{13,14}

Automated HPLC and SFC enantiomeric screening methods have been widely used in the pharmaceutical industry to rapidly determine the optimal enantioseparation conditions.^{15–17} Previously, we demonstrated the utility and application of automated, intelligent four-channel parallel SFC/MS-MUX to rapidly screen, identify, and optimize separation conditions of (primarily) racemic sample mixtures for enantiopurifications.^{18,19} Compared with other parallel chiral LC methods cited in literature,^{16,20,21}

*Correspondence to: Lu Zeng, Department of Analytical Chemistry, Takeda San Diego, Inc., 10410 Science Center Drive, San Diego, CA 92121, USA. E-mail: lu.zeng@takedasd.com

Received for publication 6 November 2007; Accepted 1 February 2008

DOI: 10.1002/chir.20553

Published online 1 April 2008 in Wiley InterScience (www.interscience.wiley.com).

our approach combined innovations in instrument hardware, software, and enantioseparation strategies. We coined the technique "Intelligent Parallel Optimization for Chiral SFC Separations" (IPOCSS). Using the IPOCSS interface, we showed that a single sample mixture can undergo a comprehensive method development screen (i.e. four-columns by six modifiers; 24 unique modifier/column combinations) in as little as 30 min. Furthermore, utilizing custom intelligent decision-making software to navigate the screening process, it was possible to automatically terminate the data acquisition once user-defined criteria (minimum R_s , t_R , peak area, etc.) were satisfactorily met. Thus, a significant amount of time, solvent usage, and resources was saved while productivity and throughput are increased.

To evaluate and characterize compound libraries containing one or more stereocenters for % *ee* determinations required a modification of our previously reported IPOCSS screening strategy from a method development and optimization tool to a rapid, high-throughput enantiomeric purity assessment tool. Automated method development for rapid % *ee* determinations is complicated by the presence of trace amounts of minor enantiomers. The problem is exacerbated when applied to large compound libraries with diverse chemical structures, varying enantiopurities, and multiple stereocenters. To address these issues, we modified the IPOCSS program so as to allow it to function as a tool for rapid, high-throughput enantiomeric purity assessment tool. The new enhancements were made to support the characterization of two internally synthesized compound libraries—"Library A," an 11-component library and "Library B," a 225-component library—with structurally diverse chemical scaffolds (across Libraries A and B), stereogenic centers (within Libraries A and B) and varying enantiopurities. Experimental screening conditions were modified to balance fast analysis times while maintaining suitable enantioselectivity for accurate % *ee* determinations.

MATERIALS AND METHODS

Chemicals and Reagents

Liquid CO₂ (SFE/SFC grade) was obtained from Airgas, Inc. (Radnor, PA). HPLC-grade (0.2 μ m filtered) organic modifiers, methanol (MeOH), 2-propanol (2-PrOH), and acetonitrile (ACN) were obtained from Fisher Scientific (Fair Lawn, NJ). 1-Propanol (1-PrOH) was obtained from Alfa Aesar (Ward Hill, MA) and ethanol (EtOH) was obtained from Acros Organics (Morris Plains, NJ). Ammonium acetate (AAc), ammonium trifluoroacetate (ATFAc), and warfarin were obtained from Sigma-Aldrich (St. Louis, MO). Compound libraries were synthesized at Takeda San Diego. Library A components (11 compounds, 1 mg each) were diluted with MeOH to 0.1 mg/ml before analysis. Library B samples (225 compounds) were received as 10 mM stock solutions MeOH/DMSO (50:50) in a 96-well plate. Solvent was evaporated overnight using a MiniVap (SPEWare, Baldwin Park, CA) and the compounds were reconstituted to 0.1 mg/ml in MeOH before analyses.

Chirality DOI 10.1002/chir

Chiral Chromatographic Conditions

All chiral SFC columns used were coated polysaccharide Chiralpak AD-H, AS-H and Chiralcel OJ-H, OD-H (all 2.1 \times 150 mm, 5 μ m) purchased from Chiral Technologies, Inc. (West Chester, PA). A mobile phase composition of CO₂/organic modifier (60:40, v/v) was used with modifier screening hierarchical progression scheme: MeOH > EtOH > 2-PrOH > 1-PrOH > ACN. Mobile phase was delivered at 5 ml/min and split to the four columns enabling a 1.25 ml/min per column flow rate. The outlet pressure was regulated at 100 bar. It has been shown that adding basic additives such as AAc and ATFAc to organic modifiers can aid in enantioselectivity, improved peak shape and enhanced MS ionization with polysaccharide CSPs for the analysis of basic compounds.^{22–25} To support the characterization of Library A and Library B, 10 mM of AAc was added to MeOH, EtOH, 2-PrOH, and 1-PrOH while 10 mM of ATFAc was added to ACN (due to AAc's low solubility in ACN).

SFC/MS-MUX Instrumentation and Configuration

All chiral analyses were performed on a Waters ZQ 2000 Micromass[®] single quadrupole mass spectrometer (Waters Corp., Milford, MA) equipped with a multiplex (MUX) four-channel electrospray ion source coupled to a Berger SFC Analytix[™] Dual Pump Fluid Control Module (FCM 1100), Modifier Fluid Control Module (FCM 1200), and a TCM 2000 column oven (Mettler-Toledo/AutoChem, Columbia, MD). Mass spectrometric data acquisition was performed using Positive-Ion Electrospray Ionization (ESI+) detection in the Selected Ion Recording (SIR) mode with 0.1 sec dwell time; the inter-spray scan delay time was 0.1 sec/channel with 0.8 sec total cycle time. Ion source conditions were used as follows: sprayer voltage, 3.2 kV; cone voltage, 25 V; desolvation temperature, 350°C; source temperature, 150°C; desolvation gas flow, 650 l/h and cone gas flow, 30 l/h. Injections were made using an HTS PAL autosampler (LEAP Technologies, Carrboro, NC). A 20 μ l injection of sample was made and distributed evenly across each of the four-columns operated in parallel chromatography mode. A make-up flow of 0.05% formic acid in MeOH/H₂O (90:10, v/v) at 0.02 ml/min per channel was added post-column to each of the four column effluent flow streams prior to entering the MUX interface. MassLynx[™] acquired and monitored data simultaneously from the four-channel mobile phase streams. Figure 1 illustrates the complete SFC/MS-MUX system configuration.

Chiral Screening Methodology and Strategy

Intelligent parallel optimization for chiral SFC separations. As previously reported, IPOCSS integrates both SFC/MS-MUX hardware and Waters/Berger software components to navigate the screening process by automatically submitting samples, monitoring runs, processing and analyzing data, intelligently judging optimal separation conditions, and deciding how to proceed in the screen progression.¹⁹ The entire sequence is guided by an in-house custom intelligent decision-making software program

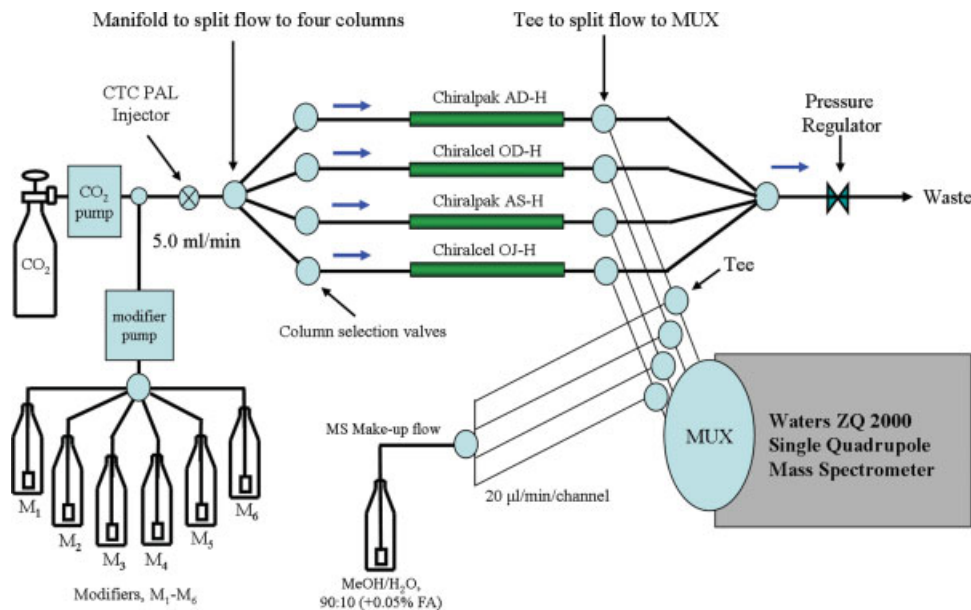


Fig. 1. Schematic representation of the SFC/MS-MUX parallel four-channel configuration used for enantioselective screening. M₁–M₆ correspond to each modifier attached to the 6-port stream selector valve. [Color figure can be viewed in the online issue, which is available at www.interscience.wiley.com.]

written in Microsoft[®] Visual Basic[®] 6.0. To initiate an IPOCSS screen, the user enters MassLynx[™] methods and parameters (tune, inlet, MS, SFC, modifier priority, resolution requirements, etc.) into the *Configuration* panel and then imports a sample list text file—containing sample name, molecular weight and vial position—using the *Import Sample List* button. Pressing the *Start* button initiates the automatic screen, enabling IPOCSS to perform the flow scheme progression that was described previously.¹⁹ Peak integrations are performed by OpenLynx[™], while IPOCSS applies the following equation (according to USP)²⁶ to calculate peak resolution values (R_s):

$$R_s = 2 \times (t_{R2} - t_{R1}) / (W_2 + W_1)$$

where t_{R2} and t_{R1} are the retention times (in min) of the second and first eluting peaks, respectively, and W_2 and W_1 are the peak widths (in min, 10% valley definition) of the second and first eluting peaks, respectively.

After a sample has completed one solvent cycle (5 min run), IPOCSS automatically calculates and quantifies key screening parameters from the run—retention times (t_R), peak widths, resolution (R_s) and % *ee*—to gauge the analysis “success” using a specific column and modifier combination. IPOCSS then evaluates and compares the results against the user-defined criteria to judge if further solvent cycles are necessary to satisfy the user-defined criteria. If R_s has not been adequately met, IPOCSS automatically screens the next modifier in the procession to evaluate its selectivity behavior. If R_s has been adequately met, IPOCSS terminates the screening process and determines the “optimal” separation conditions based on the largest observed R_s . The original purpose of IPOCSS was to rapidly develop optimal chiral chromatographic conditions

of racemates to support enantiopurifications. Thus, the software and criteria that controlled IPOCSS were designed to handle samples containing approximate equal proportions of each enantiomer pair; whose mass spectral peak abundances and ion intensities would be approximately equal in magnitude.

IPOCSS Enhancements to support high throughput and % *ee* determinations. Modifications to the IPOCSS program were required in order to rapidly assess enantiomeric purity of compound libraries, where sample mixtures contain varying degrees of enantiomeric ratios (scalemic mixtures). Two crucial user-definable features were added to IPOCSS control software interface to aid in the identification of peaks exhibiting relative small MS peak intensities: (1) Minimum Area (MA), a peak integration-defining parameter in which an absolute minimum area threshold is defined and must be satisfactorily met for IPOCSS to identify a peak as legitimate instead of as chemical noise or other chromatographic impurity; and (2) Minimum % Base Peak (MBP), a % *ee* qualifier where the relative % area of the smaller peak (compared to the larger peak) must meet or exceed a set value in order for a peak to be considered. Adding these two features to the IPOCSS program enabled us to readily assess % *ee* values in scalemic sample mixtures containing trace amounts of an enantiomer.

RESULTS AND DISCUSSION

Enantiomeric Purity Assessment of a Small Compound Library

Library A was a small, structurally similar set of 11 internally synthesized compounds that was screened to: (1)

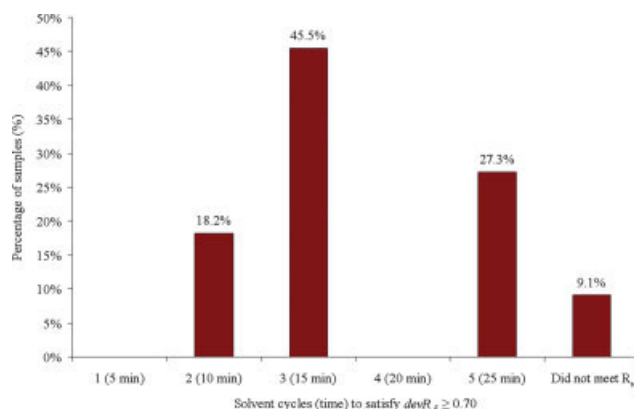


Fig. 2. Percentage of samples that met R_s ($R_s \geq 0.70$) in a given solvent cycle (time) for Library A. [Color figure can be viewed in the online issue, which is available at www.interscience.wiley.com.]

verify enantiomeric purity and (2) enantiopurification feasibility. The following criteria were used in the IPOCSS Configuration panel: $R_s = 0.70$, MA = 3000, and MBP = 30%. Setting R_s to ensure IPOCSS would terminate the method development process once the observed R_s has been satisfactorily met. The 40% organic modifier hierarchical progression scheme was: MeOH > EtOH > 2-PrOH > 1-PrOH > ACN.

The following factors were considered in selecting the initial screening conditions that balanced both speed of analysis and overall purity calculation accuracy: (a) Using <40% modifier generally retains molecules longer on the column, generating run times of 5 min and (b) Resolution $R_s \geq 0.70$ is considered an acceptable value for assessing enantiopurification feasibility. With the current configuration, a single sample can undergo a comprehensive method development screen (i.e. parallel four-columns across five modifiers) with 20 unique column/modifier conditions in as little as 25 min; the shortest run time is as little as 5 min if the criteria have been met satisfactorily within any of the first modifier/four-column combinations.

The success rate for achieving an observed $R_s \geq 0.70$ within five solvent cycles was 90.9% (10/11) for all 11 samples in Library A. No compounds achieved the defined minimum R_s using a single solvent cycle (5 min). 18.2% of the samples (2/11) required 2 cycles (10 min), 45.5% of the samples (5/11) required 3 cycles (15 min), 27.3% of the samples (3/11) required 5 cycles (25 min) and the remaining 9.1% of the compounds (1/11) did not meet the R_s criterion (see Fig. 2). The largest observed R_s with corresponding modifier, column and calculated % ee value are shown in Table 1. Compound **A-11** exhibited the largest observed R_s (equal to 1.89) with 2-PrOH on AS-H within a 15-min total screening time. The modifiers that yielded the highest success rates of meeting R_s criterion were 2-PrOH and ACN. Nine of 11 compounds exhibited the largest R_s on an AS-H column.

Shorter screening times are possible if R_s has been satisfactorily met within the first or second solvent cycles. Such an example is illustrated with Compound **A-4** in Table 2. $R_s = 0.68$ (3.23% ee) was observed with MeOH (first cycle) while EtOH (second cycle) yielded $R_s = 1.04$

(7.05% ee) both on AS-H. Compound **A-7** required a full screen (i.e. 4 columns \times 5 modifiers) and R_s was ultimately achieved using ACN on an OD-H column (see Fig. 3). Only marginal enhancements in enantioselectivity were observed until arriving at ACN, where $R_s = 0.83$ (3.26% ee) was achieved on OD-H (Table 2). Despite taking 25 min to reach R_s , the total screening time is significantly shorter when compared to non-parallel-based screening methods (e.g. serially based methods would have taken 104 min).

Despite Library A primarily consisting of racemates (Table 1), several compounds contained 2 chiral centers with small amounts of diastereomeric “impurities” present in the sample mixtures. One of the challenges we encountered with the library was IPOCSS erroneous peak selection of nontargeted peaks. Compound **A-9** exhibited such behavior where the majority of the targeted enantiomers were principally equal in proportion; however, small amounts of diastereomer “impurities” were observed, as listed in Table 2 on OD-H and AD-H with MeOH and on all four columns with EtOH. Conversely, the impurity was not observed with 2-PrOH on any column. Expanded chromatograms showing the impurity along with the calculated relative diastereomer percentage (E_d) and absolute integrated area (A_d) are displayed in Figure 4. As evidenced in Figure 4, selecting a large enough MA and MBP is critical in reducing erroneous peak selection. With MeOH, AD-H yielded $E_d = 4.86\%$ and $A_d = 2831$, while OD-H yielded $E_d = 15.71\%$ and $A_d = 17831$. As the IPOCSS Configuration was set to MA = 3000 and MBP = 30%, it was unable to select the diastereomer in OD-H because R_s was below the setting ($R_s = 0.55$). Moreover, none of the diastereomer proportions was large enough with EtOH to be identified as a legitimate peak. Improved R_s was observed across cycles 1–3 with AS-H displaying superior enantioselectivity and a final $R_s = 1.02$ (3.74% ee) with 2-PrOH.

Identifying diastereomers is important for characterizing sample mixtures containing multiple chiral centers, especially when one diastereomer is targeted for enantiopurification. The technique enabled us to properly identify and

TABLE 1. Screening results of Library A displaying largest R_s with corresponding column, mobile phase, R_s and % ee

Sample	Chiral column ^a	Mobile phase ^{b,c}	R_s	% ee
A-1	AS-H	2-PrOH	0.76	5.20
A-2	AS-H	2-PrOH	0.71	7.23
A-3	AS-H	2-PrOH	0.70	5.27
A-4	AS-H	EtOH	1.04	7.05
A-5	OD-H	ACN	1.11	8.13
A-6	AS-H	ACN	0.74	2.00
A-7	OD-H	ACN	0.82	3.26
A-8	AS-H	2-PrOH	0.56	9.03
A-9	AS-H	2-PrOH	1.02	3.74
A-10	AS-H	EtOH	0.83	8.17
A-11	AS-H	2-PrOH	1.89	14.00

^a“AD-H” and “AS-H” indicates ChiralpakTM AD-H and AS-H, respectively. “OD-H” and “OJ-H” indicates ChiralcelTM OD-H and OJ-H, respectively.

^bMobile phase composition was CO₂/modifier (60:40, v/v).

^cEtOH and 2-PrOH contained 10 mM of ammonium acetate (AAc) as additive; ACN contained 10 mM of ammonium trifluoroacetate (ATFAc) as additive.

TABLE 2. Screening results for samples A-2, A-4, A-7, and A-9 with chromatographic parameters (t_R [min], R_s , and % ee)

Samples	Chiral column ^a	Mobile phase ^b											
		40% MeOH ^c				40% EtOH ^c				40% 2-PrOH ^c			
		t_{R1}	t_{R2}	R_s	% ee	t_{R1}	t_{R2}	R_s	% ee	t_{R1}	t_{R2}	R_s	% ee
A-2	AD-H	0.74	0.74	0.00	–	0.69	0.69	0.00	–	0.71	0.71	0.00	–
	OD-H	1.03	1.03	0.00	–	1.03	1.03	0.00	–	0.73	1.22	2.58	20.00
	AS-H	0.65	0.75	0.38	6.03	0.63	0.79	0.58	8.92	1.05	1.41	0.71	7.23
A-4	OJ-H	0.52	0.52	0.00	–	0.55	0.55	0.00	–	0.72	0.72	0.00	–
	AD-H	0.84	0.84	0.00	–	0.69	0.69	0.00	–				
	OD-H	0.88	0.88	0.00	–	0.75	0.75	0.00	–				
A-7	AS-H	0.77	0.97	0.68	3.23	0.85	1.29	1.04	7.05				
	OJ-H	0.45	0.45	0.00	–	0.45	0.45	0.00	–				
	AD-H	0.91	0.91	0.00	–	0.73	0.95	0.68	19.07	0.81	1.10	0.63	15.59
A-9	OD-H	0.90	0.90	0.00	–	0.75	0.75	0.00	–	0.88	1.03	0.44	39.13
	AS-H	0.63	0.63	0.00	–	0.63	0.72	0.32	21.14	0.99	1.32	0.56	29.92
	OJ-H	0.50	0.50	0.00	–	0.49	0.49	0.00	–	0.59	0.59	0.00	–
A-9	AD-H	0.93	0.93	0.00	–	0.78	0.78	0.00	–	0.79	0.79	0.00	–
	OD-H	0.66	0.88	0.55	68.58	0.76	0.76	0.00	–	0.95	0.95	0.00	–
	AS-H	0.70	0.80	0.34	4.45	0.75	0.99	0.54	12.38	1.39	2.33	1.02	3.74
	OJ-H	0.50	0.50	0.00	–	0.52	0.52	0.00	–	0.64	0.64	0.00	–

The IPOCSS-selected optimal (largest observed R_s) results are highlighted in bold, while the IPOCSS-calculated erroneous results are underlined.

–, selectivity not observed; blank, not screened due to R_s being satisfied with previous run.

^a“AD-H” and “AS-H” indicates ChiralpakTM AD-H and AS-H, respectively; “OD-H” and “OJ-H” indicates ChiralcelTM OD-H and OJ-H, respectively.

^bMobile phase composition was CO₂/modifier (60:40, v/v).

^cMeOH, EtOH, 2-PrOH, and 1-PrOH contained 10 mM of ammonium acetate (AAc) as additive.

^dACN contained 10 mM of ammonium trifluoroacetate (ATFAc) as additive.

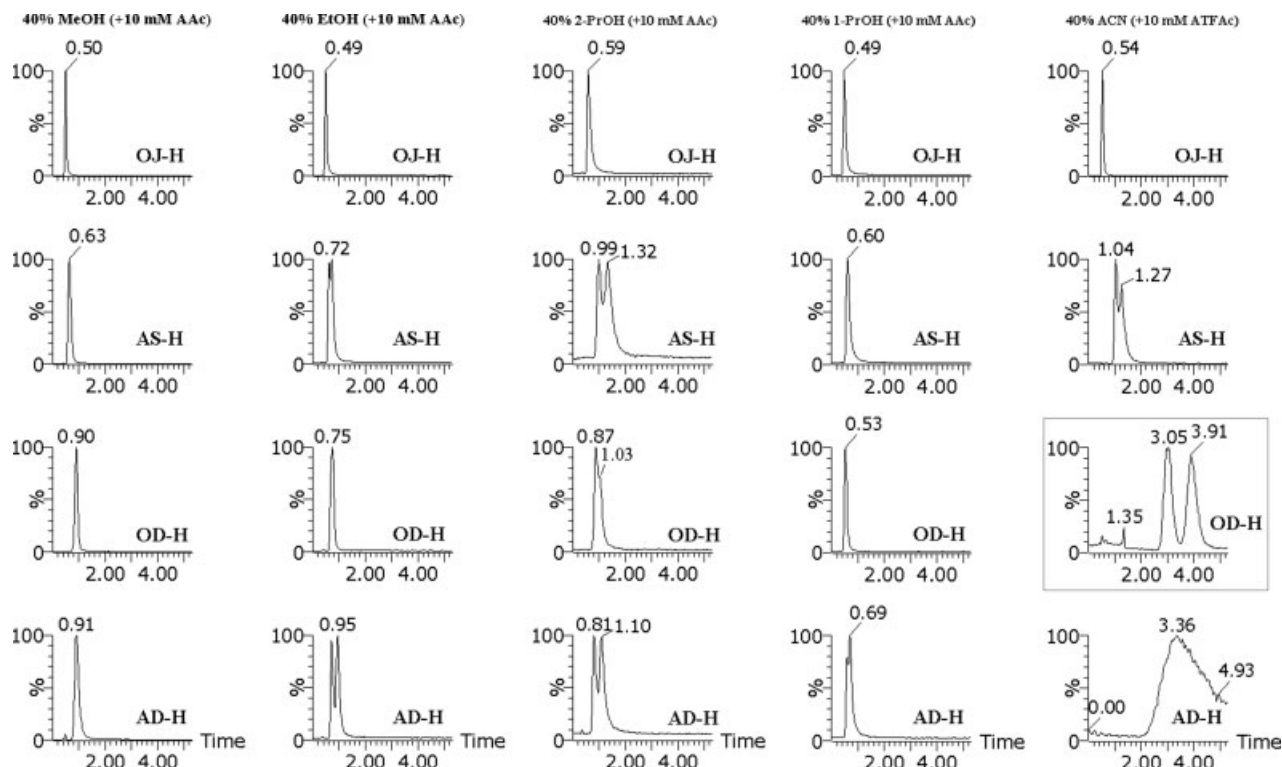


Fig. 3. Screening results of A-7 indicating modifier progression scheme (from left to right) to attain R_s ; $R_s = 0.83$ (3.26% *ee*) was achieved within 25 min on OD-H with 40% ACN (boxed).

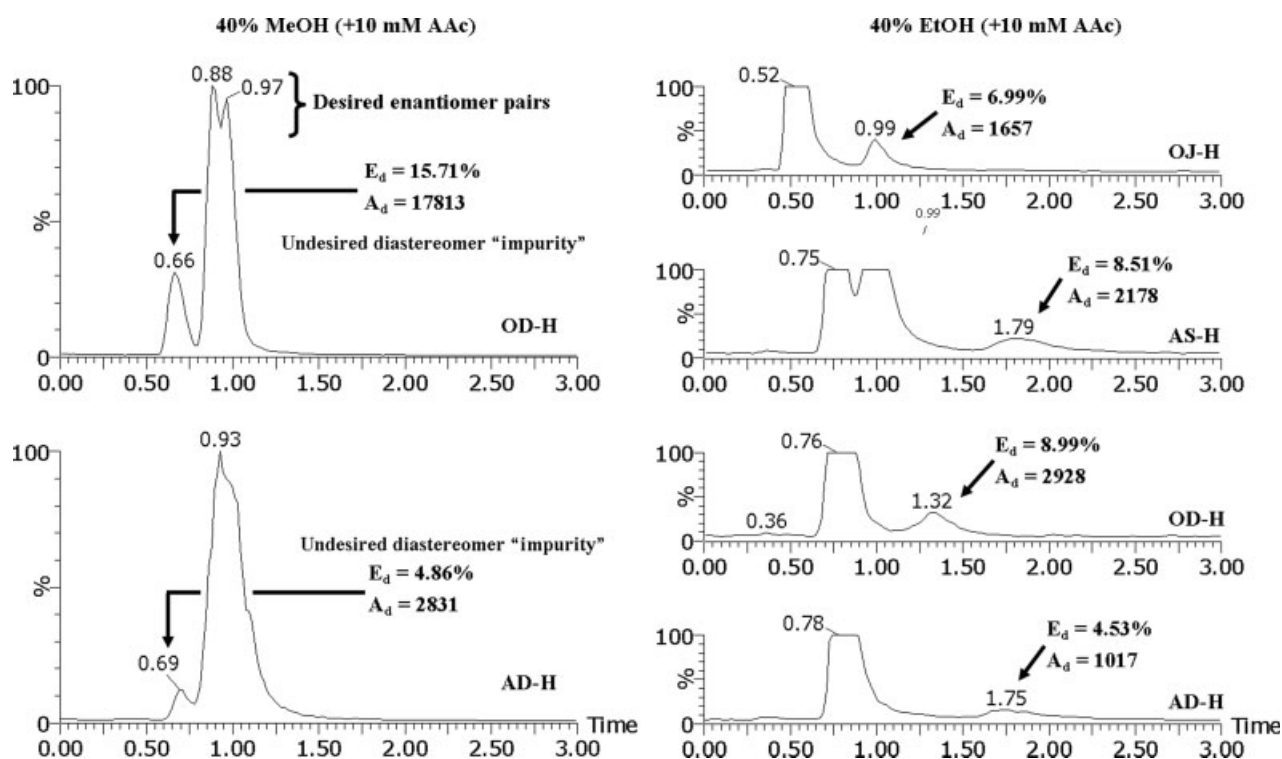


Fig. 4. Expanded chromatograms of A-9 screening results. Small amounts of diastereomer impurities were identified on AD-H and OD-H with MeOH and AD-H, OD-H, AS-H, OJ-H with EtOH and their relative percentage proportions (E_d) and absolute integrated areas (A_d).

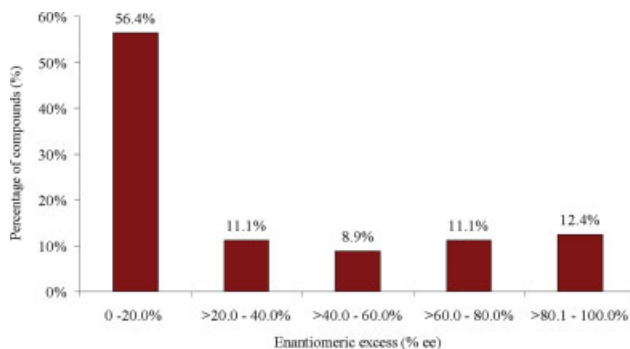


Fig. 5. Range of enantiopurities observed in Library B. [Color figure can be viewed in the online issue, which is available at www.interscience.wiley.com.]

substantiate the existence of diastereomers due to the same molecular ions observed in the chromatogram. Employing other detection methods (i.e. UV) would not differentiate between diastereomers and other unidentified small impurities in the sample mixture. Future work on diastereomer elucidation may perhaps include the use of an ion trap mass spectrometer (MS^n) to distinguish enantiomers from diastereomers based on the MS fragmentation pattern differences, as recently reported by Badaloni et al.²⁷

Enantiomeric Purity Assessment of Library B

Library B was a large, structurally similar set of 225 internally synthesized compounds that was screened to

determine % *ee* values without further method refinement, optimization, or enantiopurification. The screening strategy used for Library B was adopted from the one used for Library A to balance both speed of analysis while maintaining accurate purity calculations. The following criteria were used in the IPOCSS Configuration panel: $R_s = 1.5$, MA = 500, and MBP = 1%. Setting MA = 500 ensured trace peaks were not overlooked, and similarly, MBP = 1% made certain that small enantiomers in the samples with large % *ee* values were properly identified. Setting $devR_s = 1.5$ anticipated chromatographic baseline separation to accurately quantify a % *ee* and increases the likelihood of achieving a full 3-modifier screen. The 40% organic modifier hierarchical progression scheme was: MeOH > EtOH > 2-PrOH. With the current configuration, a single sample could undergo a comprehensive method development screen (i.e. parallel four-columns across three modifiers) with 12 unique column/modifier conditions in as little as 15 min; the shortest run time is as little as 5 min if criteria have been satisfactorily met within any of the first modifier/four-column combinations.

Library B compounds were primarily scalemic mixtures with varying degrees of enantiomeric ratios. Figure 5 displays the range of enantiopurities obtained from the screen: approximately half of the samples (56.4%) exhibited enantiopurity values close to racemates (0–20.0% *ee*), while the remainder displayed a range of % *ee* values (between 20.0 and 100% *ee*). Purity values within the 80.1–100% *ee* range (12.4% of the total samples) posed challenges in accurate identification and quantification of trace

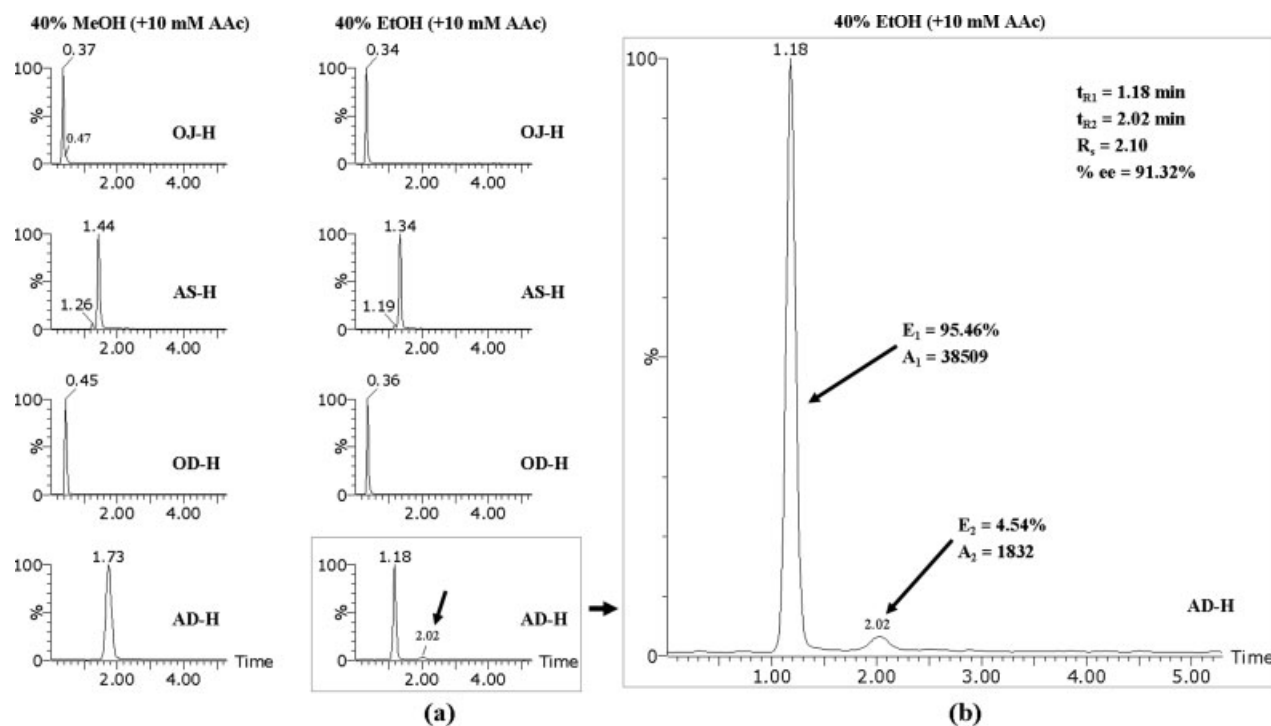


Fig. 6. Screening results of B-113. (a) $R_s = 2.1$ (91.32% *ee*) was achieved within 10 min on AD-H with 40% EtOH (boxed). (b) Magnified view highlighting elution order with relative percentage proportions (E_d) and absolute integrated areas (A_d). Elution order reversal of the minor enantiomer was observed comparing OJ-H ($t_{R1} = 0.47$ min) and AS-H ($t_{R1} = 1.26$ min) with MeOH and between AD-H ($t_{R2} = 2.02$ min) and AS-H ($t_{R1} = 1.19$ min) with EtOH.

TABLE 3. Screening results of select samples from Library B exhibiting high, middle, and low % ee values comparing influence of the CSP and modifier conditions on chromatographic parameters, t_R (min), R_s , % ee and enantiomer elution order (EEO)

Sample	Chiral Column ^a	Mobile phase ^b														
		40% MeOH ^c						40% EtOH ^c						40% 2-PrOH ^c		
		<i>t</i> _{R1}	<i>t</i> _{R2}	<i>R</i> _s	% <i>ee</i>	EEO ^d	<i>t</i> _{R1}	<i>t</i> _{R2}	<i>R</i> _s	% <i>ee</i>	EEO ^d	<i>t</i> _{R1}	<i>t</i> _{R2}	<i>R</i> _s	% <i>ee</i>	EEO ^d
B-85	AD-H	/	/	0.00	–	–										
	OD-H	0.80	0.80	0.00	–	–										
	ASH	2.48	2.84	0.96	76.06	min→maj										
	OJ-H	1.01	2.03	1.92	75.42	maj→min										
	AD-H	1.73	1.73	0.00	–	–	1.18	2.02	2.10	91.32	maj→min					
B-113	OD-H	0.45	0.45	0.00	–	–	0.36	0.36	0.00	–	–					
	ASH	1.26	1.44	0.84	91.28	min→maj	1.19	1.34	0.82	91.82	min→maj					
	OJ-H	0.37	0.47	0.70	85.96	maj→min	0.34	0.34	0.00	–	–					
	AD-H	2.05	2.05	0.00	–	–	1.21	2.56	1.12	49.24	maj→min	0.89	1.94	2.34	42.96	maj→min
	OD-H	0.68	0.68	0.00	–	–	0.55	0.55	0.00	–	–	0.51	0.51	3.00	–	–
B-127	ASH	0.50	0.70	0.80	45.24	min→maj	0.45	0.58	0.80	47.78	min→maj	0.43	0.57	0.80	41.84	min→maj
	OJ-H	0.67	0.81	0.76	52.70	min→maj	0.57	0.57	0.00	–	–	0.47	0.47	0.00	–	–

–, selectivity not observed; blank; not screened due to R_s being satisfied with previous run; /, peak eluted after 5 min acquisition time.

^a“AD-H” and “AS-H” indicates Chiralpak™ AD-H and AS-H, respectively; “OD-H” and “OJ-H” indicates Chiralcel™ OD-H and OJ-H, respectively.

^bMobile phase composition was CO₂ (l)/modifier (60:40, v/v).

^cMeOH, EtOH and 2-PrOH contained 10 mM of ammonium acetate (AAC) as additive.

^dEnantiomer elution order (EEO) denoted: “min→maj” correlates to minor enantiomer preceding elution over major enantiomer (and vice versa).

amounts of enantiomer impurities in these samples. The new enhancements in IPOCSS played a key role in properly identifying these small peaks as further discussed below.

Enantiomeric Elution Order and Method Accuracy

Enantiomeric elution order of trace analytes in multi-component mixtures plays an important role in accurately determining chromatographic parameters.^{3,28} Elution order reversal and enantioselectivity is influenced by both modifiers and chiral selectors used in enantioseparations.²⁹ The following discussion of three examples highlight the importance of elution order in relation to enantioselectivity and accurate % *ee* values; elution order reversal was observed on multiple columns across several modifier conditions.

Compound **B-113** had a high % *ee* value (>90%) and was used to illustrate the successful implementation of the new IPOCSS software enhancements to accurately identify and measure trace amounts of minor enantiomers present in scalemic mixtures. The modifier screen progression is illustrated in Figure 6 where the minor enantiomer was properly identified and quantified among multiple columns within 10 min (two solvent cycles). Table 3 lists the screening results, demonstrating the consistently large % *ee* values across multiple CSPs and modifiers. Enantioselectivity was observed with MeOH on AS-H ($R_s = 0.84$, 91.28% *ee*) and OJ-H ($R_s = 0.70$, 85.96% *ee*); however, EtOH exhibited superior selectivity over MeOH on AD-H ($R_s = 2.10$, 91.32% *ee*) and marginal selectivity on AS-H ($R_s = 0.82$, 91.82% *ee*). Enantioselectivity was not observed on OD-H and OJ-H with EtOH. Since R_s was suitably met on AD-H with EtOH, IPOCSS terminated further solvent progression yielding satisfactory R_s and % *ee* within 10 min.

Elution order reversal was observed between AS-H and AD-H with EtOH (see Fig. 6). Since the minor enantiomer on AD-H was sufficiently separated from the major enantiomer, it was possible to derive an accurate % *ee*. Even though baseline resolution was not achieved with MeOH and EtOH on AS-H, the % *ee* values were in agreement with those obtained from the separation on AD-H with EtOH ($R_s = 2.10$). This suggests that accurate and consistent % *ee* values may be achieved even when baseline separation is not achieved, provided the minor enantiomer elutes prior to the major one.

Compound **B-85** had a medium % *ee* value (20–89%). Elution order reversal was observed on AS-H and OJ-H with MeOH, whereas enantioselectivity was not observed on AD-H or OD-H (see Fig. 7). The minor enantiomer eluted prior to the major enantiomer on AS-H with an $R_s = 0.96$ and 76.06% *ee*, whereas the elution order on OJ-H was reversed ($R_s = 1.92$ and 75.42% *ee* on OJ-H). Despite reduced selectivity on AS-H relative to OJ-H (Table 3), the % *ee* values across columns were in good agreement.

Compound **B-127** had a small % *ee* value (<20%), exhibiting elution order reversal behavior between AS-H and AD-H with both EtOH and 2-PrOH (see Fig. 8). The minor enantiomer eluted prior to the major enantiomer on AS-H,

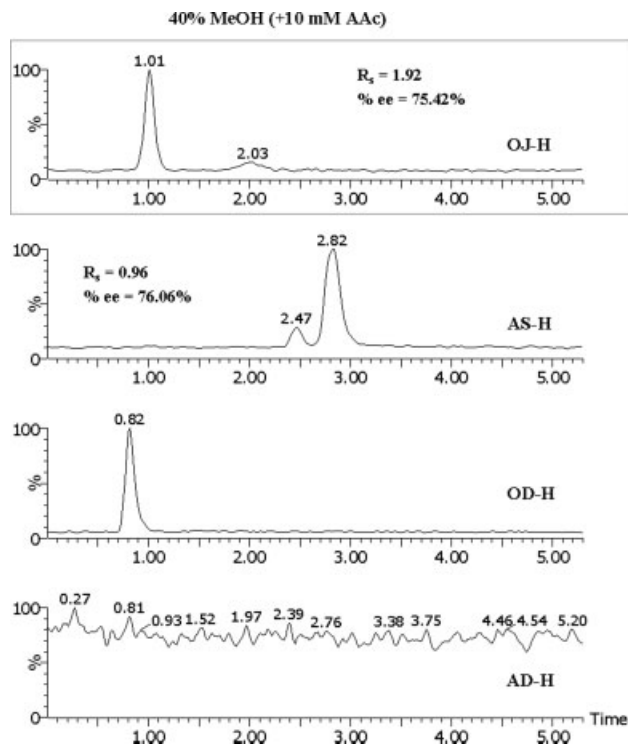


Fig. 7. Screening results of B-85. Minor enantiomer elution order reversal with the CSP-dependent difference in selectivity was observed; $R_s = 1.92$ (75.42% *ee*) on OJ-H and an $R_s = 0.96$ (76.06% *ee*) was achieved within 5 min using 40% MeOH. Optimal screening conditions are boxed. Compound eluted past 5 min acquisition time on AD-H.

whereas the elution order was reversed on AD-H. Figure 8 and Table 3 illustrate the results from a complete screen where the % *ee* values for both AS-H and AD-H with 2-PrOH were in agreement with each other despite the large disparity in observed R_s : on AD-H, $R_s = 2.34$, 42.96% *ee* and on AS-H, $R_s = 0.80$, 41.84% *ee*. IPOCSS correctly identified AD-H with 2-PrOH as the optimal screening combination.

Overall, Library B exhibited few incorrect peak selections due to isobaric mass interference. In most cases, the compounds exhibited sharp peak shapes with high signal-to-noise ratios. Potential challenges would arise if, for instance, MA was set too high. In this instance, smaller peak areas would not be properly recognized due to their relatively low intensity in the sample mixture. Additionally, inaccurate % *ee* determinations would occur when nonsymmetrical peaks (non-Gaussian) and/or two peaks of differing relative areas were observed in the chromatographic separation. One way to correct this is to implement a modified R_s function, as shown by Cai and Wu.³⁰

CONCLUSION

Software enhancements—addition of MA and MBP criteria to IPOCSS—were implemented to our in-house automated SFC/MS-MUX screening system to rapidly assess enantiomeric purities of two compound libraries exhibiting a varying array of % *ee* values.

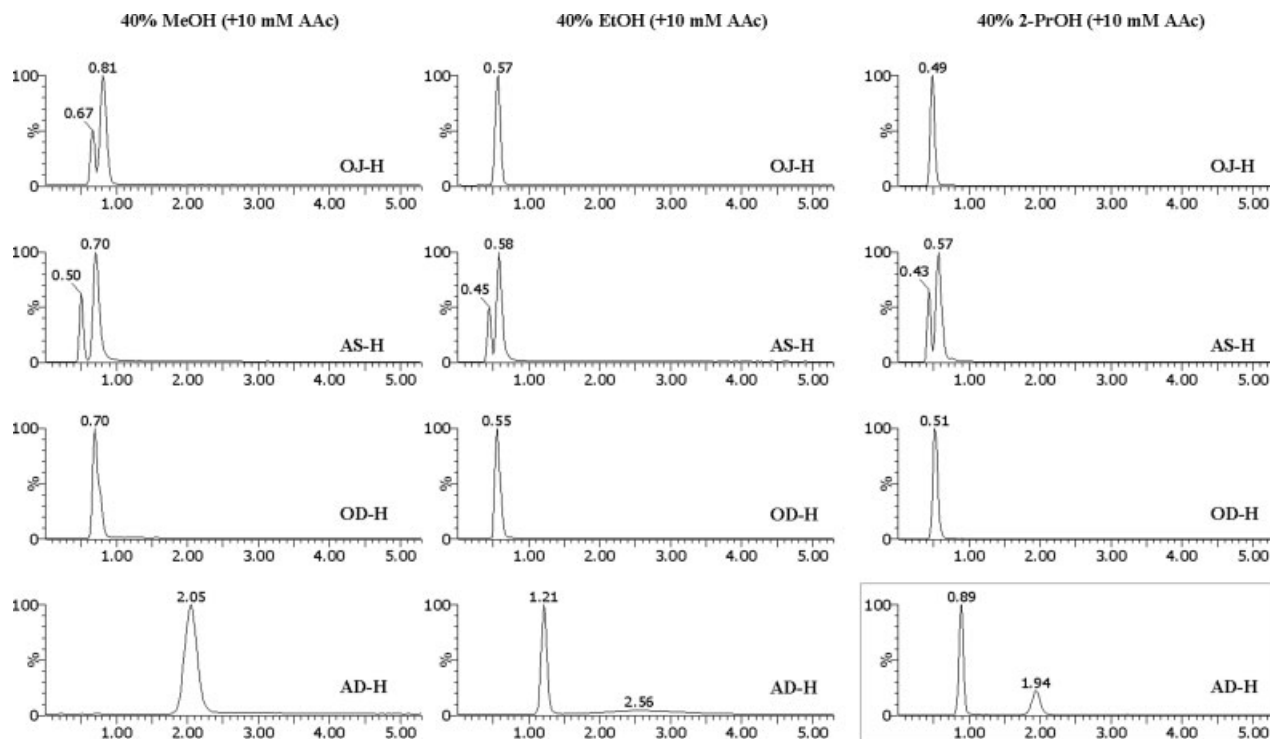


Fig. 8. Screening results of B-127 displaying the difference in enantioselectivity and elution order reversal amid several CSPs and modifier conditions. Optimal screening conditions were achieved with an $R_s = 2.34$ (42.96% *ee*) within 15 min on AD-H using 40% 2-PrOH (boxed).

An 11 compound library (Library A) was screened to evaluate enantiomeric purity and enantiopurification feasibility. A 90.9% success rate of resolving each enantiomer pair at $R_s \geq 0.70$ within ≤ 25 min was achieved. The screening process satisfactorily resolved 54.5% of the samples within 15 min using 2-PrOH. Most of the samples (81.8%) exhibited the largest R_s on AS-H.

A 225 compound library (Library B) was evaluated to quickly assess accurate enantiomeric purities over a broad range of % *ee* values. Approximately half of the samples (56.4%) exhibited purity values close to racemates (0–20.0% *ee*), while the remainder of the samples displayed a range of % *ee* values (between 20.0 and 100% *ee*). Several compounds in the library displayed elution order reversal across various modifiers and CSPs. Overall, the minor enantiomers that eluted prior to the major exhibited much smaller observed R_s values than those that eluted after the major enantiomer; however, this decrease in selectivity did not negatively affect the % *ee* accuracy as the values were in agreement with values obtained from separations where the minor enantiomer was baseline resolved after the major enantiomer.

To address situations in which nonsymmetrical peak shapes and/or differing relative peak abundances are observed, future software enhancements should be considered: (a) fine-tune the integration methods IPOCSS uses to calculate resolution values for peaks exhibiting large % *ee* values and (b) enable IPOCSS to evaluate small peaks with elution order reversal as an additional criterion for selecting optimal separation conditions.

Chirality DOI 10.1002/chir

The new screening strategy to assess enantiomeric purity has resulted in the implementation of an internal routine, analytical service to support medicinal chemistry drug discovery programs at Takeda San Diego, Inc.

ACKNOWLEDGMENTS

The authors would like to thank Dr. Stephen Gwaltney, Dr. Sheldon Cao, and Mr. Jun Feng for providing compound libraries (A and B) for the studies.

LITERATURE CITED

1. Caner H, Groner E, Levy L. Trends in the development of chiral drugs. *Drug Discov Today* 2004;9:105–110.
2. Zhang Y, Wu D, Wang-Iverson DB, Tymiak AA. Enantioselective chromatography in drug discovery. *Drug Discov Today* 2005;10:571–577.
3. Gübitz G, Schmid MG. Chiral separation by chromatographic and electromigration techniques. A review. *Biopharm Drug Dispos* 2001; 22:291–336.
4. Yamamashi E. Polysaccharide-based chiral stationary phases for high-performance liquid chromatographic enantioseparation. *J Chromatogr A* 2001;906:105–125.
5. Kartoza I, Kanyonyo M, Happaerts T, Lambert DM, Scriba GKE, Chankvetadze B. Comparative HPLC enantioseparation of new chiral hydantoin derivatives on three different polysaccharide type chiral stationary phases. *J Pharm Biomed Anal* 2002;27:457–465.
6. Phinney KW. SFC of drug enantiomers. *Anal Chem* 2000;72:204A–211A.
7. Terfloth G. Enantioseparations in super- and subcritical fluid chromatography. *J Chromatogr A* 2001;906:301–307.

8. Williams KL, Sander LC, Wise SA. Comparison of liquid and supercritical fluid chromatography using naphthylethylcarbamoylated- β -cyclodextrin chiral stationary phases. *J Chromatogr A* 1996;746:91–101.
9. Chester TL, Pinkston JD. Supercritical fluid and unified chromatography. *Anal Chem* 2002;74:2801–2812.
10. Toribio L, Nozal MJ, Bernal JL, Alonso C, Jimenez J. Comparative study of the enantioselective separation of several antiulcer drugs by high-performance liquid chromatography and supercritical fluid chromatography. *J Chromatogr A* 2005;1091:118–123.
11. Borman P, Boughtflower B, Cattanaach K, Crane K, Freebairn K, Jonas G, Mutton I, Patel A, Sanders M, Thompson D. Comparative performances of selected chiral HPLC, SFC, and CE Systems with a chemically diverse sample set. *Chirality* 2003;15:S1–S12.
12. Finn MG. Emerging methods for the rapid determination of enantiomeric excess. *Chirality* 2002;14:534–540.
13. Smith RM. Supercritical fluids in separation science—the dreams, the reality and the future. *J Chromatogr A* 1999;856:83–115.
14. Combs MT, Ashraf-Khorassani M, Taylor LT. Packed column supercritical fluid chromatography-mass spectroscopy: A review. *J Chromatogr A* 1997;785:85–100.
15. Villeneuve MS, Anderegg RJ. Analytical supercritical fluid chromatography using fully automated column and modifier selection valves for the rapid development of chiral separations. *J Chromatogr A* 1998;826:217–225.
16. Zhang Y, Watts W, Nogle L, McConnell O. Rapid method development for chiral separation in drug discovery using multi-column parallel screening and circular dichroism signal pooling. *J Chromatogr A* 2004;1049:75–84.
17. Maftouha M, Granier-Loyaux C, Chavana E, Marini J, Pradines A, Heydenb YV, Picarda C. Screening approach for chiral separation of pharmaceuticals Part III. Supercritical fluid chromatography for analysis and purification in drug discovery. *J Chromatogr A* 2005;1088:67–81.
18. Zeng L, Xu R, Kassel DB. Parallel SFC/MS combined with intelligent column selection for high throughput chiral optimization and separation. Proceedings of the 53rd ASMS Conference on Mass Spectrometry and Allied Topics 2005, San Antonio, TX.
19. Zeng L, Xu R, Laskar DB, Kassel DB. Parallel supercritical fluid chromatography/mass spectrometry system for high throughput enantioselective optimization and separation. *J Chromatogr A* 2007;1169:193–204.
20. Sajonz P, Gong X, Leonard WR, Biba M, Welch CJ. Multiparallel chiral method development screening using an 8-channel microfluidic HPLC system. *Chirality* 2006;18:803–813.
21. Sajonz P, Schafer W, Gong X, Shultz S, Rosner T, Welch CJ. Multiparallel microfluidic high-performance liquid chromatography for high-throughput normal-phase chiral analysis. *J Chromatogr A* 2007;1145:149–154.
22. Berger TA. Separation of polar solutes by packed column supercritical fluid chromatography. *J Chromatogr A* 1997;785:3–33.
23. Bakhtiar R, Tse FLS. High-throughput chiral liquid chromatography/tandem mass spectrometry. *Rapid Commun Mass Spectrom* 2000;14:1128–1135.
24. White C, Burnett J. Integration of supercritical fluid chromatography into drug discovery as a routine support tool II. Investigation and evaluation of supercritical fluid chromatography for achiral batch purification. *J Chromatogr A* 2005;1074:175–185.
25. Pinkston JD, Stanton DT, Wen D. Elution and preliminary structure-retention modeling of polar and ionic substances in supercritical fluid chromatography using volatile ammonium salts as mobile phase additives. *J Sep Sci* 2004;27:115–123.
26. USP. The United States Pharmacopeia, XX Revision. p 943–946.
27. Badaloni E, Cabri W, Ciogli A, Deias R, Gasparrini F, Giorgi F, Vigevani A, Villani C. Combination of HPLC “Inverted Chirality Columns Approach” and MS/MS detection for extreme enantiomeric excess determination even in absence of reference samples. Application to camptothecin derivatives. *Anal Chem* 2007;79:6013–6019.
28. Perry JA, Rateike JD, Szczerba TJ. Eluting trace components before major constituents: I. Sensitivity enhancement in analytical determinations of optical purity. *J Chromatogr A* 1987;389:57–64.
29. Gyllenhaal O, Stefansson M. Reversal of elution order for profen acid enantiomers in packed-column SFC on Chiralpak AD. *Chirality* 2005;17:257–265.
30. Cai CP, Wu NS. A practical resolution function. *Chromatographia* 1990;30:400–404.

Use of Large-Scale Chromatography in the Preparation of Armodafinil

WILLY HAUCK,¹ PHILIPPE ADAM,² CHRISTELLE BOBIER,^{2*} AND NELSON LANDMESSER³

¹Novasep Inc., Boothwyn, Pennsylvania

²Novasep SAS, Pompey, France

³Cephalon Inc., West Chester, Pennsylvania

ABSTRACT Armodafinil, the (*R*)-enantiomer of modafinil, is a medication used to treat the excessive sleepiness associated with narcolepsy, obstructive sleep apnea/hypopnea syndrome, and shift work sleep disorder. We report here the chemical development of armodafinil and the investigations that led to a commercial route to prepare this pure enantiomer. Three synthetic approaches were used to provide the chiral sulfoxide. Resolution via preferential crystallization was used for phase I clinical trials and was subsequently replaced by chiral chromatography, enabling us to pursue a rapid filing and registration of the API. Finally, the commercial route was developed and employed asymmetric oxidation catalyzed by a titanium(IV) isopropoxide and diethyl tartrate system. The advantages of choosing a chromatographic development pathway to expedite registration while concurrently developing an economical chiral synthesis route is discussed in the context of armodafinil development. *Chirality* 20:896–899, 2008. © 2008 Wiley-Liss, Inc.

KEY WORDS: continuous chromatography; chiral chromatography; asymmetric oxidation; asymmetric synthesis; preferential crystallization; armodafinil; chiral sulfoxide; preparative HPLC; continuous processes

INTRODUCTION

Armodafinil (2-[(*R*)-(diphenylmethyl)sulfinyl]acetamide) (Fig. 1) is a wakefulness-promoting agent used for the treatment of excessive sleepiness associated with narcolepsy, obstructive sleep apnea, and shift work sleep disorder. Armodafinil is a second generation therapy and is a single enantiomer formulation of modafinil that has been approved for the same indications.

The challenge in this process development was to find a viable and economic synthetic route while also shortening development times to introduce the product more quickly to the market. It was, therefore, interesting to choose a continuous chiral chromatographic process, to file the molecule as soon as possible and concurrently work on the asymmetric process development in the laboratory for the long-term commercial supply. This strategy can be successful and allows the pharmaceutical company to reduce the time to market launch by up to 2 yr.

CHROMATOGRAPHY

HPLC is well known by analytical specialists as a powerful method for both optical and chemical purity measurement. Unfortunately, chromatography is rarely considered as a way of pure enantiomer production, even if it is a good alternative to the other techniques.¹

Some commercialized APIs such as sertraline (Zoloft[®]),² escitalopram (Cipralex[®]/Lexapro[®]), levitiracetam (Keppra[®]), radafaxine, and pagoclone³ are produced via chromatography and demonstrate how powerful chiral chromatography can be. Commercial production at tons to 100s tons scale shows it can be the most cost-effective production method for chiral manufacturing.

Preparative HPLC can be easily scaled-up for production of pure enantiomers by transposing analytical conditions to a larger column and increasing amounts of feed injected. Continuous chromatography (SMB, VARICOL[®]) is designed for binary separations and is very well adapted for chiral resolution of a racemate. The optimization of these processes is done after just a few laboratory measurements and the application of modeling and simulation software. The development and optimization of continuous chromatography can take place in parallel with the first production by HPLC in order to save time.

To prepare armodafinil by chiral chromatography, the simplest route was to resolve readily available racemic modafinil.⁴ The strategy that we developed was the following:

- To determine solubility of substrate in common eluent solvents,
- To screen a large number of chiral stationary phases (CSPs) and chiral intermediates,

*Correspondence to: Christelle Bobier, Novasep SAS, Pompey, France. E-mail: christelle.bobier@novasep.com

Received for publication 7 February 2008; Accepted 13 February 2008

DOI: 10.1002/chir.20564

Published online 27 May 2008 in Wiley InterScience (www.interscience.wiley.com).

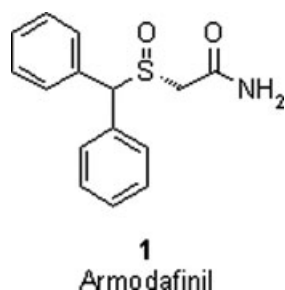


Fig. 1. Structure of Armodafinil (2-[(*R*)-(diphenylmethyl)sulfinyl]acetamide).

- To optimize the eluent system for use with the selected CSP/intermediate,
- To demonstrate the selected conditions on analytical and pilot scale, and
- To develop a process for large-scale separation.

During the development study, the aim was to select the most productive and robust stationary phase and mobile phase for the separation of modafinil enantiomers. Our method development typically began with a screening of different CSPs (from Daicel, Shiseido, Kromasil, Merck KgaA or Regis) and a screening of different eluents (ethanol, methanol, heptane, isopropanol, or a mix of them). Based on the analyte solubility (greatest in MeOH 20 g/l at 20°C), selectivity and productivity, Chiralpak AD 20 μ m (Chiral Technologies) was selected as the CSP for the process. Conditioning of the CSP with isopropanol after column packing and prior to the VARICOL[®] separation in methanol was found to improve the efficiency and selectivity of the separation and contributed to the robustness of the final process.

A complementary study was performed to define the appropriate conditions on a 30-cm I.D. column HPLC. When 5 mg were injected onto the analytical column, every 4 min, (*R*)-modafinil was recovered within specifications of yield (90%) and purity (99.0%). The corresponding amount to be injected onto the 30-cm I.D. column is 21.27 g per injection.

With these studies in hand, the separation was carried out using a 30-cm I.D. HPLC column installation. For the early clinical studies, a total of 61.3 kg of (*R*)-modafinil were produced with a yield of 93%. During three consecutive batches of this first production campaign, the specific productivity obtained was 0.3 kg (*R*)-modafinil/kg CSP/day. The optical purity was between 99.2 and 99.7% and the chemical purity was more than 99.9%. This amount of (*R*)-modafinil was obtained over 3 mo.

In parallel with the HPLC production campaign and with the perspective of large-scale production, a pilot study on a VARICOL[®] Lab system, equipped with six columns of 2.5-cm I.D., was run to demonstrate the feasibility of the process and to identify robust operating conditions for production on the VARICOL[®] 6-200 (six columns of 20-cm I.D.). The operating ranges were characterized by numerical simulations and the working conditions were found through this process demonstration (specific productivity

= 0.48 kg (*R*)-modafinil/kg CSP/day). The VARICOL[®] Lab was operated under these conditions for a period of over 10 days in order to process 1 kg of feed material and to assess the eluent recycling. The parameters implemented in the VARICOL[®] production were within the range of the predicted parameters as defined in the simulation study.

The numerical simulation showed that better performances (purity, productivity, and yield) were obtained with the VARICOL[®] process when compared with the SMB process, and also defined an upper limit for (*S*)- and (*R*)-modafinil content in the recycled eluent. On the other hand, maximum water content in the eluent was experimentally set at 5000 ppm. Content of undesired enantiomer was set to a limit ± 0.007 g/l for the mobile phase and ± 1 g/l when the eluent is used for feed preparation.

For phase III clinical supply, 540 kg of (*R*)-modafinil (99% o.p.) was produced on a VARICOL[®] unit composed of six columns of 20-cm I.D. packed with Chiralpak AD 20 μ m as stationary phase and using pure methanol as mobile phase. The productivity obtained during the 8 mo production campaign was 0.5 kg (*R*)-modafinil/kg CSP/day, chromatographic yield was 93% and recovery yield of (*R*)-modafinil, including subsequent drying process, was 77.6%. The optical purity of the desired enantiomer was greater than 99.2% and the chemical purity was 99.7%.

The next step of the study was to characterize the (*R*)-modafinil separation robustness from a racemate feed stock with a new impurity profile on a VARICOL[®] Lab pilot unit. This study provided the necessary information to define critical parameters and their proven acceptable ranges; to determine the maximum impurity levels needed to reach chemical purity specifications; to evaluate the new packing batches using the new feed stock (CSP stability, protocol for IPA conditioning, residual content of IPA in methanol); and to evaluate the stability of purified (*R*)-modafinil in its solid form (at 40 and 65°C for 8 days under nitrogen atmosphere).

A rationale was developed to define the residence time of *rac*-modafinil, (*R*)-modafinil, and methanolic solutions to control the stability profile in the continuous chiral separation process including process validation batches and production of commercial launch quantities. On an industrial VARICOL[®] unit (composed of six columns of 30-cm I.D.), the stationary phase was stable after the processing of 10 metric tons of racemate.

Chiral chromatography quickly produced the required amount of armodafinil for clinical trials and registration of the molecule. The development of the method from the feasibility study to the scale-up and process validation at three different commercial production sites equipped with two unit sizes (30- and 45-cm I.D. columns) took only 23 mo.

Eventually, chiral chromatography will not be selected as the route for long-term commercial production. Racemization of the undesired enantiomer was not possible for this molecule, and the starting material (modafinil) is costly. We, therefore, had to develop a more cost-effective route.

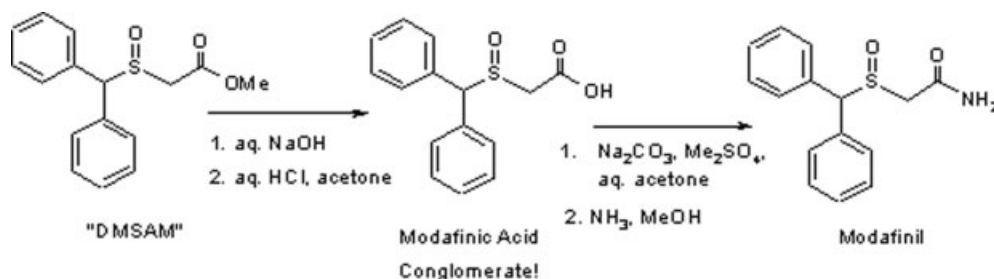


Fig. 2. Formation of Modafinic acid and conversion to Modafinil.

CRYSTALLIZATION

A classical method useful for the separation of enantiomers is the preparation and fractional recrystallization of their respective diastomeric salts. This well-known method is only possible when the racemate to be resolved is capable of forming a diastomeric salt and when the purified enantiomer can be regenerated from the salt. Another method for the separation of enantiomers involves the preferential crystallization of a conglomerate, when a racemate exists as a true eutectic mixture. This situation is estimated to apply to about 5% of all organic compounds.

During the early stage of armodafinil development, it was discovered that an intermediate in the synthesis of racemic modafinil could be easily converted to its carboxylic acid derivative and that the derivative, modafinic acid, exists as a true eutectic mixture or conglomerate. This conglomerate could be separated into its corresponding enantiomers by preferential crystallization, utilizing an auto-seeded programmed polythermal preferential crystallization (AS3PC) method⁵ (see Fig. 2).

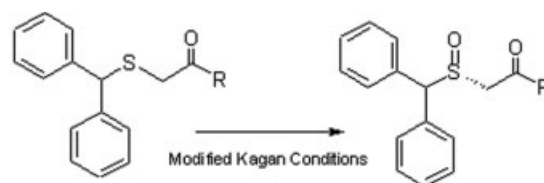
The AS3PC method of preferential crystallization takes advantage of the unique quality of conglomerates and a protocol that involves seeding a solution of the racemate with one of the pure enantiomers. This seeding process results in the crystallization of the enantiomer that now is present in excess. Filtration to collect the solid provides the first enantiomer in high chiral purity, while the mother liquor remaining is now highly enriched in the second enantiomer. At this point in the process, additional racemate is added to the mother liquor. The resulting solution is now enriched in the second enantiomer which crystallizes again in high chiral purity. Upon collection of the second enantiomer by filtration, the mother liquor that remains is now highly enriched in the first isomer. By adding additional racemate to the solution, the cycle is extended and both of the enantiomers can be harvested in alternating batches. In the case of modafinic acid, we have processed enantiomers through over 35 cycles in a pilot plant cGMP environment. A total of 85 kg of (*R*)-modafinic acid was produced by this method over four batches. The optically pure acid was subsequently converted to the API in a two-step synthetic process.

Although the AS3PC method of preferential crystallization allowed us to provide API for early preclinical and clinical studies, we quickly realized that the process was limiting and labor intensive. In the absence of a process for the racemization of the undesired enantiomer, the

theoretical yield for any crystallization process is only 50%. Since it seemed that this process would not prove to be adequately robust on commercial scale, it was decided to focus resources on an asymmetric synthesis.

ASYMMETRIC SYNTHESIS

A strategy for the asymmetric synthesis of armodafinil was developed based upon the groundbreaking work of Kagan and coworkers.⁶ This chemistry utilizes a chiral titanium complex catalyzed cumene hydroperoxide oxidation of a sulfide substrate to provide chiral sulfoxides with good optical activity. We found the Kagan method to be quite useful but also to be substrate dependant. Several sulfide derivatives of modafinil were screened to determine a starting point for optimization. From this initial screen, the sulfide amide substrate provided excellent op-



Entry	R	Yield	% ee
1	OMe	50 %	65
2	OH	ND	0
3	NH ₂	70%	>98

Solvent	% ee	LCAP Armod.	Yield
Toluene	93	>99	92 %
Ethyl acetate	99.5	>99	75 %
Methylene chloride	98	>98.5	61 %
Acetonitrile	99.3	>98.5	70 %
THF	99.7	>99	50 %
Acetone	99.6	>99	45 %

Fig. 3. Effect of substrate and solvent on the yield and enantiomeric excess of the asymmetric oxidation. (LCAP Armod. is the liquid chromatography area percent of Armodafinil. It is a measure of the chemical purity.) [Color figure can be viewed in the online issue, which is available at www.interscience.wiley.com.]

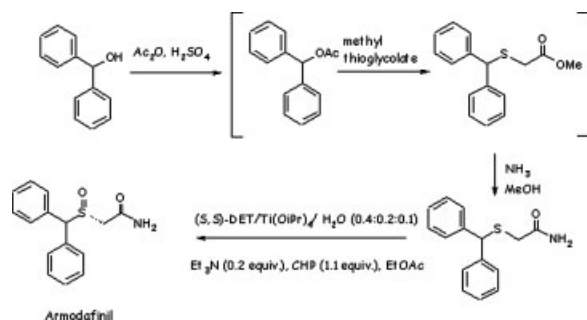


Fig. 4. Asymmetric synthesis of Armodafinil.

tical purity and was identified as a starting point for further optimization (see Fig. 3).

Once the sulfide amide was identified as the preferred substrate, a group of several parameters were studied in an effort to optimize the conditions for maximizing yield and chiral purity. The parameters studied included were the following: the choice of solvent, water stoichiometry, Ti catalyst stoichiometry, (S,S)-DET (diethyl tartrate) stoichiometry, cumene hydroperoxide stoichiometry, and catalyst contact time. The final optimized conditions provided an asymmetric oxidation process suitable for commercial scale manufacturing yielding the API in 75% isolated yield and >99.5% optical purity.⁷

The asymmetric oxidation offers several advantages over the separation processes. The process begins with relatively cheap achiral raw materials and overall is a true catalytic process. The result is a process that is economically favorable as compared with separation methods. In addition, the armodafinil isolated from the asymmetric synthesis process is typically >99% chemical purity and >99.5% optical purity and meets the specification in every way for API armodafinil. The final commercial manufacturing process is shown below (see Fig. 4).

CONCLUSION

Chiral chromatography enabled us to shorten the time to regulatory submission and approval of Nuvigil[®] (armodafinil). The process also provides extremely pure API for clinical use. This is a testament to the purity of modafinil, the starting material for the process, and the value of large-scale chiral chromatography as a purification tool.

The large-scale preparation of armodafinil was quickly achieved, thanks to chromatography. Classical batch

HPLC was used to supply the API for early clinical trials, while the optimization, validation, and multisite implementation of a commercial production was achieved using VARICOL[®] continuous chromatography.

For this particular program, the chiral separation was the final process step, and the undesired enantiomer could not be recycled by racemization. Consequently, the global yield and cost of goods were not the most favorable. As the chromatographic process guaranteed the scale-up and the supply of Armodafinil, we could develop in parallel an efficient asymmetric synthesis that further improved cost of goods and could be introduced as a postapproval change for long-term commercial production.

This example shows that chiral chromatography should be systematically evaluated for large-scale API manufacturing to shorten the time to market even, if the ultimate cost of goods targets cannot be achieved with the technology.

ACKNOWLEDGMENTS

Cephalon: John Mallamo, Conrad Kowalski, Gilles Serure, Gerard Duret, Laurence Prat, Francois Rebiere, Pierre Leproust, Stéphanie Graf, Laurent Courvoisier, Dominique Klien, Guy Piacenza, Sebastien Rose, Nelson Landmesser, Stuart Dodson, and Michael Kress. Chiral Technologies: James Lee and Tom Lewis. Novasep: Jean Bléhaut, Félicie Denet, Manuel Marques, Yvan Ruland, Eric Lang, Kevin Duffield. IRCOF-University of Rouen: Prof. Gérard Coquerel, Marie-Noëlle Petit, Franck Mallet, and Nicolas Wermester.

LITERATURE CITED

1. Francotte ER. Enantioselective chromatography as a powerful alternative for the preparation of drug enantiomers. *J Chromatogr A* 2001;906:379–397.
2. Quallich GJ. Development of the commercial process for Zolofit/Sertraline. *Chirality* 2005;17:S120–S126.
3. Stuk TL, Assink BK, Bates RC, Erdman DT, Fedij V, Jennings SM, Lassig JA, Smith RJ, Smith TL. An efficient and cost effective synthesis of Pagoclone. *Org Process Res Dev* 2003;7:851–855.
4. Hauck W, Ludemann-Hombourger O, Ruland Y, Landmesser N, Mallamo J. Methods for the separation of modafinil. *Int. Patent WO 2006/030278*.
5. Collet A, Brienne MJ, Jacques J. Optical resolution by direct crystallization of enantiomer mixtures. *Chem Rev* 1980;80:215–230.
6. Brunel J-M, Diter P, Duestsch M, Kagan HB. Highly enantioselective oxidation of sulfides mediated by a chiral titanium complex. *J Org Chem* 1995;60:8086.
7. Rebiere F, Duret G, Prat L. Process for enantioselective synthesis of single enantiomers of modafinil and related compounds by asymmetric oxidation. *Int. Patent WO 2005/028428*.

Cellulose tris(3,5-dimethylphenylcarbamate)-Based Chiral Stationary Phases as Effective Tools for Enantioselective HPLC Separation of Structurally Different Disubstituted Binaphthyls

LUCIE LOUKOTKOVÁ,¹ MILENA RAMBOUSKOVÁ,¹ ZUZANA BOSÁKOVÁ,^{1*} AND EVA TESAŘOVÁ²

¹Faculty of Science, Department of Analytical Chemistry, Charles University in Prague, 128 43 Prague 2, Czech Republic

²Faculty of Science, Department of Physical and Macromolecular Chemistry, Charles University in Prague, 128 43 Prague 2, Czech Republic

ABSTRACT Cellulose tris(3,5-dimethylphenylcarbamate)-based chiral stationary phases (CSPs) were used for a study of the HPLC retention and enantioseparation behavior of 2,2'-disubstituted or 3,2,2'-trisubstituted 1,1'-binaphthyls and 8,3'-disubstituted 1,2'-binaphthyls. The effects of the mobile phase composition in normal- (NP) and reversed-phase (RP) separation modes were investigated. The NP mobile phases contained *n*-hexane and propane-2-ol at various volume ratios, the RP ones were obtained by mixing acetonitrile with water or a 20 mM phosphate buffer of pH 6.0 or 3.0. The RP separation mode has been found more suitable for enantioresolution of most of the analytes. The best enantioseparation of 2,2'-diacetyl-1,1'-binaphthyl, 2-hydroxy-2'-(phenylamino)-1,1'-binaphthyl-3-carboxylic acid and 2-amino-2'-hydroxy-1,1'-binaphthyl-3-carboxylic acid was obtained in the mobile phase of ACN/20 mM phosphate buffer, pH 3.0, 40/60 (v/v), whereas *N*-(2'-hydroxy-1,1'-binaphthyl-2-yl)acetamide, *N*-(3'-methoxy-1,2'-binaphthyl-8-yl)acetamide, and *N*-(3'-hydroxy-1,2'-binaphthyl-8-yl)acetamide yielded better results in ACN/water at the same v/v ratio. The analyte–CSP interaction mechanism was found to be temperature independent but the enantioresolution improved at an elevated temperature. The mechanism of the enantioselective discrimination is discussed on the basis of the thermodynamic parameters obtained. Semi-preparative separation conditions have been proposed for 2-amino-2'-hydroxy-1,1'-binaphthyl-3-carboxylic acid, *N*-(3'-methoxy-1,2'-binaphthyl-8-yl)acetamide, and *N*-(3'-hydroxy-1,2'-binaphthyl-8-yl)acetamide. *Chirality* 20:900–909, 2008. © 2008 Wiley-Liss, Inc.

KEY WORDS: liquid chromatography; chiral separation; cellulose-based chiral stationary phase; atropisomers; substituted binaphthyls

INTRODUCTION

Over the last two decades, high-performance liquid chromatography (HPLC) has become one of the most common techniques in chiral separations. HPLC has also been successfully employed for determination of the optical purity of newly synthesized organic compounds.

Two approaches can, in general, be used for the preparation of optically pure or enriched organic compounds. The first approach is based on a synthesis of the racemate. A disadvantage of this approach lies in the necessity of subsequent isolation of individual enantiomers. The racemate can either be transformed into pairs of diastereoisomers which can be resolved by achiral liquid chromatography, or separated directly in a chiral environment. The other approach, asymmetric synthesis, is a direct synthesis of enantiomers, using suitable optically pure ligands acting as catalysts. The chiral ligands in asymmetric reactions must have stable configurations (they must be resistant toward racemization) and a high optical purity is required.

Binaphthyl derivatives have been extensively used to control many asymmetric processes and have demon-

strated outstanding chiral discrimination properties, due to their unique properties derived from their rigidity, chirality and spatial arrangement. Most of 1,1'-binaphthyl molecules are *C*₂ symmetric with two identical naphthyl units often substituted in the 2,2'-positions. Chirality of these compounds is caused by restricted rotation of atoms or groups of atoms around the single bond on the binaphthyl skeleton (axial chirality, atropisomerism). Increased hindrance to rotation at the pivotal 1,1'-bond makes these molecules potential candidates for enantioseparation.¹ The best representatives of the binaphthyl group are 2,2'-dihy-

Contract grant sponsor: Ministry of Education, Youth and Sports of the Czech Republic Long-Term Research Plan; Contract grant numbers: MSM0021620857.

Contract grant sponsors: Ministry of Education, Youth and Sports of the Czech Republic, Kontakt ME 895.

*Correspondence to: Zuzana Bosáková, Faculty of Science, Department of Analytical Chemistry, Charles University in Prague, Albertov 2030, 128 43 Prague 2, Czech Republic. E-mail: bosakova@natur.cuni.cz

Received for publication 26 September 2007; Accepted 14 March 2008

DOI: 10.1002/chir.20585

Published online 13 June 2008 in Wiley InterScience (www.interscience.wiley.com).

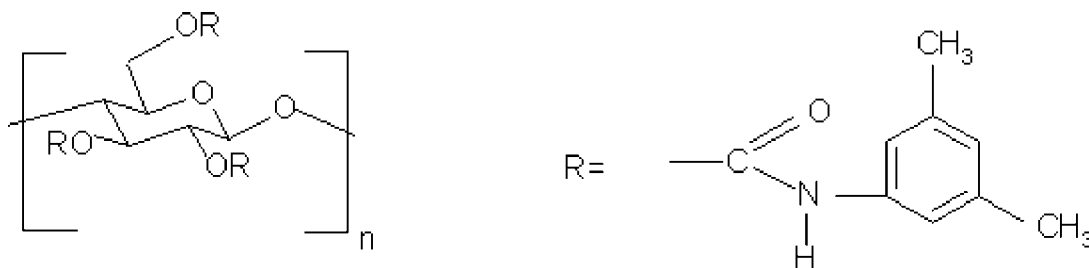


Fig. 1. The structure of cellulose tris(3,5-dimethylphenylcarbamate).

droxy-1,1'-binaphthyl (1,1'-bi-2,2'-naphthol, BINOL, OBIN),²⁻⁴ 2,2'-diamino-1,1'-binaphthyl (BINAM) and 2,2'-bis(diphenylphosphino)-1,1'-binaphthyl (BINAP)^{5,6} which have been used to develop many related chiral auxiliaries. Chiral stationary phases (CSPs) based on binaphthyl derivatives have also been prepared.⁷ The recent developments in the field of new chiral binaphthyl catalysts are focused on the preparation of derivatives with non-identical groups in various positions⁸ and to a shifting the classical 1,1'-chiral axis to other positions.⁹ Efforts in the molecular architecture of these ligands are oriented toward creating a stable chiral environment for asymmetric reactions providing a high degree of enantiopurity.

Polysaccharides belong to biopolymers that are capable of resolving a great variety of enantiomers. CSPs based on derivatized cellulose are widely used for enantioseparations.¹⁰⁻¹⁶ Cellulose tris(3,5-dimethylphenylcarbamate) CSPs (see Fig. 1) exhibit a very good resolution for a variety of stereochemically interesting organic molecules and chiral drugs.¹⁴ These CSPs contain polymeric chains of derivatized D-(+)-glucose residues in β -1,4 linkages which create a well-defined chiral environment (chiral groove) of a high rigidity. The polar carbamate groups are oriented inward the groove and the hydrophobic aromatic groups outward it. The former allow H-bonding and the latter π - π interactions with the analytes. The chiral recognition is based on stereogenically different fit of enantiomers into the chiral cavities; the enantioselective interaction is stabilized by other bonding types (H-bonding, π - π interactions, dipole-dipole interaction, steric effect).¹⁶ Cellulose tris(3,5-dimethylphenylcarbamate) CSPs are available in two basically different designs - coated and recently also immobilized ones. An advantage of the immobilized version¹⁷⁻¹⁹ lies in its compatibility with various mobile phases (MPs), compared with the limited versatility of coated CSPs.

The type of CSP and the mobile phase composition strongly affect the retention and enantioseparation behavior of chiral compounds. Another important factor influencing the retention and chiral separation is the temperature. The synthesized asymmetric catalysts should have stable configurations and thus the temperature is a very important optimizing parameter. The van't Hoff plots²⁰⁻²² ($\ln k$ versus $1/T$) permit a simple prediction whether the retention and enantioseparation mechanism is temperature dependent or not.

Most papers on the binaphthyl-based ligands found in the literature deal with their synthesis. Enantioselective

HPLC has been used in some cases to control the enantiomeric purity or the yield of the final products. However, the separation conditions, including characterization of the separation systems, have not usually been adequately described. Only a few articles pay attention to the enantioseparation. Cellulose- or amylose-based columns in the normal separation mode have mostly been used. The following systems have been used for the separation of some atropisomers contained in the set studied by us. 2,2'-Diacyl-1,1'-binaphthyl (1) has been separated on both amylose- and cellulose-based CSPs in the MPs composed of 1-5% of propane-2-ol (*v*) in *n*-hexane.²³⁻²⁵ *O'*,*S*-1,1'-Binaphthyl-2,2'-diyl bis(dimethylcarbamothioate) (4) and *O*,*O'*-1,1'-binaphthyl-2,2'-diyl bis(dimethylcarbamothioate) (5) have been enantioseparated with *n*-hexane/ethanol 90/10 (v/v) on cellulose-based and amylose-based CSPs, respectively.²⁶ 2,2'-Dihydroxy-1,1'-binaphthyl (8) has been separated into the enantiomers on an amylose-based CSP in a mobile phase of pure methanol,¹³ on a cellulose-based CSP using *n*-hexane/butanol 90/10 (v/v) as a mobile phase,²⁷ or on a cellulose tris(5-fluoro-2-methylphenylcarbamate)-based CSP with *n*-hexane/propane-2-ol 90/10 (v/v) mobile phase.¹⁶

Recently, seven symmetrically 2,2'-disubstituted 1,1'-binaphthyls (OBIN, its ether and ester derivatives and its dibromo-substituted analog) have been studied on cellulose tris(3,5-dimethylphenylcarbamate) CSP in normal separation mode.²⁸ OBIN, 2,2'-diamino-1,1'-binaphthalene and 1,1'-bi-2-naphthol bis(trifluoromethane sulfonate) have been separated on newly developed synthetic polymeric chiral stationary phases - P-CAP, P-CAP-DP, DEABV, and DPEVB.²⁹ However, to the best of our knowledge, no suitable method for direct chiral separation of a set of structurally different binaphthyl enantiomers has so far been published.

In view of these facts and the need of organic chemists for chiral separations of the racemates of binaphthyl derivatives, this work is aimed to study the retention and enantioseparation of binaphthyl derivatives on two coated cellulose tris(3,5-dimethylphenylcarbamate) CSPs, one designed for the normal separation mode and the other one for the reversed-phase mode, under various experimental conditions, including the mobile phase composition, the buffer pH, and the temperature. A simple analytical method is proposed for chromatographic screening, with a possibility for easy switching to a semipreparative mode.

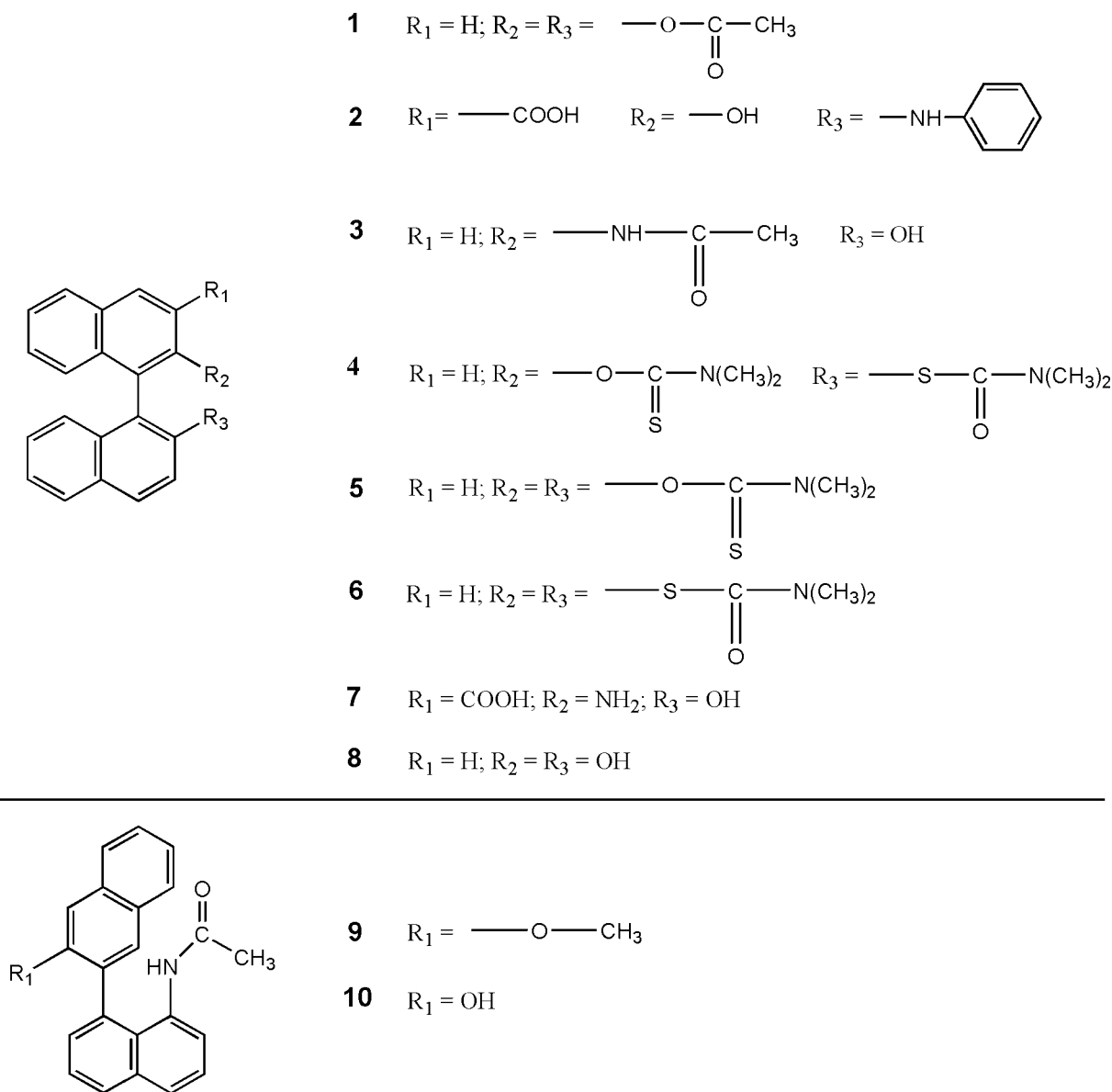


Fig. 2. Structures of the studied binaphthyl derivatives; samples **1–8** belong to the group of 2,2'-disubstituted or 2, 3, 2'-trisubstituted 1,1'-binaphthyls. Samples **9** and **10** belong to the group of 8,3'-disubstituted 1,2'-binaphthyls.

EXPERIMENTAL

Chemicals

n-Hexane, propane-2-ol and acetonitrile (ACN) were purchased from Sigma-Aldrich (St. Louis, MO), all of HPLC grade; $\text{NaH}_2\text{PO}_4 \cdot 2\text{H}_2\text{O}$ from Penta (Chrudim, Czech Republic), acetic acid (HAc) and sodium hydroxide from Lachner (Neratovice, Czech Republic); all of p.a. purity. Deionized water was used (Milli-Q water purification system Millipore, Milford, MA).

All the studied analytes (see Fig. 2) have been synthesized as racemates at the Department of Organic Chemistry, Faculty of Science, Charles University in Prague. The synthesis of analyte **1** has been described in Refs. 30 and 31. The synthesis of methylesters of analytes **2** and **7** has

been published in Ref. 8 and their transformation into analytes **2** and **7** in Ref. 32. The synthesis of analytes **3**, **4**, **5**, **6**, and **8** has been described in Ref. 26 (in the case of analyte **3**, racemic 2-amino-2'-hydroxy-1,1'-binaphthyl has been used as the precursor³³). The synthesis of analytes **9** and **10** has been described in Ref. 9.

Instrumentation

The HPLC equipment (Dionex Softron, Germering, Germany) involved a P 580A LPG pump, an UV-vis detector type UVD 170S and a Rheodyne injection valve Model 7725i (Cotati, CA) with a 20- μL sample loop (if not indicated otherwise). The samples were injected with Hamilton syringes (Reno, Nevada). The data were handled using

TABLE 1. Effect of the propane-2-ol content on the chromatographic data of the selected analytes

Sample	<i>n</i> -hexane/propane-2-ol (v/v)											
	95/5			90/10			80/20			70/30		
	<i>k</i> ₁	<i>R</i>	α	<i>k</i> ₁	<i>R</i>	α	<i>k</i> ₁	<i>R</i>	α	<i>k</i> ₁	<i>R</i>	α
1	0.58	1.23	1.28	0.55	0.91	1.20	0.53	0.81	1.15	0.50	0.74	1.13
4	1.24	1.90	1.35	1.05	1.87	1.33	1.00	1.64	1.30	0.92	1.38	1.24
9	13.43	4.92	1.59	6.46	4.62	1.46	4.24	4.60	1.43	3.88	4.55	1.40
10	7.48	4.98	1.77	3.95	4.80	1.69	2.20	4.73	1.65	1.58	4.70	1.64

Experimental conditions: stationary phase, CHIRALCEL OD-H; mobile phase, *n*-hexane/propane-2-ol at various volume ratios, flow rate 0.7 ml/min, UV detection, 254 nm; *k*₁, retention factor of the first eluted enantiomer; α, selectivity; *R*, enantioresolution.

the PC Chromeleon software (Dionex Corporation, Sunnyvale, CA).

The temperature was controlled using a Mistral column thermostat Model Spark (Mistral, Emmen, The Netherlands). An ultrasonic bath Ultrasonic LC30H (Elma, Prague, Czech Republic) was used for degassing the MPs. The buffer pH was adjusted with a pH-meter Model 3510 (Jenway, Felsted, England).

The two cellulose-based chiral stationary phases, Chiralcel OD-H (150 mm × 4.6 mm I.D., cellulose tris(3,5-dimethylphenylcarbamate) coated on silica gel, particle size 5 μm) designated for normal separation mode and Chiralcel OD-RH (150 mm × 4.6 mm I.D., cellulose tris(3,5-dimethylphenylcarbamate) coated on silica gel, particle size 5 μm) designated for reversed-phase separation mode, were purchased from Daicel (Chiral Technologies Europe, Illkirch, France).

Separation Conditions

Normal separation mode. The MPs consisted of *n*-hexane (HEX) and propane-2-ol (IPA) at various volume ratios.

Reversed-phase separation mode. The MPs contained ACN as the organic modifier and water or a 20 mM phosphate buffer, pH 3.0 or 6.0. The pH of the buffer solution was adjusted with phosphoric acid to the required value prior to adding the organic modifier.

Racemates of individual 2,2'-disubstituted or 3,2,2'-trisubstituted 1,1'-binaphthyls and 8,3'-disubstituted 1,2'-binaphthyls were dissolved in ACN; the concentrations of the solutions injected were 0.5 mg/ml (if not indicated otherwise). The samples were stored at 5°C. The mobile phase flow rate was 0.7 ml/min.

The UV detection was performed at a wavelength of 254 nm. The measurements were carried out at 22°C and the temperature effect was studied within the range, 5–40°C.

RESULTS AND DISCUSSION

CSPs based on cellulose tris(3,5-dimethylphenylcarbamate) exhibit a particularly high chiral recognition for a variety of racemic compounds. Applicability of coated versions of these CSPs to MPs of various polarities is limited.¹⁴ Therefore, two cellulose tris(3,5-dimethylphenylcarbamate) bonded CSPs have been examined—one designed for

normal mode and the other for reversed-phase separations of the synthesized atropisomers of differently substituted binaphthyls.

Normal Separation Mode

Based on the structure of the substituted binaphthyls,¹⁶ the normal phase separation mode (with Chiralcel OD-H column) was the first choice for the study of the retention and enantioseparation behavior of the selected 1,1'- and 1,2'-binaphthyl derivatives. The MPs were prepared by mixing *n*-hexane and propane-2-ol at various volume ratios, ranging from 5 to 80 vol % of propane-2-ol. In general, higher propane-2-ol contents resulted in a lower retention, however, analytes **2** and **7** did not elute in any mobile phase tested. Table 1 summarizes the chromatographic data of the analytes, showing at least partial enantioresolution within reasonable retention times. The baseline enantioseparation of analyte **4** was achieved in a very short separation time in the mobile phase with 20 vol % propane-2-ol (see Fig. 3A). In comparison with the retention of the 1,1'-binaphthyl derivatives listed in Table 1, it is obvious that both the disubstituted 1,2'-binaphthyls exhibit longer retention times (particularly sample **9**) with markedly higher values of enantioresolution (see Fig. 3B) which are just slightly affected by changes in the mobile phase composition.

The increasing retention with decreasing propane-2-ol content seems to have a stereoselective character for all the derivatives, as it is accompanied by increased enantioresolution. The results given in Table 1 support the assumption that propane-2-ol, as the polar constituent of the mobile phase, competes with the analytes for the polar interaction sites of the chiral selector (namely, carbamate groups)³⁴ which play an important role in chiral discrimination.

Reversed-Phase Separation Mode

Considering the properties of the analytes studied, their solubility and unknown *pK*_a values, the reversed-phase separation system has been developed, composed of a Chiralcel OD-RH column and ACN with water or a 20 mM phosphate buffer, pH 3.0 or 6.0, as the mobile phase constituents. The influence of the ACN content in the ACN/water MPs on the retention factors, enantioresolution and the selectivity can be seen in Table 2. As expected, lower ACN contents result in a higher retention of all the analy-

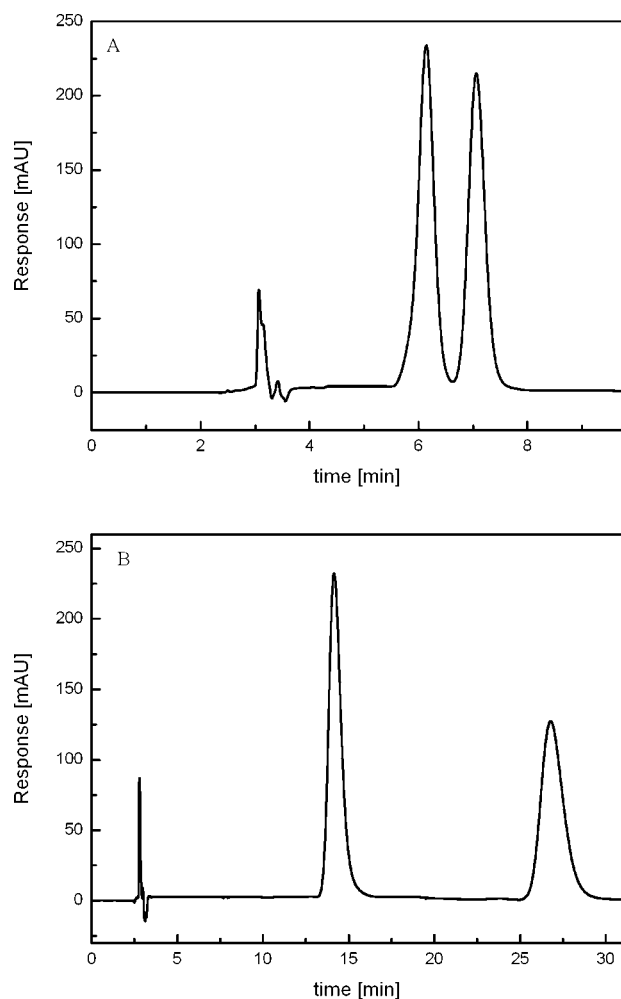


Fig. 3. Enantioseparation of analyte **4** (A) and analyte **9** (B) *n*-hexane/propane-2-ol, 80/20 (v/v), Chiralcel OD-H (150 mm × 4.6 mm I.D.), UV detection, 254 nm, mobile phase flow rate, 0.7 ml/min.

tes. At the two lowest ACN contents (30 and 40% of ACN), analytes **1**, **4**, **5**, **6**, **8**, and **9** exhibit very long retention times. In general, increased retention times result in an improved enantioresolution of most of the analytes. No partial enantioresolution has been observed for samples **2**, **5**, **6**, and **8**, all of them from the family of 2,2'-disubstituted or 3,2,2'-trisubstituted 1,1'-binaphthyls. On the contrary, both the representatives of 8,3'-disubstituted 1,2'-binaphthyls (analytes **9** and **10**) provide high values of enantioresolution, even in MPs with high ACN contents. Compound **7** (possessing —COOH, —NH₂ and —OH groups) has shown rather high sensitivity to the ACN/water ratio. No other analyte studied offers such possibilities for hydrogen bonding; both hydrogen donor and acceptor groups are available in analyte **7**.

The results obtained in the buffered medium, 20 mM phosphate buffer, pH 3.0 or 6.0, with varying ACN content, are summarized in Table 3. The ACN/buffer ratios have been selected considering the results obtained in the ACN/water MPs (Table 2). The influence of the ACN con-

TABLE 2. Effect of the acetonitrile content on the chromatographic data of all the studied binaphthyl derivatives

Sample	ACN/water (v/v)																	
	80/20			70/30			60/40			50/50			40/60			30/70		
	k_1	R	α	k_1	R	α	k_1	R	α	k_1	R	α	k_1	R	α	k_1	R	α
1	1.00	0.00	1.00	1.84	0.00	1.00	2.61	0.65	1.05	7.22	1.09	1.04	26.28	1.10	1.04	\times	\times	\times
2	0.13	0.00	1.00	0.15	0.00	1.00	0.27	0.00	1.00	0.41	0.00	1.00	2.43	0.00	1.00	9.63	0.00	1.00
3	0.37	0.40	1.14	0.41	1.00	1.15	0.75	1.22	1.16	1.69	1.75	1.15	4.63	2.54	1.15	20.58	3.24	1.17
4	1.58	0.66	1.06	2.02	0.77	1.06	4.51	1.03	1.06	13.40	1.24	1.06	\times	\times	\times	\times	\times	\times
5	1.68	0.00	1.00	2.30	0.00	1.00	5.62	0.00	1.00	19.53	0.00	1.00	\times	\times	\times	\times	\times	\times
6	1.36	0.00	1.00	1.66	0.00	1.00	3.35	0.00	1.00	9.18	0.00	1.00	\times	\times	\times	\times	\times	\times
7	0.00	0.00	1.00	0.14	0.64	1.93	0.31	1.38	2.58	1.44	1.68	1.53	2.86	1.85	1.55	10.45	1.43	1.62
8	0.54	0.00	1.00	0.68	0.00	1.00	1.30	0.00	1.00	3.62	0.00	1.00	10.26	0.00	1.00	\times	\times	\times
9	1.77	3.56	1.31	1.43	3.83	1.36	2.59	4.52	1.35	5.90	5.49	1.36	16.40	6.28	1.36	22.40	6.35	1.35
10	0.95	2.81	1.34	0.77	3.01	1.40	1.32	3.93	1.41	2.96	4.97	1.40	7.10	5.84	1.40	12.10	5.94	1.40

×, retention time of analyte was longer than 120 min. Experimental conditions: stationary phase—CHIRALCEL OD-RH; mobile phase—acetonitrile/water at various volume ratios, flow rate 0.7 ml/min, UV detection, 254 nm; for the parameter symbols see Table 1.

TABLE 3. Effect of the acetonitrile content and buffer pH on the chromatographic data of all the studied binaphthyl derivatives

Sample	ACN/20 mM phosphate buffer, pH 6.0						ACN/20 mM phosphate buffer, pH 3.0					
	60/40			50/50			40/60			50/50		
	k_1	R	α	k_1	R	α	k_1	R	α	k_1	R	α
1	3.41	0.66	1.04	7.07	0.73	1.05	28.06	0.78	1.05	2.74	0.63	1.05
2	0.23	0.00	1.00	0.40	0.00	1.00	1.55	0.00	1.00	1.12	0.00	1.00
3	0.67	1.35	1.18	1.68	1.69	1.15	4.76	2.12	1.15	0.79	1.25	1.16
4	5.88	1.05	1.06	13.23	1.12	1.07	×	×	×	4.77	0.95	1.06
5	7.51	0.00	1.00	18.50	0.00	1.00	×	×	×	5.14	0.00	1.00
6	4.36	0.00	1.00	8.54	0.00	1.00	×	×	×	3.13	0.00	1.00
7	0.16	0.86	1.44	0.25	1.34	1.48	0.61	2.42	1.46	1.02	4.37	1.55
8	1.75	0.00	1.00	3.46	0.00	1.00	8.83	0.00	1.00	1.43	0.00	1.00
9	3.20	4.54	1.37	5.80	4.94	1.37	16.67	5.27	1.37	2.74	4.41	1.37
10	1.66	3.97	1.52	2.81	4.40	1.40	7.17	5.18	1.42	1.35	3.68	1.41

×, retention time of analyte was longer than 120 min. Experimental conditions: stationary phase—CHIRALCEL OD-RH, mobile phase—acetonitrile/20 mM phosphate buffer, pH 6.0 or 3.0, at three volume ratios, flow rate 0.7 ml/min, UV detection, 254 nm; for the parameter symbols see Table 1.

tent in the buffered MPs on the retention is similar to that observed in the unbuffered separation systems, i.e., a decrease in the ACN content leads to a higher retention, with better values of enantioresolution for most of the analytes. The effect of the phosphate buffer pH is illustrated in Figure 4. The retention is increased and the resolution substantially improved at lower pH values.

Comparing the results obtained in the unbuffered and buffered MPs with the same ACN contents (Table 2 vs. Table 3), differences in the retention and enantioseparation can mostly be found in the MPs with the lowest ACN content (40 vol %) and at the lower buffer pH value (3.0). These differences are most pronounced for samples **1** (2,2'-diacetyl-1,1'-binaphthyl), **2** (2-hydroxy-2'-(phenylamino)-1,1'-binaphthyl-3-carboxylic acid) and **7** (2-amino-2'-hydroxy-1,1'-binaphthyl-3-carboxylic acid). The enantioresolution of these three compounds has been improved in the buffered mobile phase (pH 3.0) whereas the retention factors have been affected in different ways. The reduced retention of compound **1** in the mobile phase with the phosphate buffer, pH 3.0, is still accompanied by an increased resolution value. The samples **2** and **7** contain in their structures functional groups capable of creating hydrogen bonds. The H-bonding interactions are stereoselective and an increase in their strength results in a stronger retention and improved enantioseparation in the separation system with the cellulose tris(3,5-dimethylphenylcarbamate) chiral selector and the mobile phase buffered to pH 3.0. As the strength of the hydrogen bonding is considerably influenced by the organic modifier present in the mobile phase, the differences are more pronounced in the MPs with low ACN contents. Comparing the separation behavior of analytes **2** and **7** in identical MPs demonstrates that the bulky aromatic substituent of the amino group near the OH group in analyte **2** substantially reduces the strength of the stereoselective H-bonding. This result can be documented on higher retention versus lower resolution values of analyte **2** against analyte **7** (viz. Table 3). Similar behavior has already been observed by

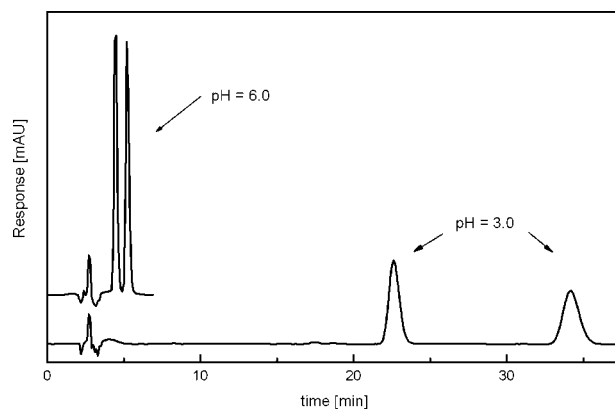


Fig. 4. A chromatogram of enantioseparation of sample **7**, ACN/20 mM phosphate buffer, pH 3.0 or 6.0, 40/60 (v/v), Chiralcel OD-RH (150 mm × 4.6 mm I.D.), UV detection, 254 nm, mobile phase flow rate, 0.7 ml/min.

other authors³⁴ for 2,2'-dihydroxy-1,1'-binaphthyl versus 10,10'-dihydroxy-9,9'-biphenanthryl.

Unfortunately, no partial enantioresolution has been observed for samples **5**, **6**, and **8**. These analytes have the most symmetrical structure of all the compounds studied, which is difficult to enantioresolve. Moreover, samples **5** and **6** (with identical bulky substituents in positions 2,2') have no suitable ionizable groups for enantioselective interactions. Analogously, analyte **4** has no suitable ionizable groups but the substitution is less symmetrical. Compound **8** also has a symmetrical substitution of the basic skeleton and the substituents in the 2,2'-positions can readily form intramolecular H-bonds and thus block the stereoselective interaction with the chiral selector and so the separation becomes much more difficult. This conclusion is supported by the fact that in methanol containing MPs, in which MeOH plays the role of an H-donor, the enantioseparation can easily be attained.¹³

The replacement of water with the buffer solution only slightly affects the retention and enantioresolution of 8,3'-disubstituted 1,2'-binaphthyls. The retention factor values and the high values of enantioresolution remain almost unchanged. The steric arrangement of this type of derivatives probably improves their fitting to the chiral cavities of cellulose tris(3,5-dimethylphenylcarbamate) and a substitution, especially in position 8, provides a supplementary (suitable) stereoselective interaction.

To summarize, the interaction mechanism of the analytes studied can be based on the steric fit of corresponding parts of these compounds into the CS groove and to polar interactions between polar substituents on the binaphthyl with the carbamate residues of the cellulose derivatives. The polar carbamate groups are believed to be the most important sites for chiral discrimination.³⁴ In addition, π - π interactions between the phenyl ring of the CS and the naphthyls of the analytes (or also CH- π interactions) contribute to the chiral separation.

Based on the results attained in the reversed-phase separation mode, the best mobile phase composition for 3 analytes from the set of 10 compounds (analytes **1**, **2**, and **7**) has been ACN/20 mM phosphate buffer, pH 3.0, 40/60 (v/v). Compounds **3**, **9**, and **10** have yielded better results in ACN/water at the same v/v ratio.

The resolution values obtained for analytes **9** and **10** in the ACN/water mobile phase enable direct use of the method developed in a semipreparative mode. As a compromise among the demands on the solubility, retention times and resolution, the mobile phase composition ACN/water 60/40 (v/v) has been selected for analytes **9** and **10**. A slightly modified mobile phase composition [ACN/0.1% acetic acid, pH 3.3 60/40 (v/v)] has been used for analyte **7**. Overload conditions have been attained by using various injection volumes (10, 50, and 100 μ l) at the same concentration of analytes **7**, **9**, and **10**, i.e., 5.0 mg/ml. A sufficient enantioresolution has been preserved up to the injection volume, 50 μ l (see Fig. 5).

Temperature Study

The role of the temperature is very important in chiral separations and thus it has been studied in detail for analytes **1**, **3**, **7**, **9**, and **10**. The solvation effect of the environment, the mobile phase in our case, affects the conformation of compounds and their interaction with chiral selectors. We have studied it on the MPs of ACN/water and ACN/20 mM phosphate buffer, pH 3.0, at a ratio of 40/60 (v/v). The ACN content in the MPs has been based on our results given above (section Reversed-Phase Separation Mode). The temperature effect has been examined within the range, 5–40°C. (Regarding the stability of the CSP, it was impossible to increase the temperature range to higher values.) van't Hoff dependences* have been plotted. The slopes ($-\Delta H^0/R$) and regression coefficients of

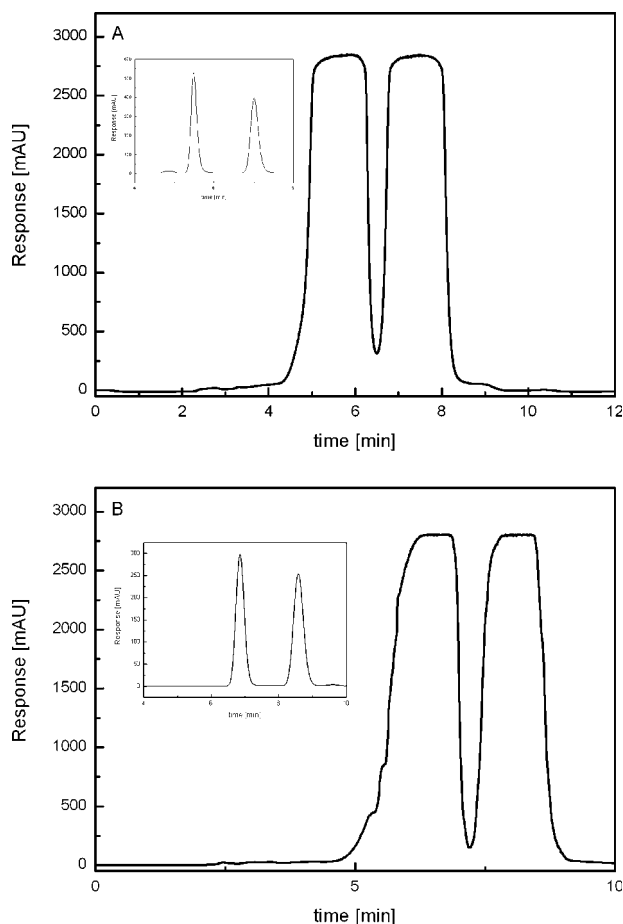


Fig. 5. Chromatograms of enantioseparation of samples **7** (A) and **10** (B) under semipreparative conditions. Separation conditions: Chiralcel OD-RH (150 mm \times 4.6 mm I.D.); mobile phase compositions: (A) ACN/1%HA, pH 3.3 60/40 (v/v) and (B) ACN/water 60/40 (v/v); UV detection, 254 nm, mobile phase flow rate, 0.7 ml/min. Injected sample amount, 250 μ g (sample concentration, 5.0 mg/ml, sample volume, 50 μ l). Insert: The enantioseparations under analytical conditions—sample concentration, 0.5 mg/ml, sample volume, 10 μ l.

tes **1**, **3**, **7**, **9**, and **10**. The solvation effect of the environment, the mobile phase in our case, affects the conformation of compounds and their interaction with chiral selectors. We have studied it on the MPs of ACN/water and ACN/20 mM phosphate buffer, pH 3.0, at a ratio of 40/60 (v/v). The ACN content in the MPs has been based on our results given above (section Reversed-Phase Separation Mode). The temperature effect has been examined within the range, 5–40°C. (Regarding the stability of the CSP, it was impossible to increase the temperature range to higher values.) van't Hoff dependences* have been plotted. The slopes ($-\Delta H^0/R$) and regression coefficients of

* $\ln k = -\left(\frac{\Delta H^0}{R}\right) \frac{1}{T} + \left(\frac{\Delta S^0}{R}\right) + \ln \Phi$, where k is the retention factor, ΔH^0 and ΔS^0 represent the differences in the standard enthalpy and entropy, respectively, when an enantiomer transfers from the mobile to the stationary phase, R is the universal gas constant, T is the temperature, and Φ the phase ratio.

TABLE 4. Results calculated from van't Hoff plots obtained for the individual atropisomers

Mobile phase		ACN/water, 40/60 (v/v)		ACN/20 mM phosphate buffer, pH 3.0, 40/60 (v/v)	
Analyte	Retention factor	$-\frac{\Delta H^0}{R}$ (10^3 K)	Regression coefficient	$-\frac{\Delta H^0}{R}$ (10^3 K)	Regression coefficient
1	k_1	1.255	0.9982	1.062	0.9991
	k_2	1.275	0.9982	1.164	0.9992
3	k_1	1.044	0.9991	0.831	0.9987
	k_2	1.091	0.9991	0.870	0.9988
7	k_1	1.415	0.9883	1.335	0.9930
	k_2	1.621	0.9899	1.596	0.9933
9	k_1	0.986	0.9917	1.053	0.9934
	k_2	0.940	0.9891	1.007	0.9925
10	k_1	1.027	0.9973	0.895	0.9964
	k_2	1.158	0.9965	1.005	0.9976

ΔH^0 , difference in the standard enthalpy; R , universal gas constant.

the linear $\ln k$ versus $1/T$ plots obtained for each pair of the atropisomers are summarized in Table 4. The retention decreases with increasing temperature. The highest sensitivity to temperature changes (the highest slope value) is exhibited by analyte **7**, offering three functional groups, $-\text{COOH}$, $-\text{NH}_2$ and $-\text{OH}$, for hydrogen bonding (as discussed in section Reversed-Phase Separation Mode). As the slopes represent the value, $-\Delta H^0/R$, in van't Hoff plots, the positive values indicate that adsorption of both the atropisomers of all the analytes is an exothermic process. Higher slopes (see Table 4) for both the enantiomers in water than in the buffered mobile phase have been observed for analytes **1**, **3**, **7**, and **10**, whereas sample **9** has higher slopes in phosphate buffer MPs. Analyte **9** also exhibits exceptional behavior regarding the comparison of the first and second eluting enantiomer. A higher slope value has been obtained for the less retained atropisomer of **9** (than for the more retained one) whereas the opposite results have been observed for all the other derivatives.

The regression coefficients obtained from the van't Hoff plots constructed for individual enantiomers approach unity. This confirms the assumption that the retention mechanism is independent of the temperature in both the MPs. The linearity of the dependences also indicates that the CS does not change (there is no change in the conformation) within the studied temperature range.

The dependence of enantioresolution on the temperature is not as straightforward as is the retention. Chiral resolution is strongly affected by the chemical structure (and spatial arrangement) of the analytes. The most pronounced effect of the temperature on enantioresolution has been observed for both the 1,2'-binaphthyl derivatives (samples **9**, **10**). The dependences of enantioresolution of racemates **9** and **10** are not monotonous. Their R -values increase with increasing temperature, attain a maximum value at $T = 30^\circ\text{C}$ and then slightly decrease. This result can be explained by a decrease in the rigidity of the stereochemical arrangement of the atropisomers at a certain temperature.

Enantioselectivity can better be described by the differences in the thermodynamic parameters.[†] The difference clearly shows the impact of stereoselective interactions on enantioresolution (compared to the non-enantioselective ones, which only contribute to the retention but have no positive effect on enantioseparation). The values of the differences in the adsorption (interaction) enthalpy and entropy for the individual atropisomers can be obtained if $\ln \alpha$ is plotted against $1/T$. The results for the unbuffered and buffered separation systems [Chiralcel OD-RH column and MPs composed of ACN/water or ACN/20 mM phosphate buffer, pH 3.0, 40/60 (v/v)] are summarized in Table 5. In general, the enthalpy term has a higher impact on the separation in the temperature range measured. The negative $\Delta(\Delta H^0)$ values indicate that the adsorption of the atropisomer with a higher affinity to the stationary phase is exothermic, and thus is favored. Higher absolute values of the differences in the enthalpy and entropy have resulted from the separation system with the buffered mobile phase. The highest absolute $\Delta(\Delta H^0)$ value has been obtained for compound **7** with the best enantioselectivity in both the MPs. The negative $\Delta(\Delta S^0)$ values indicate a decrease in the degree of freedom if the analytes interact with the CSP. The exceptional behavior of analyte **9**, which exhibits positive values for both $\Delta(\Delta H^0)$ and $\Delta(\Delta S^0)$, indicates that the interaction is thermodynamically favorable for the opposite atropisomer. The $\Delta(\Delta G^0)$ values calculated for the experimental temperature, 22°C , are always negative. This result is in accordance with the fact that all the pairs of atropisomers listed in Table 5 have been successfully separated. The best selectivity and resolution have been observed for analyte **7** in the buffered mobile phase, in which the highest absolute $\Delta(\Delta G^0)/$

[†] $\ln \alpha = \frac{-\Delta(\Delta G^0)}{RT} = \frac{-\Delta(\Delta H^0)}{RT} + \frac{\Delta(\Delta S^0)}{R}$, where α is enantioselectivity, $\Delta(\Delta H^0)$, $\Delta(\Delta S^0)$, and $\Delta(\Delta G^0)$ represent the differences in ΔH^0 , ΔS^0 , and ΔG^0 (ΔG^0 is the difference in the standard Gibbs energy when an enantiomer transfers from the mobile to the stationary phase) for a given pair of enantiomers, respectively, R is the universal gas constant and T is the temperature.

TABLE 5. Thermodynamic parameters of enantioseparation of selected analytes

MP Analytes	ACN/water, 40/60 (v/v)			ACN/20 mM phosphate buffer, pH 3.0, 40/60 (v/v)		
	$\Delta(\Delta H^0)$ (kJ mol ⁻¹)	$\Delta(\Delta S^0)$ (J K ⁻¹ mol ⁻¹)	$\Delta(\Delta G^0)^a$ (kJ mol ⁻¹)	$\Delta(\Delta H^0)$ (kJ mol ⁻¹)	$\Delta(\Delta S^0)$ (J K ⁻¹ mol ⁻¹)	$\Delta(\Delta G^0)^a$ (kJ mol ⁻¹)
1	-0.19	-0.30	-0.10	-0.94	-2.23	-0.28
3	-0.32	0.15	-0.36	-0.32	0.17	-0.37
7	-1.61	-1.81	-1.08	-2.15	-3.30	-1.18
9	0.27	3.68	-0.81	0.39	4.11	-0.82
10	-1.08	-0.88	-0.82	-1.10	-0.90	-0.83

MP—mobile phase; $\Delta(\Delta H^0)$, $\Delta(\Delta S^0)$, $\Delta(\Delta G^0)$ —differences in ΔH^0 , ΔS^0 , and ΔG^0 between the pairs of atropisomers.

^a $T = 22^\circ\text{C}$ (295.15 K).

value has been obtained. The thermodynamic results are in a good agreement with the chromatographic data given in Tables 2 and 3.

CONCLUSIONS

Cellulose tris(3,5-dimethylphenylcarbamate)-based chiral stationary phases have been found suitable for enantioseparation of most (7 from 10) of the studied binaphthyl derivatives. A slightly elevated temperature, 30°C , improves the enantioresolution. The separation system has also been proposed for semipreparative application (for analytes **7**, **9**, and **10**), which can be used for the preparation of these catalysts for asymmetric syntheses. The representatives of 8,3'-disubstituted 1,2'-binaphthyls (analytes **9** and **10**) have been separated with the highest values of enantioresolution in all the MPs tested. This result can be attributed to the proper fit of these derivatives into the helical structure of cellulose. In addition, π - π interactions of the aromatic parts of the analytes with the tris(3,5-dimethylphenylcarbamate) substituent on cellulose and hydrogen bonding or dipole-dipole interactions contribute to the enantiodiscrimination process. In the group of the 1,1'-binaphthyl derivatives, the best enantioseparation has been attained for analyte **7**, which offers functional groups required for H-bonding.

The comparison of the two separation modes studied (normal- and reversed-phase) shows that only analyte **4** from the family of 1,1'-binaphthyl derivatives and the two 8,3'-disubstituted 1,2'-binaphthyls can be baseline resolved in the normal phase separation mode, whereas the reversed-phase mode provides a more universal application.

The temperature studies confirm the independence of the retention mechanism on the temperature, whereas the enantioresolution is temperature dependent. The differences in the thermodynamic parameters obtained in the optimized separation systems confirm that the interaction of atropisomers with the chiral stationary phase is a favored process. The resultant thermodynamic data are in good agreement with the chromatographic results.

LITERATURE CITED

- Pu L. 1,1'-Binaphthyl dimers, oligomers, and polymers: molecular recognition, asymmetric catalysis, and new materials. *Chem Rev* 1998;98:2405-2494.
- Noyori R, Tomino I, Tanimoto Y, Nishizawa M. Rational designing of efficient chiral reducing agents. Highly enantioselective reduction of aromatic ketones by binaphthol-modified lithium aluminium hydride reagents. *J Am Chem Soc* 1984;106:6709-6717.
- Simonsen KB, Svenstrup N, Roberson M, Jørgensen KA. Development of an unusually highly enantioselective hetero-diels-alder reaction of benzaldehyde with activated dienes catalyzed by hypercoordinating chiral aluminum complexes. *Chem Eur J* 2000;6:123-128.
- Dabbagh HA, Najafi-Chermahini A, Banibairami S. A new family of bis-tetrazole (BIZOL) BINOL-type ligands. *Tetrahedron Lett* 2006;47:3929-3932.
- McCarthy M, Guiry PJ. Axially chiral bidentate ligands in asymmetric catalysis. *Tetrahedron* 2001;57:3809-3844.
- Yamano T, Yamashita M, Adachi M, Tanaka M, Matsumoto K, Kawada M, Uchikawa O, Fukatsu K, Ohkawa S. Approach to the stereoselective synthesis of melatonin receptor agonist Ramelteon via asymmetric hydrogenation. *Tetrahedron: Asymmetry* 2006;17:184-190.
- Shuichi O, Shijo M, Tanaka H, Miyano S. Chiral stationary phases consisting of axially dissymmetric 2'-substituted-1,1'-binaphthyl-2-carboxylic acids bonded to silica gel for high-performance liquid chromatographic separation of enantiomers. *J Chromatogr* 1993;645:17-28.
- Kočovský P, Vyskočil Š, Smrčina M. Non-symmetrically substituted 1,1'-binaphthyls in enantioselective catalysis. *Chem Rev* 2003;103:3213-3245.
- Vyskočil Š, Meca L, Tišlerová I, Cisarová I, Poláček M, Harutyunyan SR, Belokon YN, Stead RMJ, Farrugia L, Lockhart SC, Mitchell WL, Kočovský P. 2,8'-Disubstituted-1,1'-binaphthyls: a new pattern in chiral ligands. *Chem Eur J* 2002;8:4633-4648.
- Okamoto Y, Kawashima M, Hatada K. Useful chiral packing materials for high-performance liquid chromatographic resolution of enantiomers: phenylcarbamates of polysaccharides coated on silica gel. *J Am Chem Soc* 1984;106:5357-5359.
- Okamoto Y, Kaida Y. Resolution by high-performance liquid chromatography using polysaccharide carbamates and benzoates as chiral stationary phases. *J Chromatogr A* 1994;666:403-419.
- Yashima E. Polysaccharide-based chiral stationary phases for high-performance liquid chromatographic enantioseparation. *J Chromatogr A* 2001;906:105-125.
- Tachibana K, Ohnishi A. Reversed-phase liquid chromatographic separation of enantiomers on polysaccharide type chiral stationary phases. *J Chromatogr A* 2001;906:127-154.
- Aboul-Enein HY, Ali I. Applications of polysaccharide-based chiral stationary phases for resolution of different compound classes. In: Gübitz G, Schmid MG, editors. *Methods in molecular biology*, Vol. 243. Chiral separations: methods and protocols. Totowa: Humana; 2004. Chapter 6, pp 186-187.
- Chankvetadze B, Ikai T, Yamamoto C, Okamoto Y. High-performance liquid chromatographic enantioseparations on monolithic silica columns containing a covalently attached 3,5-dimethylphenylcarbamate derivative of cellulose. *J Chromatogr A* 2004;1042:55-60.

16. Okamoto Y, Yashima E. Polysaccharide derivatives for chromatographic separation of enantiomers. *Angew Chem Int Ed* 1998;37:1020–1043.
17. Ghanem A. Exploring solvent versatility in immobilized cellulose-based chiral stationary phase for the enantioselective liquid chromatographic resolution of racemates. *J Sep Sci* 2007;30:1019–1028.
18. Zhang T, Nguyen D, Franco P, Murakami T, Ohnishi A, Kurosawa H. Cellulose 3,5-dimethylphenylcarbamate immobilized on silica—A new chiral stationary phase for the analysis of enantiomers. *Anal Chim Acta* 2006;557:221–228.
19. Ali I, Aboul-Enein Y. Impact of immobilized polysaccharide stationary phases on enantiomeric separations. *J Sep Sci* 2006;29:762–769.
20. Cabrera K, Jung M, Fluck M, Schurig V. Determination of enantiomerization barriers by computer simulation of experimental elution profiles obtained by high-performance liquid chromatography on a chiral stationary phase. *J Chromatogr A* 1996;731:315–321.
21. Schurig V. Peak coalescence phenomena in enantioselective chromatography. *Chirality* 1998;10:140–146.
22. Tesarová E, Bosáková Z. The factors affecting the enantiomeric resolution and racemisation of oxazepam, lorazepam and promethazine on macrocyclic antibiotics-bonded chiral stationary phases. *Chem Anal (Warsaw)* 2003;48:439–451.
23. Huang J, Chen H, Zhang P, Li T. Preparation and evaluation of proline-based chiral columns. *Anal Chem* 2005;77:3301–3308.
24. Huang J, Chen H, Zhang P, Li T. Improvement of proline enantioselective stationary phases by replacing the 9-fluorenylmethoxycarbonyl group. *J Chromatogr A* 2006;1109:307–311.
25. Huang J, Chen H, Zhang P, Li T. Improvement of proline enantioselective stationary phases by varying peptide length and linker. *J Chromatogr A* 2006;1113:109–115.
26. Smrčina M, Vyskočil Š, Polívková J, Poláková J, Sejbal J, Hanuš V, Polášek M, Verier H, Kočovský P. Axially chiral 1,1'-binaphthyls with non-identical groups in 2,2'-positions. Synthesis of the enantiomerically pure 2-hydroxy-2'-thiol and substituted 2-amino-2'-thiols. *Tetrahedron: Asymmetry* 1997;8:537–546.
27. Li CP, Yang HL, Li JH, Shan WG. Enantioseparation of 2,2'-dihydroxy-1,1'-binaphthyl and 2-amino-2'-hydroxy-1,1'-binaphthyl and 2,2'-diamine-1,1'-binaphthyl on chiral stationary phase by high performance liquid chromatography. *Chinese J Anal Chem* 2006;34:1133–1136.
28. Weng W, Zhan F, Fu J, Li T, Chen X, Huang X. Enantioseparation of binaphthol and its derivatives on cellulose tris(3,5-dimethylphenyl carbamate). *Chromatographia* 2008;67:119–123.
29. Han X, Berthod A, Wang C, Huang K, Armstrong DW. Super/Subcritical fluid chromatography separations with four synthetic polymeric chiral stationary phases. *Chromatographia* 2007;65:381–400.
30. Chandra KL, Saravanan P, Singh RK, Singh VK. Lewis acid catalyzed acylation reactions: scope and limitations. *Tetrahedron* 2002;58:1369–1374.
31. Ballini R, Bosica G, Carloni S, Ciaralli L, Maggi R, Sartori G. Zeolite HSZ-360 as a new reusable catalyst for the direct acetylation of alcohols and phenols under solventless condition. *Tetrahedron Lett* 1998;39:6049–6052.
32. Vyskočil Š. Synthesis of new non-symmetrically substituted derivatives of 1,1'-binaphthyl by oxidative cross-coupling using substituted 2-naphthol and 2-naphthylamines. Diploma Thesis, Faculty of Science, Charles University, Prague; 1994.
33. Smrčina M, Lorenc M, Hanuš V, Kočovský P. A facile synthesis of 2-amino-2'-hydroxy-1,1'-binaphthyl and 2,2'-diamino-1,1'-binaphthyl by oxidative coupling using copper (II) chloride. *Synlett* 1991;4:231–232.
34. Yashima E, Yamamoto Ch, Okamoto Y. NMR studies of chiral discrimination relevant to the liquid chromatographic enantioseparation by a cellulose phenylcarbamate derivative. *J Am Chem Soc* 1996;118:4036–4048.

Chiral Recognition via Helical Sense and Phase in a Crystalline Supramolecular Array of Intermeshed Triple-Helices

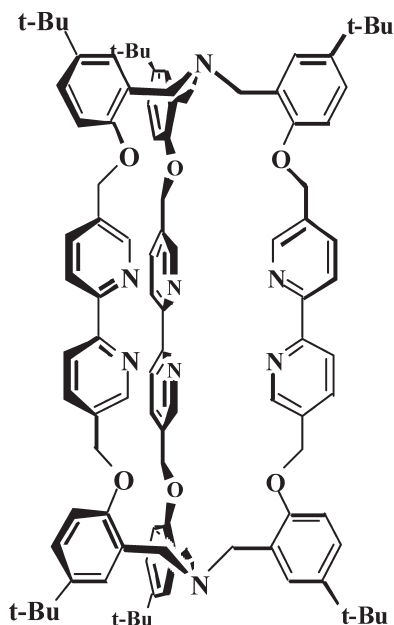
ROBERT GLASER*

Department of Chemistry, Ben-Gurion University of the Negev, Beer-Sheva 84105, Israel

ABSTRACT Hexatertiary butyl-substituted D_3 -symmetrical cage ligands composed of octahedral bidentate complexes of Ni(II) or Cu(II) ligated on either side to triskelion arrangements of three salicyl rings bound to a central nitrogen hub atom exhibit triple-helical conformations. Maximization of intermolecular aromatic–aromatic interactions between these complexes promote extended tongue and groove interleaving and affords a supramolecular array of diastereomeric intermeshed C_3 -symmetrical triple-helices perpetuating sideways throughout alternating enantiomeric layer stacks in the entire $P3$ space group crystal lattice. Chiral recognition within these supramolecular ensembles is based upon the principles of helical sense and phase. A discussion of the symmetry, mechanical and chemical factors, and constraints influencing the formation of these self-assembled crystalline supramolecular ensembles will be presented. *Chirality* 20:910–918, 2008. © 2008 Wiley-Liss, Inc.

KEY WORDS: helical stereochemistry; supramolecular ensembles; intermeshing helices; interleaving helices; chiral recognition

INTRODUCTION



Triple-helical complexes of cage ligand **1** with four different divalent metal ions [Ni(II), Cu(II), Fe(II), and Mn(II)] have recently been reported by Lindoy and coworkers.^{1,2} The cage ligand is composed of three *o,o'*-bipyridinyl moieties whose *para*-positioned methylene

carbons are directly ligated to salicyl group oxygen atoms. Each of the three strands is bound together via ligation of the salicyl methylene carbons to a common nitrogen cap affording a tripod-type moiety.^{1,2} Metal binding to the three bipyridinyl units in **1** resulted in three-bladed propeller chiral geometries of the type that are well-known for tris-chelate complexes of metals.^{1,2} The single-crystal X-ray crystallographically determined structures of the four hexatertiary butyl-substituted derivatives have also been briefly discussed and coordinates are to be found in the Cambridge Structural Database (CSD).³ The CSD refcodes for these complexes are IRA-CIN [Ni(II)], ECAKEZ [Cu(II)], ECAKAV [Fe(II)], and ECAKID [Mn(II)]. Linkage of the chiral propeller to the salicyl tripod entity causes the entire molecule to be twisted into a triple-helical-like geometry.

The nitrogen lone pairs on the tripod-like caps may exhibit different tropicities vis-à-vis the metal [e.g., *exo*–*exo* or *endo*–*endo* arrangements (or perhaps in principle even a mixture?)]. The authors reported that semiempirical

Dedicated to Kurt Mislow (Princeton University) on the occasion of his 84th birthday. ... כבוד חכמים ינחלו ... "the wise shall inherit honor" ... Pirke Aboth, verse VI:3.

*Correspondence to: Robert Glaser, Department of Chemistry, Ben-Gurion University of the Negev, Beer-Sheva 84105, Israel.
E-mail: rglaser@bgu.ac.il

Received for publication 25 June 2007; Accepted 7 February 2008

DOI: 10.1002/chir.20562

Published online 1 April 2008 in Wiley InterScience (www.interscience.wiley.com).

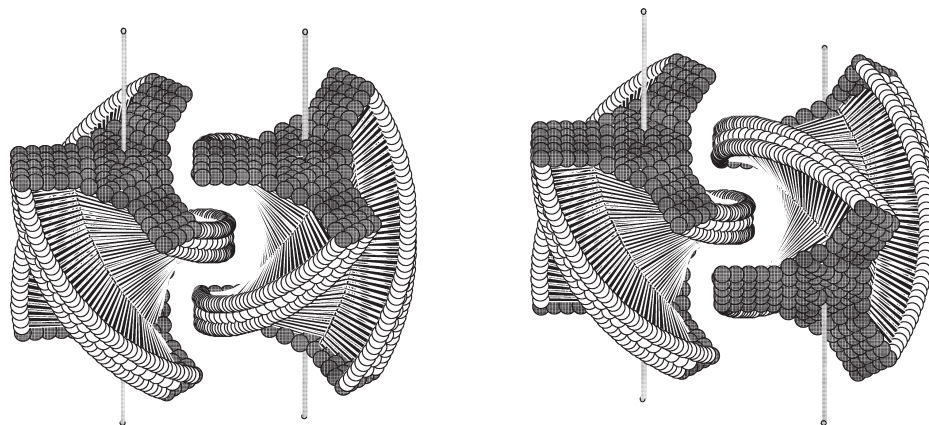
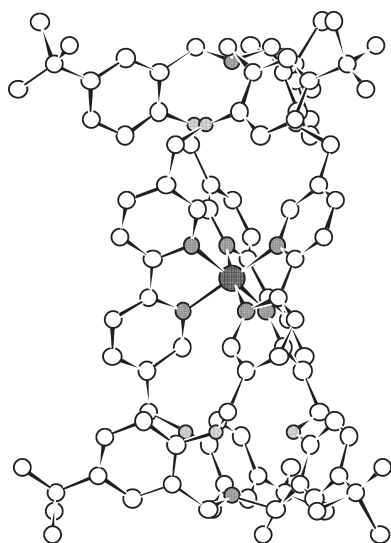
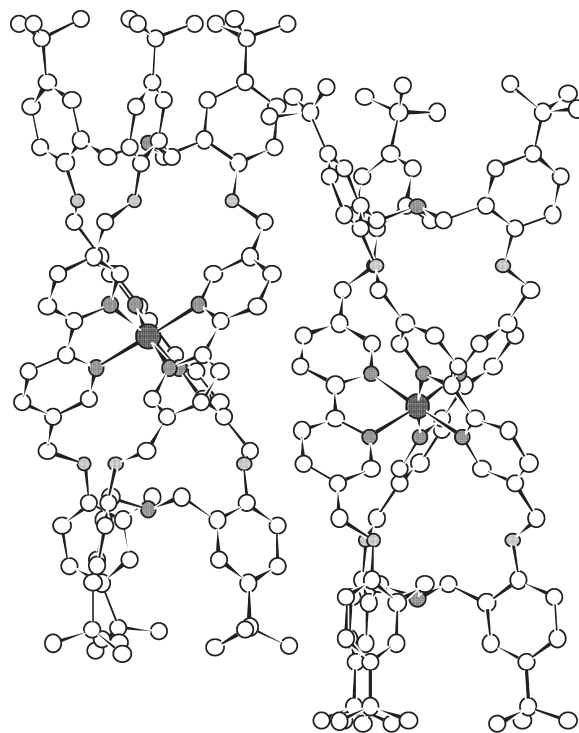


Fig. 1. Pair of structures on the left: heterochiral tongue-in-groove intermeshing between $[M]$ -5 and $[P]$ -5 gears. Pair of structures on the right: homochiral intermeshing between $[M]$ -5 and $[M]$ -5 gears.

(PM3) computational studies showed little difference in the heats of formation for the exo-exo or endo-endo nitrogen lone pair arrangements in diastereomeric complexes of **1**.¹ Crystalline complexes with Fe(II) and Mn(II) exhibited endo-endo nitrogen lone-pairs, e.g., $[P]$ -2 for Fe(II), while they were disposed in an exo-exo manner for the analogous solid-state complexes with Ni(II) and Cu(II).² The latter set of triple-helical complexes crystallized with two crystallographically independent molecules of opposite handedness, $[P]$ -3 and $[M]$ -4.^{1,2} All the cage ligand **1**/divalent metal complexes occupy a special position of threefold rotational symmetry in their respective P -3 [Ni(II), Cu(II)], and R -3c [Fe(II), Mn(II)] trigonal space group crystals.^{1,2} The Ni(II)/Cu(II) complexes intermesh in a “tongue and groove” manner reminiscent of two interlocking gear wheels.^{1,2} No intermeshing of triple helices was observed in crystalline complexes with Fe(II) and Mn(II).²



$[P]$ -2



$[P]$ -3

$[M]$ -4

One may envision two modes for the “tongue and groove” intermeshing of helices, see Figure 1. These modes exist for intermeshing single helices as well as for multiplexes.⁴ The important ability of gears and screws to intermesh are a well-known mechanical principle. Gear intermeshing also provides a basis for chiral recognition.⁴ Consider two three-bladed helical gears (worm gears). The axes of two intermeshed *heterochiral* helices (ensemble $[M]$ -(5): $[P]$ -(5)) are parallel while those of the two intermeshed *homochiral* helices (diastereomeric ensemble $[M]$ -(5): $[M]$ -(5)) are skewed, see Figure 2.⁴ It is apparent that the heterochiral schematic gear arrangement is analo-

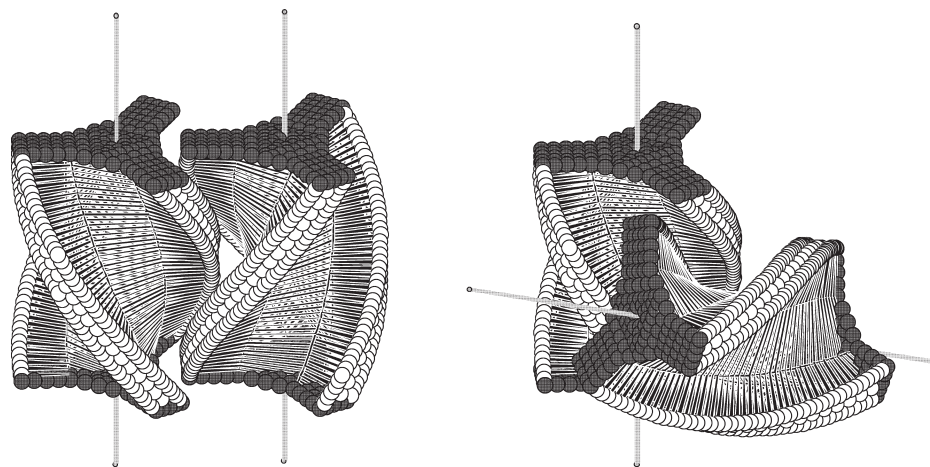


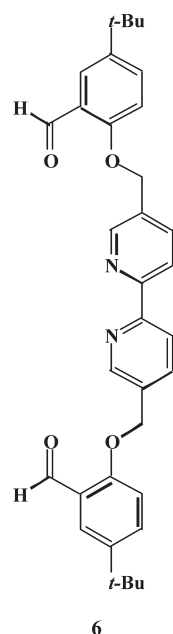
Fig. 2. Pair of structures on the left: Chiral recognition of $[M]\text{-}5\text{:}[P]\text{-}5$ intermeshed gears oriented to depict the parallel screw axes. Pair of structures on the right: diastereomeric $[M]\text{-}5\text{:}[M]\text{-}5$ gear ensemble with skewed axes.

gous to that depicted for the above-mentioned crystalline-state molecular ensemble of $[P]\text{-}3\text{:}[M]\text{-}4$ Ni(II) complexes. An in-depth discussion of the symmetry, mechanical, and chemical factors and constraints influencing the formation of these ensembles within the crystal is warranted since they actually represent examples of helical chiral recognition and supramolecular self-assembly based on the principles of helical sense and phase.

DISCUSSION

It was reported that the ^1H NMR spectrum at 298 and 318 K of the free cage ligand **1** exhibited only two methylene-proton singlet resonances in the aliphatic region: δ 3.80 ($-\text{CH}_2\text{N}-$) and δ 5.02 ($-\text{CH}_2\text{O}-$).² The singlet multiplicity was attributed to conformational interconversion.² The NMR results are clearly indicative of either inherent or time-averaged D_{3h} -symmetry in solution whereby the methylene-protons in each geminal pair are either inherently enantiotopic within an achiral entity and hence isochronous, or they are dynamically enantiotopic at the fast exchange limit for interconversion between chiral D_3 -symmetry enantiomeric conformers. Ligation of Fe(II) ions to either the dialdehyde precursor **6**, while it was ascribed to a fixed conformation for the complex with **1**.² A sufficient cause for the observation of anisochronous methylene protons in both cases is simply based on symmetry considerations, while the degree of rotational restriction is really a secondary matter. Metal octahedral complexation with the bipyridyl bidentate moieties within either open (**6**) or cage ligands (**1**) affords D_3 -symmetry three-bladed propeller chiral rigid geometries in both cases. Perpendicular to the C_3 -axis axis are three coplanar C_2 -axes transversing the metal, and not through the methylene carbon atoms. Thus, the methylene protons are now

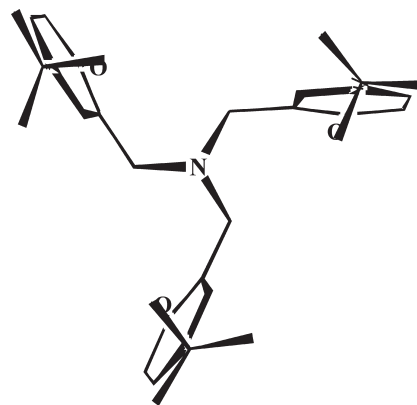
diastereotopic and hence this is sufficient cause for anisochronism. It remains to be proven whether or not there is restricted rotation about the $\text{Ar}-\text{CH}_2-\text{O}$ bonds in the case of the complex with **6**, although it is highly likely that this is true for the case of the complex with **1**. The methylene protons are diastereotopic in any event. What is important is that the C_2 -rotation axes through the metal in the propeller cause CH_2O and CH_2N methylene subunits in one half of the molecule to be homotopically isochronous with each of their corresponding counterparts within the other half of the molecule. Thus, the C_3 -axes of the Fe(II) complexes with **1** or **6** are both palindromic in solution. While ^1H NMR data were only available for the triple helical Fe(II) complex with **1**,² it is expected that the solution-state complexes of Mn(II), Ni(II), and Cu(II) with this same cage ligand will also show D_3 -symmetry in solution.



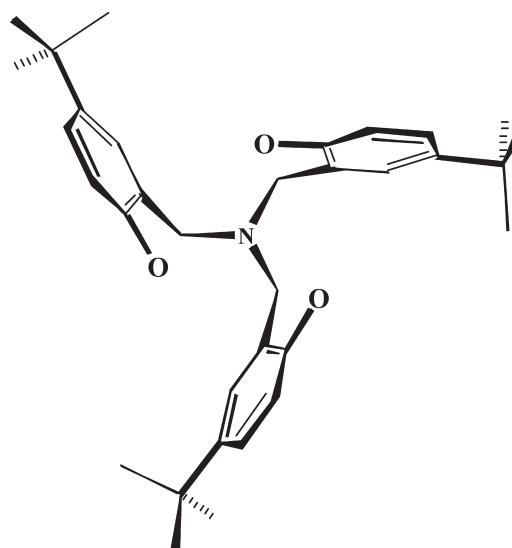
There are relatively small cell-axes differences for the Ni(II) and Cu(II) {values in braces} crystals: $a = b = 15.9763(19)$ { $15.9603(16)$ } Å, $c = 51.131(9)$ { $51.157(7)$ } Å. On the other hand, these cell-axes differences are larger for the Mn(II) and Fe(II) {values in braces} crystals: $a = b 17.478(8)$ { $17.638(19)$ } Å, $c = 91.68(6)$ { $92.448(19)$ } Å. A relatively small 0.051 Å RMS difference was found for the superimposition of all corresponding nonhydrogen atoms (with the exception of all methyl carbons and disordered *t*-Bu quaternary carbons) within the **[P]-3:[M]-4** intermeshed Ni(II) complexes upon corresponding atoms in the isostructural Cu(II) analogue. A much larger 0.303 Å RMS difference was measured for the analogous superimposition of similar atoms in the nonintermeshed twisted triple-strand conformers of the isostructural Mn(II) and Fe(II) pair. The difference in magnitudes between these RMS differences is correlated with the M–N mean bond lengths in the complexes: similar 2.142(6) {2.104(7)} Å Cu–N {Ni–N} values versus dissimilar 2.232(2) {1.797(2)} Å Mn–N {Fe–N} values.

Describing the geometry of metal complexes such as **2-4** as “triple helices” or “triplexes” is an approximation since the molecules are obviously not oligomers of repeat units, nor are they regular. Each triple helical molecule is actually composed of two different structural regions, each having local threefold rotational symmetry. With this idealization in mind, it is reasonable to refer to these complexes as three intertwined homotopic [*P*]- or [*M*]-helices in the general sense. The two regions are a three-bladed propeller with a metal atom at the hub directly linked to a triskelion arrangement composed of three salicyl rings ligated to a central nitrogen hub atom. The three salicyl rings are each skewed (rather than “paddle”-like) versus the N-lone pair axis. The triskelion [*P*]-helicity [torsion angle LP–N...C_{ipso}–C_{ortho}–9(3)° for the Ni(II)/Cu(II) complexes and –23(2)° for the Fe(II)/Mn(II) complexes] is correlated with [*P*]-metal-atom propeller helicity. Edge-differentiation of the two *ortho*-positions of the salicyl rings results in *syn* or *anti* arrangements for the O-atom relative to the N-lone pair hub-axis. Thus, the *Cortho* carbon noted in the aforementioned torsion angle is substituted with either a proton (for the *exo-exo* Ni(II)/Cu(II) complexes) or an oxygen (for the *endo-endo* Fe(II)/Mn(II) complexes). Since triskelions are disk-like, they have tropicity [*clockwise* or *counterclockwise* directionality] which is relative to the particular side from which it is viewed. In order to compare the triskelion tropicities [directionalities] they should be excised from their respective molecules and superimposed so that they are both viewed from the same side. When this is performed for complexes with the same metal-atom propeller helicity, the triskelion tropicities are identical when the *isolated* triskelion fragments are removed from either an *exo-exo* complex (see **7**) or from an *endo-endo* diastereomeric complex (see **8**). Since a triskelion salicyl oxygen always is linked to a methylene in the *p,p'*-substituted bipyridyl propeller unit of the cage ligand, it follows that the nitrogen lone-pair will have an *exo* disposition for the –9(3)° torsion angle LP–N...C_{ipso}–C_{ortho} triskelions while it will be *endo* for the –23(2)° torsion angle counterparts. It is readily apparent that the *tert*-butyl

groups are disposed differently in the two triskelion moieties. The substituents point outwards in the *endo-endo* case and are more parallel and closer to the helical axes in the *exo-exo* arrangement. On the basis of these observations, one would expect the *tert*-butyl groups to engender considerable steric hindrance for intermeshing in the case of the Fe(II)/Mn(II) complexes.



7



8

The metal-propeller chirality is induced outward into the *t*-butyl *p*-substituted salicyl-ring regions on either side. The rings themselves are constrained to remain in close proximity to the threefold axis by virtue of their ligation to the nitrogen triskelion hub. Three H₂C–O bonds connect the metal propeller region with the triskelion propeller region. For metal propeller [*P*]-helicity, *exo-exo* Ni(II)/Cu(II) complexes of **1** have (pyridinyl)C_{ipso}–H₂C–O–C_{ipso}(salicyl) antiperiplanar-type torsion angles of +155(9)° while this angle has a –122(2)° (–)-anticlinal value in the *endo-endo* Fe(II)/Mn(II) complexes of **1**.

Thus, propeller helicity induces a particular triskelion tropicity via the short $\text{H}_2\text{C}-\text{O}$ single-bond spacers between the two types of structural unit. The result is a triple helical-like unit approximating a twisted three-bladed gear whose diameter is $\approx 11\text{--}12\text{ \AA}$, and whose helical pitch is about $47\text{ \AA}/\text{turn}$ (based on the solid-state Ni(II) structures). The about 23 \AA length of the triple-helical molecules represents slightly more than one-third of a full turn.

The ligation of $\text{Ni(II)}/\text{Cu(II)}$ to **1** affords a complex with either right- and left-handed helicity in acetonitrile solution. In principle, both homochiral and heterochiral ensembles of intermeshed triple helices are possible upon crystallization of the racemic mixture. It will be shown that there are chemical, mechanical, and symmetry reasons for the following solid-state stereochemical observations: (1) the two intermeshing helices have a heterochiral relationship rather than a homochiral relationship; (2) one metal atom is displaced by about 2.4 \AA from its neighbor when they intermesh; (3) the dimensions of the two helices differ slightly from one another so that they do not represent a true pair of enantiomers; and (4) each helix is nonpalindromic in terms of its structural dimensions.

Although it was not commented upon in the original reports,^{1,2} there appears to be an attractive force (a chemical constraint) between the two triple helices which plays a dominant role in the formation of a very particular self-assembled extended supramolecular array within the entire crystal lattice. We suggest that this force is based upon intermolecular aromatic–aromatic interactions which have recently been reviewed.⁵ In particular, edge-to-face arrangements of aromatic rings are known to be very favorable.⁶ According to an analysis of side-chain interactions in proteins, Burley and Petsko considered two aromatic residues to interact if the distance between phenyl centroids was less than 7 \AA .⁷ They noted that the most favored distance was 5 \AA , and the most favored dihedral angle was 90° .⁷ A typical phenyl–phenyl interaction was reported to have an energy between -4 to -8 kJ mol^{-1} based upon nonbonded potential energy calculations.⁷ From our inspection of the IRACIN and ECAKEZ crystal structures it appears that phenyl–phenyl interactions influence the particular geometry of association between the two triple-helical molecules. There are 11 aromatic rings involved in intermolecular aromatic–aromatic interactions between the **[P]-3** and **[M]-4** triple-helical constituents of the Ni(II) or Cu(II) ensembles. The distances between the aromatic ring centroids involved in these interactions vary from 4.58 to 6.60 \AA with the mean distance being $5.6(7)\text{ \AA}$, see Figure 3. Aromatic–aromatic interactions are expected to be maximized within the entire space between two parallel heterochiral axes, as opposed to existing within only a smaller volume at the nexus between skewed homochiral axes. The observation of self-assembled heterochiral intermeshing triple-helical molecules within the crystal lattice appears to be the result of this chemical imperative. Moreover, the entire architecture of the crystal lattice appears to be governed by this principle. The strength of these attractive interactions is probably augmented by the fact that the aromatic rings play a dual role of being both the “tongue” and the “groove.”

Chirality DOI 10.1002/chir

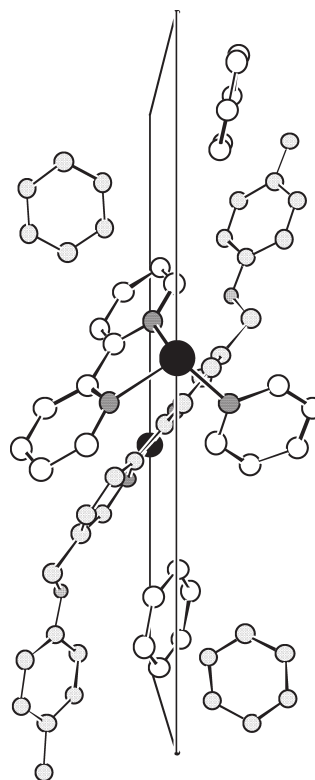


Fig. 3. Arrangement of aromatic rings involved in the “tongue-in-groove” intermeshing between the closer to viewer **[P]-3** and more distant **[M]-4** (shaded atoms) molecules vis-à-vis the plane containing the two helical axes.

It goes without question that the solid-state stereochemistry of the ensemble of two Ni(II) or of two Cu(II) complexes is intimately related to their packing within the crystal lattice. Therefore, a brief discussion of the particular space group symmetry is a logical place at which to begin. For both metals, the ensemble of two intermeshing triple-helices crystallizes in the trigonal space group $P\bar{3}$ and with the same packing motif.^{1,2} Since the crystalline ensembles of the two metals are isostructural,^{1,2} bonding parameters from now on will refer only to the Ni(II) crystal for simplicity. The $P\bar{3}$ unit cell consists of side c perpendicular to a rhombical parallelepiped base consisting of two fused equilateral triangles generating the short diagonal so that a 120° angle exists between the two equal length sides a and b , see Figure 4.⁸ As a result, the unit cell may be considered to be composed of two fused equilateral triangular subunit prisms. The symmetry operations within the cell include a C_3 rotation axis [dashed line] whose length runs through the middle of each equilateral triangular prism (i.e., parallel to the c side) and exits at the midpoints of the top and bottom ends of the subunit. The midpoint of each of the three rectangular faces of the triangular prism is a point of inversion. Finally, each c -axis itself is coincidental with a C_3 rotation axis passing through an inversion center (an inversion-triad).

The general positions of symmetry in a crystal are those chirotopic positions whose local site symmetry exhibits only the trivial symmetry operations of identity and transla-

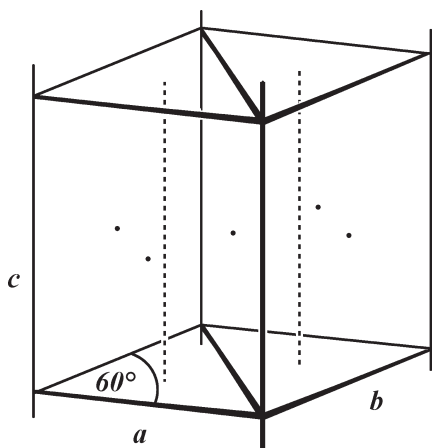


Fig. 4. The $P3$ unit cell with side c perpendicular to the a - b plane, and 120° angle γ between the a - and b -axes. The centers of inversion are depicted as points, the C_3 rotation axes are shown as dashed lines, and the C_3 rotation axes passing through inversion centers are the c -axes.

tion. All molecules (achiral or chiral) are fully desymmetrized to C_1 upon occupancy of general positions of symmetry within the crystal lattice. Six complete asymmetric general positioned molecules [three d,l -pairs] are needed to exemplify all the symmetry operations in space group $P3$. The metal complexes with the cage ligand **1** will be depicted in cartoon form as threefold gears as a heuristic device in the stereochemical discussion of helical interactions within the solid-state ensembles. The asymmetry of the slightly distorted triplexes arises from the fact that the C_3 -axis is between three triple helices rather than between the three strands of a symmetrical single triple helix. Thus, there is a diastereotopic symmetry relationship between the three component strands within each triple helix, and the two ends are nonpalindromic. The inversion center at the midpoint of the common fused face of the two equilateral triangular prism subunits generates a set of three enantiomeric distorted [P]-triple helices which are homotopic about the second C_3 -axis. Note that because of the threefold symmetry axes, one of equilateral triangular prism subunits of the unit cell contains molecules of only one handedness, while the other prism contains only molecules of the opposite handedness. There is no symmetry requirement that the axes of generally positioned helices be parallel to each other nor to the C_3 -axes. Maximization of aromatic-aromatic interactions are expected to be unattainable under these conditions.

Packing considerations may be such that the C_3 -axes in both [**P**]-**3** and [**M**]-**4** may coincide with those in the $P3$ space group and thus enable the complexes to occupy special positions of threefold rotational symmetry in the crystal. The symmetry elements of both the object and special site must be identical for the occupancy of a special position to be allowed. However, this unanimity of symmetry elements does not provide sufficient cause for the special arrangement to occur. It is quite commonly observed that symmetrical molecules occupy general positions of symmetry upon entering a crystal lattice. This is usually attributed to optimization of packing efficiency which appears to

triumph over the preservation of symmetry. As a result, the geometries of these molecules are distorted somewhat from ideality and are completely desymmetrized down to C_1 -symmetry. However, the converse of the special position symmetry argument is always true. A molecule may never occupy a site of special symmetry if it itself does not possess the exact same symmetry element as that of the site. Consider an arrangement whereby each triplex now occupies a different crystallographic threefold axis of rotational symmetry (see enantiomeric gear ensemble **9** in Fig. 5). Now, only two specially positioned Ni(II)/Cu(II) triple helical molecules [a single d,l -pair] are required to exemplify all of the symmetry operations of the $P3$ space group, and the unit-cell volume will accordingly shrink by two-thirds compared to that for the general positioned case. All strands of each triple helix are now internally homotopic so the solution-state D_3 -symmetry molecule has only been desymmetrized down to C_3 [rather than complete desymmetrization to C_1 for general position occupancy].

David Avnir's Continuous symmetry measure (CSM) of a structure is a normalized root-mean-square distance function from the closest structure which has the desired symmetry, i.e., the nearest perfectly symmetric object with the desired symmetry.⁹⁻¹¹ In our case C_2 -symmetry will be the desired ideal relationship between top and bottom halves of the Ni(II)/Cu(II) complexes. A CSM S_{C_2} = integer "0" value would be measured if a C_2 -axis passed through the metal and perpendicular to the threefold axis in the crystal. All t -butyl groups were removed from the CSM calculations since some of them were disordered. The S_{C_2} -values measured for the top and bottom halves within the excised Ni(II) propeller unit in the [**P**]-**3** and [**M**]-**4** complexes are 0.0919 and 0.1392, respectively. Similarly, CSM S_{C_2} values comparing the relationship between complete exo-exo salicyl triskelion units (minus the t -butyl groups) on either side of the metal propeller are 0.0548 and 0.0670 for the [**P**]-**3** and [**M**]-**4** complexes, respectively. Clearly, there is less solid-state distortion of C_2 -rotational symmetry between selected corresponding atoms in the two triskelion units than there is for the two Ni(II) propeller unit halves. These CSM S_{C_2} values quantitatively show that the geometries of the top and bottom halves within each complex have been slightly distorted from ideal identity, i.e., the complexes are nonpalindromic. The finding of different CSM values for each of the two C_3 -specially positioned [**P**]-**3** and [**M**]-**4** molecules in the crystal provide further quantitative evidence that the structure of one is somewhat distorted from the other [i.e., they are diastereomeric]. In the absence of internal C_2 -symmetry and external i -symmetry constraints, all the bonding parameters between corresponding entities above and below the metal are different both in an internal and in an external comparison. For example, smaller (pyridinyl)- C_{ipso} - H_2C - O - C_{ipso} (salicyl) dihedral angle values may be correlated with smaller distances between the salicyl ring centroids at either end of the two intermeshed Ni(II) complexes, e.g., 145.0° (5.92 Å, bottom of [**P**]-**3** complex); 150.3° (6.25 Å, bottom of [**M**]-**4** complex); 160.0° (6.34 Å, top of [**P**]-**3** complex), and 166.7° (6.46 Å, top of [**M**]-**4** complex).

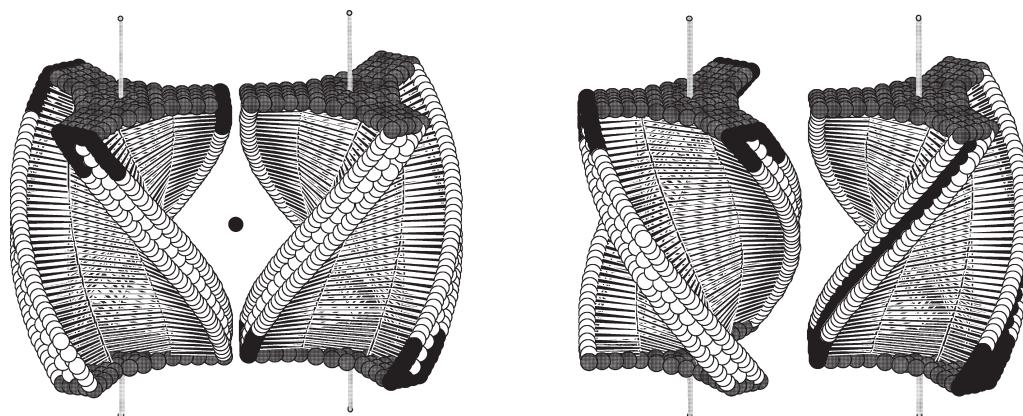
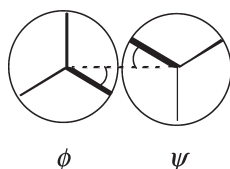


Fig. 5. Pair of structures on the left: interaxial line zero degree phase difference between inversion-center enantiomeric **[M]-9** and **[P]-9** three-bladed gears residing on three-fold rotational axes of symmetry. Pair of structures on the right: interaxial line sixty degree phase difference between diastereomeric **[M]-9** and **[P]-10** three-bladed gears residing on three-fold rotational axes of symmetry on the right.

The $P3$ inversion center ensures that both copies of oppositely handed special positioned units are enantiomers (see **[M]-9** and **[P]-9**). Again, the enantiomer of the triple helix resides in a different equilateral triangular prismatic subunit of the unit cell. Location of the heterochiral triple-helix molecules on different enantiotopic parallel C_3 -axes is a positive step towards achievement of the goal to maximize aromatic–aromatic interactions. However, parallel axes are not sufficient cause to give complete intermeshing over extended portions of the two triplexes in the crystal. In addition to parallel helical axes, the two triplexes must have a 60° phase relationship vis-à-vis the interaxial line in order to intermesh. The phase relationship between “tongue” and “groove” positions is measured in a horizontal plane perpendicular to the enantiomeric C_3 -axes, and is the summation of angles ϕ and ψ defined in drawing 11 which represent the angular displacement from the interaxial line. Inspection of assembly **[M]-9:[P]-9** in Figure 5 clearly shows that the $P3$ inversion center relates the two enantiomeric three-bladed gears with a 0° interaxial line phase difference. Intermeshing is obviously impossible since enantiotopic strands about each other. If one of the gears is rotated by 60° (see **[M]-9:[P]-10**) then the oppositely-handed strands are no longer in close juxtaposition and intermeshing may now proceed. However, the inversion center will no longer exist and the oppositely handed triplexes must hence be diastereomeric, i.e., anisometric but having the same constitution (bonding connectivity). Despite extensive intermeshing, this arrangement does not account for the $P3$ space group crystal’s inversion center.



11

General combinations of ϕ and ψ angles can produce $\phi + \psi = 60^\circ$ phase relationships in the numerous horizontal planes within the laterally intermeshed triple helices of assembly **10** because of the regular nature of the two adjacent three-bladed gear wheels in the illustration. However, the geometries of the metal complexes are far from being so regular. Figure 3 shows three sets of aromatic–aromatic interactions where a ring in one triplex points almost directly inwards towards the opposing C_3 -axis so that it is

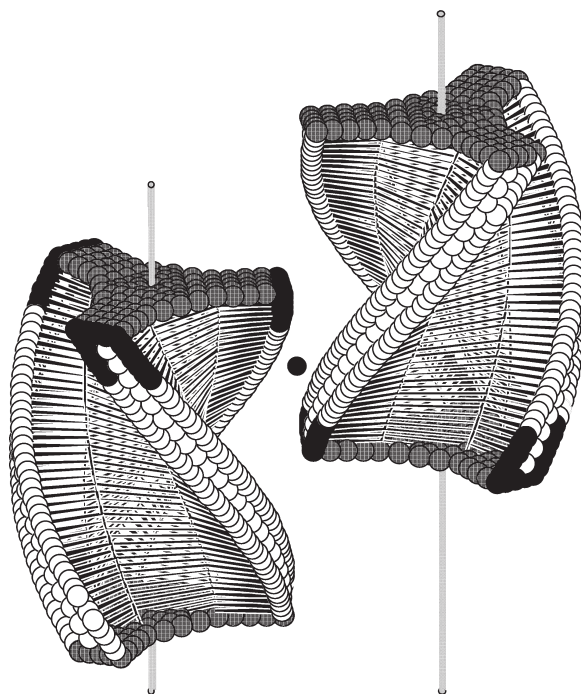


Fig. 6. Vertical shifting of one of the two triplexes in ensemble **[M]-9:[P]-10** by a distance equal to one-sixth of a turn regenerates the inversion center and aligns the gears with a 60° phase difference when measured in horizontal planes. The enantiomeric **[M]-9:[P]-9** gears in the resulting assembly may now intermesh in a region equal to one-half of their height.

located either quite close or within the plane defined by the two helical axes. In this manner it is "hugged" by two nearby aromatic rings resident in the other parallel triplex. This arrangement is actually a special case where one of the two angles is about 0° while the other one is about 60° . It suggests that 60° phase relationships produced by "general" combinations of ϕ and ψ angular relationships [i.e., not the 0° or 60° special values] would most likely engender less auspicious aromatic–aromatic interactions.

It is noted that shifting one of the abutting enantiomeric triplexes in ensemble $[M]-9:[P]-9$ by a particular vertical distance will enable both of them to now intermesh. All the cartoon-like gears depict one-third of a turn of the triplex. If one of them is shifted by a vertical height equal to that obtained in one-sixth of a turn, then both a 60° phase relationship and the inversion center are generated. However, the intermeshed region common to both gears is only one-half of their vertical height (see Fig. 6). Such a packing arrangement between the enantiomers is also unfavorable in terms of wasteful void spaces in the crystal lattice.

Attainment of extensive intermeshing, concomitant with optimum aromatic–aromatic interactions, was achieved by

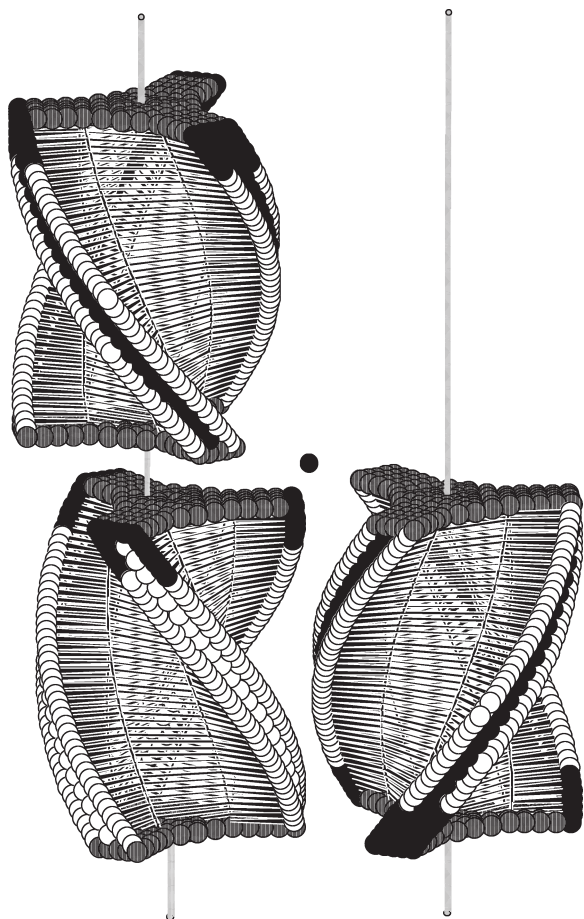


Fig. 7. Vertical pair of structures on the left: diastereomeric $[P]-10$ stacked above the homochiral $[P]-9$ triplex and twisted by 60° about the left-hand C_3 -axes. Structure on the right: $P3$ inversion center generates the $[M]-10$ triplex with a 60° phase relationship to its lateral $[P]-9$ neighbor.

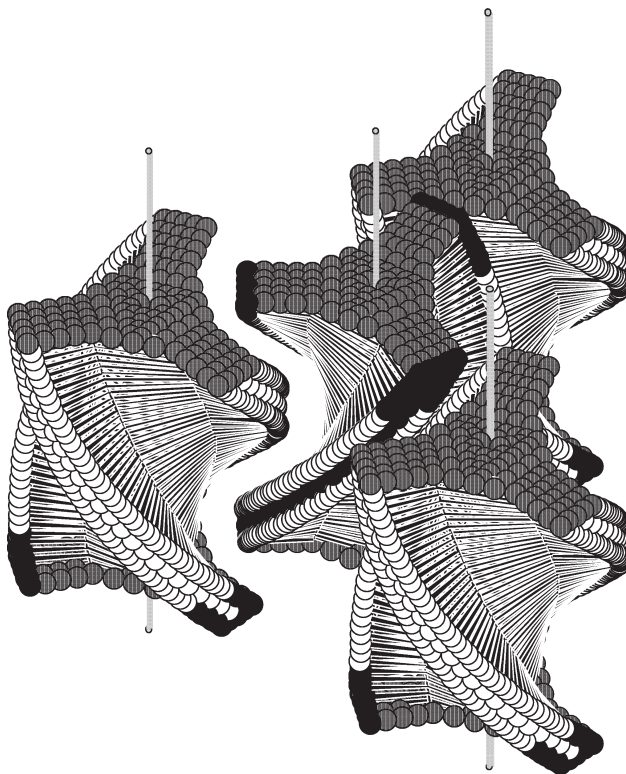


Fig. 8. One segment of the extended lateral arrangement depicting a $[P]-10$ triplex intermeshed with three neighboring diastereomeric $[M]-9$ units.

having $[P]-4$ stack on top of homochiral diastereomeric $[P]-3$ on the same C_3 -axis to generate the asymmetric unit of the $P3$ cell. This is illustrated in cartoon form by the analogous stacking of $[P]-10$ above $[P]-9$ on the left-hand C_3 -axis in Figure 7. The two distal ends of the gear stack have undergone a torsion of 60° by twisting one helix about the C_3 -axis. On a molecular level, salicyl rings in the distal ends of the stack point either directly or angularly towards the enantiomeric C_3 -axis. One ring in the $[P]-3$ end of the stack is disposed directly inwards and resides close to the interaxial plane [it is seen almost edge-on at the bottom of Fig. 3]. Two rings in the $[P]-4$ distal end of the stack straddle both sides of the same plane in an angular fashion. $[P]-4$ ring centroids have -62° and 58° torsion angles with that in the $[P]-3$ stack terminus. Thus, the $[P]-4$ salicyls will be auspiciously juxtapositioned to hug their $[P]-3$ counterpart when enantiotopically generated in $[M]-4$ by the $P3$ inversion center. Intermeshing can now proceed because of the 60° phase difference between the $[P]-3$ and $[M]-4$ lateral partners. The heterochiral $[P]-3$ and $[M]-4$ triplex diastereomers have approximate radii of $6.0(8)$ Å and reside on parallel C_3 -axis spaced about 9.2 Å apart. The c -axis distance between Ni(II)-atoms in the two intermeshing molecules is 2.405 Å which also results in a vertical shift of t -butyl groups on one triplex from those in the adjacent unit, and the common intermeshing region is about 90% of the approximately one-third turn length. Close contacts

between *t*-butyl protons in the proximate [**P**]-**3** and [**P**]-**4** stacked internal region are about 2.39 Å. Superimposition of all non-*t*-butyl group nonhydrogen atoms in [**P**]-**3** with corresponding atoms in diastereomer [**P**]-**4** gave a fairly large RMS = 0.544 Å, testifying to their anisometric relationship. Phosphorus hexafluoride anions are located both on general and on special positions of C_3 rotational symmetry (inversion triad axes) to neutralize the dicationic complexes.

Finally, one must bear in mind that the [**P**]-**3** and [**M**]-**4** diastereomeric triplexes have tongue and groove interactions and both molecules occupy special positions of threefold rotational symmetry on adjacent C_3 -axes in the *P*-**3** crystal. The three strands in the [**P**]-**3** triplex must be homotopically symmetry equivalent, and the same relationship must exist for the three strands in the diastereomeric [**M**]-**4** triplex. Therefore, intermeshing is the providence of each and every strand and groove. The result is a supramolecular array of intermeshed triple-helices perpetuated sideways throughout the entire crystal lattice. In other words, each [**P**]-**3** triplex is surrounded by three intermeshed diastereomeric [**M**]-**4** triplexes, while for each [**M**]-**4** triplex there are three intermeshed diastereomeric [**P**]-**3** triplexes, see cartoon equivalent in Figure 8. Thus, in one layer parallel to the *a*- and *b*-axes, there is a supramolecular array of intermeshed [**P**]-**3** and [**M**]-**4** diastereomers while the inversion centers generate the enantiomeric [**M**]-**3** and [**P**]-**4** diastereomeric extended array in the adjacent layers on either side. The symmetry unrelated pair of opposite handed Ni(II) triple-helices were described as a dimeric unit in the original article,² but it is clear that the interactions between the molecules in this crystal are considerably more elaborate and complex.

ACKNOWLEDGMENTS

Gratitude is expressed to Dr. David F. Perkins for bringing these intermeshing triple-helical metal complexes to his attention. Thanks are given to Prof. Moshe Karpon (Technion, Israel Institute of Technology) for discussions on *P*-**3** space group symmetry.

LITERATURE CITED

1. Perkins DF, Lindoy LF, Meehan GV, Turner P. Inherent helicity in an extended tris-bipyridyl molecular cage. *Chem Commun* 2004;152–153.
2. Perkins DF, Lindoy LF, McAuley A, Meehan GV, Turner P. Manganese(II), iron(II), cobalt(II), and copper(II) complexes of an extended inherently chiral tris-bipyridyl cage. *Proc Natl Acad Sci USA* 2006; 103:532–537.
3. Allen FH. The Cambridge structural database: a quarter of a million crystal structures and rising. *Acta Cryst B* 2002;58:380–388.
4. Glaser R. Helical Stereochemistry and chiral apple halves. II. La coupe du roi via double helical complexation using oligo(bipyridine) strands and Cu(II)/Ag(II). *Chirality* 1993;5:272–276.
5. Hunter CA, Lawson KR, Perkins J, Urch CJ. Aromatic interactions. *J Chem Soc Perkin Trans* 2001;2:651–669.
6. Hunter CA, Sanders JKM. The nature of π - π interactions. *J Am Chem Soc* 1990;112:5525–5534.
7. Burley SK, Petsko GA. Aromatic-aromatic interaction: a mechanism of protein structure stabilization. *Science* 1985;229:23–28.
8. Hahn T, editor. International tables for crystallography-space group symmetry, Vol 4. Dordrecht: Holland: International Union of Crystallography/D Reidel; 1983, p 488.
9. Zabrodsky H, Peleg S, Avnir D. Continuous symmetry measures. *J Am Chem Soc* 1992;114:7843–7851.
10. Zabrodsky H, Peleg S, Avnir D. Continuous symmetry measures. II. Symmetry groups and the tetrahedron. *J Am Chem Soc* 1993;115: 8278–8289.
11. Pinsky M, Avnir D. Continuous symmetry measures. V. The classical polyhedra. *Inorg Chem* 1998;37:5575–5582.

Analysis of the Mechanism of Asymmetric Amplification by Chiral Auxiliary *trans*-1,2-diaminocyclohexane bistriflamide

KOUCIHI ASAKURA,^{1*} YUUKI ISODA,¹ DILIP K. KONDEPUDI,² AND TOMOHIKO YAMAGUCHI³

¹Department of Applied Chemistry, Faculty of Science and Technology, Keio University, Hiyoshi, Kohoku, Yokohama 223-8522, Japan

²Department of Chemistry, Wake Forest University, Winston-Salem, North Carolina

³Nanotechnology Research Institute, National Institute of Advanced Industrial Science & Technology (AIST), 1-1-1, Higashi, Tsukuba 305-8565, Japan

ABSTRACT Asymmetric amplification is a phenomenon in which the enantiomeric excess (ee) of a product is higher than that of a chiral auxiliary for a catalyst. We analyzed the mechanism of asymmetric amplification observed in the addition of diethylzinc (Et_2Zn) to benzaldehyde (PhCHO) to synthesize 1-phenyl-1-propanol in the presence of *trans*-1,2-diaminocyclohexane bistriflamide (DCBF) and titanium tetraisopropoxide (TIOP). In a manner similar to the reaction in which 1-piperidino-3,3-dimethyl-2-butanol is a chiral auxiliary for the catalyst, when asymmetric amplification was observed, the ee of the product varied as the reaction progressed. The mechanisms of variation in ee in the two reactions, however, were different. No asymmetric amplification was observed when TIOP and PhCHO were added to a mixture of DCBF and Et_2Zn , while the ee of the product was always higher than that of DCBF when PhCHO and Et_2Zn were added to a mixture of DCBF and TIOP. In the latter case, the product ee decreased as the reaction progressed. The results indicate that DCBF forms inactive heterochiral complex causing an increase in the ee of DCBF in the solution, which is the chiral auxiliary for the catalyst. But the complex is not very stable and gradually dissociates due to the reaction with Et_2Zn . As a result, the asymmetric amplification decreases as the reaction progresses. *Chirality* 20:919–923, 2008. © 2008 Wiley-Liss, Inc.

KEY WORDS: asymmetric amplification; reservoir model; titanium tetraisopropoxide; *trans*-1,2-diaminocyclohexane bistriflamide; enantiomeric excess; diethylzinc; benzaldehyde

INTRODUCTION

In some asymmetric syntheses, enantiomeric excess (ee) of a product is higher than that of a chiral catalyst or a chiral auxiliary for the catalyst.^{1,2} The phenomenon is called asymmetric amplification, and was first noted by Kagan et al. in 1986 in the Sharpless epoxidation of geraniol.³ This finding provoked systematic studies on the analysis of the mechanism of asymmetric synthesis. Two basic kinetic models, “Reservoir model” and “ ML_2 model,” were initially proposed.^{3,4} In both models, a chiral catalyst forms inactive or weakly catalytic heterochiral dimer, so that the ee of the catalyst that is active is higher than that of the catalyst as a whole. In addition to the theoretical approaches, many examples of chemical reactions in which asymmetric amplification is observed have been found in the last two decades.^{1,2} A great variety of chiral species have been found to act as auxiliaries for the catalyst for the asymmetric amplification in 1,2-addition of diethyl zinc (Et_2Zn) to benzaldehyde (PhCHO) to synthesize 1-phenyl-1-propanol.^{5–11} Among those, very strong asymmetric amplification was found by Oguni et al. in the reaction using 1-piperidino-3,3-dimethyl-2-butanol (PDB) as a chiral auxiliary.⁵

Recently, we have analyzed the reaction and found that ee of the product varies as the reaction progresses.¹² The value of ee of the product should be constant as the reaction progresses if the mechanism of asymmetric amplification follows the “Reservoir model” or “ ML_2 model,” since the ee and concentration of the active catalyst is not a function of the concentration of reactants and the products. To explain the time variation of ee of the product, we proposed a modified Reservoir model by assuming the existence of the Michaelis–Menten type steady state. In this model, ee of the product should vary during the reaction, since the concentration of the Michaelis–Menten type intermediate is a function of reactant concentration. Noyori

Contract grant sponsor: Grant-in-Aid for Scientific Research (C) from Japan Society for Promotion of Science; Contract grant number: 17540361
Contract grant sponsor: Grant-in-Aid for the 21st Century COE program “Keio Life Conjugate Chemistry” from the Ministry of Education, Culture, Sports, Science, and Technology, Japan

*Correspondence to: Kouichi Asakura, Department of Applied Chemistry, Faculty of Science and Technology, Keio University, 3-14-1, Hiyoshi, Kohoku, Yokohama 223-8522, Japan. E-mail: asakura@appc.keio.ac.jp

Received for publication 9 May 2007; Accepted 1 February 2008

DOI: 10.1002/chir.20563

Published online 1 April 2008 in Wiley InterScience (www.interscience.wiley.com).

et al. proposed the kinetic model including a step of Michaelis–Menten type intermediate formation,¹³ for their asymmetric amplification which uses 3-*exo*-(dimethylamino) isoborneol (DAIB) as a chiral auxiliary for the catalyst.⁶ Their DAIB catalyzed asymmetric amplification, however, was little conversion-dependent.

We also have found that the reaction rate and the ee of the product differed significantly when the order of reagent addition was changed in PDB catalyzed asymmetric amplification. The phenomenon was explained by the further modification of Reservoir model that took into account not only the Michaelis–Menten type intermediate formation but also the dissociation of the reservoir.¹² Our findings showed the importance of monitoring the variation in the product ee during the reaction and systematic studies for understanding the details of the mechanism of asymmetric amplification.

There is another example of asymmetric amplification in which the order of reagent addition influences the reaction behavior.¹¹ Addition of Et₂Zn to PhCHO in the presence of stoichiometric amount of titanium tetrakisopropoxide (TIOP) and catalytic amount of *trans*-1,2-diaminocyclohexane bistriflamide (DCBF) was reported to show high enantioselectivity.^{14–18} Takahashi et al. added Et₂Zn and PhCHO into the mixture of DCBF and TIOP,^{14,15} while Walsh et al. added TIOP and PhCHO into the mixture of DCBF and Et₂Zn.^{16–18} In both cases, enantioselectivity was extremely high. However, the resulting ee of the product by the two procedures were different when DCBF was not enantiomerically pure. Kagan et al. found that asymmetric amplification was observed when they followed Takahashi et al.'s procedure, while no non-linear effect in asymmetric catalysis was observed when they employed Walsh et al.'s procedure.¹¹ In addition, when they mixed DCBF of small ee and TIOP in toluene, they found very low ee in the precipitated DCBF but the solution contained higher ee.¹⁹ This interesting behavior of the reaction motivated us to apply our analytical techniques to investigate the mechanism of the asymmetric amplification in the reaction. Since one cannot simply assume that the results of reaction with PDB as auxiliary must apply to this reaction as well, such investigations are important to unambiguously ascertain the nature of the mechanism that leads to enantiomeric amplification.

MATERIALS AND METHODS

Reagents and Solvents

Toluene was freshly distilled under argon atmosphere over sodium. Hexane solution of Et₂Zn (1.0 M) was purchased from Aldrich Chemical and TIOP was purchased from Tokyo Chemical Industry, Tokyo. Preparation of each enantiomer of DCBF was done following Walsh et al.'s method.¹⁶ (1*R*,2*R*)- or (1*S*,2*S*)-1,2-diaminocyclohexane L-tartaric acid salt purchased from Tokyo Chemical Industry, Tokyo. was dissolved in 9.0 N aqueous solution of sodium hydroxide (5.0 mL) to liberate corresponding free diamine, and it was extracted by diethyl ether (10.0 mL) twice. The solution was dried over magnesium sulfate, filtered, and concentrated to obtain (1*R*,2*R*)- or (1*S*,2*S*)-1,2-diaminocyclohexane. To a dichloromethane

(30.0 mL) solution of (1*R*,2*R*)- or (1*S*,2*S*)-1,2-diaminocyclohexane (1.09 g, 9.52 mmol) cooled at 0°C was added triethylamine (7.40 g, 42.8 mmol) and the solution was stirred for 10 min at 0°C. After cooling this mixture to –40°C, trifluoromethyl sulfonyl chloride (3.20 g, 19.0 mmol) was added and the reaction mixture was stirred for 2 h at room temperature. To the resulting solution was added 1.0 N hydrochloric acid aqueous solution (70.0 mL) to stop the reaction followed by the addition of sodium hydroxide (2.80 g, 70.0 mmol). The mixture was extracted with diethyl ether twice (40.0 and 70.0 mL) and the extract was dried over magnesium sulfate, filtered, and concentrated. The crude product was recrystallized from 1:1 hexane/chloroform to give white crystal of (1*R*,2*R*)- or (1*S*,2*S*)-DCBF.

Reaction Procedures for the Asymmetric Amplification

Following four reaction procedures were employed for 1,2-addition of Et₂Zn to PhCHO in the presence of DCBF and TIOP. In all cases, DCBF (0.240 mmol) was dissolved in 28.0 mL of dried toluene in a flame-dried Schlenk tube, and the solution was covered with argon, then following procedures were carried out.

Procedure 1: DCBF + TIOP then Et₂Zn then PhCHO. To DCBF solution was added TIOP (12.0 mmol) and the solution was stirred for 15 min at 60°C. Then the solution was cooled down to –20°C and stirred for 10 min. To this was added 1.0 M hexane solution of Et₂Zn (12.0 mL, 12.0 mmol), and the solution was stirred for 15 min at –20°C. To the resulting solution was added PhCHO (12.0 mmol) to start the reaction.

Procedure 2: DCBF + TIOP then PhCHO then Et₂Zn. To the DCBF solution was added TIOP (12.0 mmol) and the solution was stirred for 15 min at 60°C. Then the solution was cooled down to –20°C and stirred for 10 min. To this was added PhCHO (12.0 mmol), and the solution was stirred for 15 min at –20°C. To the resulting solution, 1.0 M hexane solution of Et₂Zn (12.0 mL, 12.0 mmol) was added to start the reaction.

Procedure 3: DCBF + Et₂Zn then TIOP then PhCHO. To the solution of DCBF 1.0 M hexane solution of Et₂Zn (12.0 mL, 12.0 mmol) was added, and the mixture was stirred for 15 min at 25°C. After cooling it to –20°C, the solution was stirred for 10 min at –20°C. To this TIOP (12.0 mmol) was added and the solution was stirred for 15 min at –20°C. To the resulting solution PhCHO (12.0 mmol) was added to start the reaction.

Procedure 4: DCBF + Et₂Zn then PhCHO then TIOP. To the solution of DCBF 1.0 M hexane solution of Et₂Zn (12.0 mL, 12.0 mmol) was added, and the mixture was stirred for 15 min at 25°C. After cooling it to –20°C, the solution was stirred for 10 min at –20°C. To this was added PhCHO (12.0 mmol) and the solution was stirred for 15 min at –20°C. To the resulting solution TIOP (12.0 mmol) was added to start the reaction.

In all of the above procedures, initial concentrations were 6.00×10^{-3} M for DCBF and 3.00×10^{-1} M for

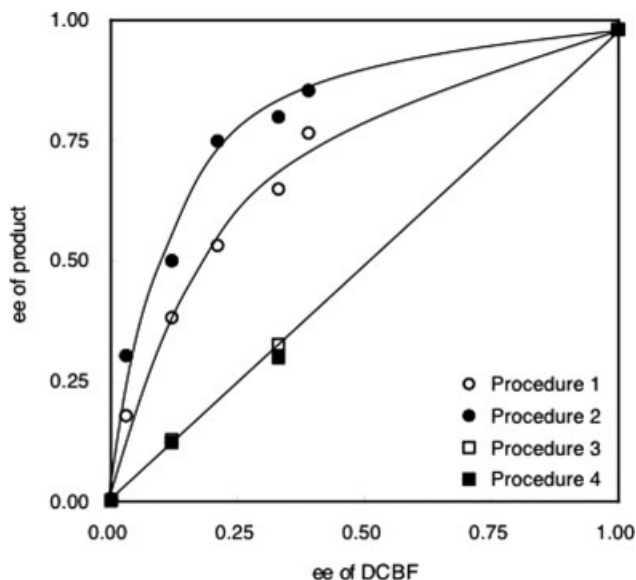


Fig. 1. The relation between the ee of DCBF and the final ee of the product by four procedures.

TIOP, PhCHO, and Et_2Zn . The temperature at which the reaction progressed is constant at -20°C . The order of reagent addition for Procedure 1 and 3 are the same as Method A and B in Kagan et al.'s report.¹¹ Since the ee of the product of the asymmetric amplification is extremely sensitive to a small difference in ee of DCBF, DCBF having a given ee was prepared at one time and used in each of the procedures.

Determination of Concentration of Reactant and Product in the Reaction System

In all cases, reaction was monitored by sampling a small portion of solution (0.30 mL) from the reaction system using a micro-syringe at prescribed times. The sample so-

lution was mixed with ethyl acetate (1.5 mL) and saturated aqueous solution of ammonium chloride (1.5 mL) in a capped bottle, and PhCHO and 1-phenyl-1-propanol extracted in the organic layer was analyzed. Quantitative analysis of PhCHO and 1-phenyl-1-propanol was done by gas chromatography (Gasukuro Kogyo GC-380). A capillary column (GL Science OV-1 NEUTRABOND-1, 0.25 mm \times 30 m) was used, and the injector, column, and detector temperatures were 300, 90, and 300°C , respectively, with carrier gas of N_2 at 0.90 mL min^{-1} . The retention time of PhCHO and 1-phenyl-1-propanol was 5.2 and 13.5 min, respectively. The ee of 1-phenyl-1-propanol was determined by high-performance liquid chromatography using a chiral column (Daicel, Chiralcel OD-H, 0.46 cm \times 25 cm). The eluent was 100:1.2 hexane/2-propanol, and the flow rate was 0.9 mL/min. The retention times of *R*- and *S*-enantiomers of 1-phenyl-1-propanol were 19.2 and 22.0 min, respectively. The ee used in this article is scale from 0 to 1.

RESULTS AND DISCUSSION

The asymmetric amplification was observed only when Procedure 1 and 2 were employed as shown in Figure 1. In both cases, DCBF was mixed with TIOP before the addition of Et_2Zn . The results correspond well with the results in the report of the Kagan et al.'s.¹¹ Not only Procedure 3 but also Procedure 4 produced no observable asymmetric amplification. The time evolutions of the concentration of the product when DCBF having ee of 0.12 was used are shown in Figure 2a. Reaction proceeded slower by Procedure 1 and 2 than by Procedure 3 and 4, indicating that the inactive heterochiral reservoir was scarcely formed when Procedure 3 and 4 are employed. In the presence of the reservoir effect, the rate of reaction should be a function of ee of catalyst and it should decrease with decreasing ee of the catalyst. As shown in Figure 2b, the

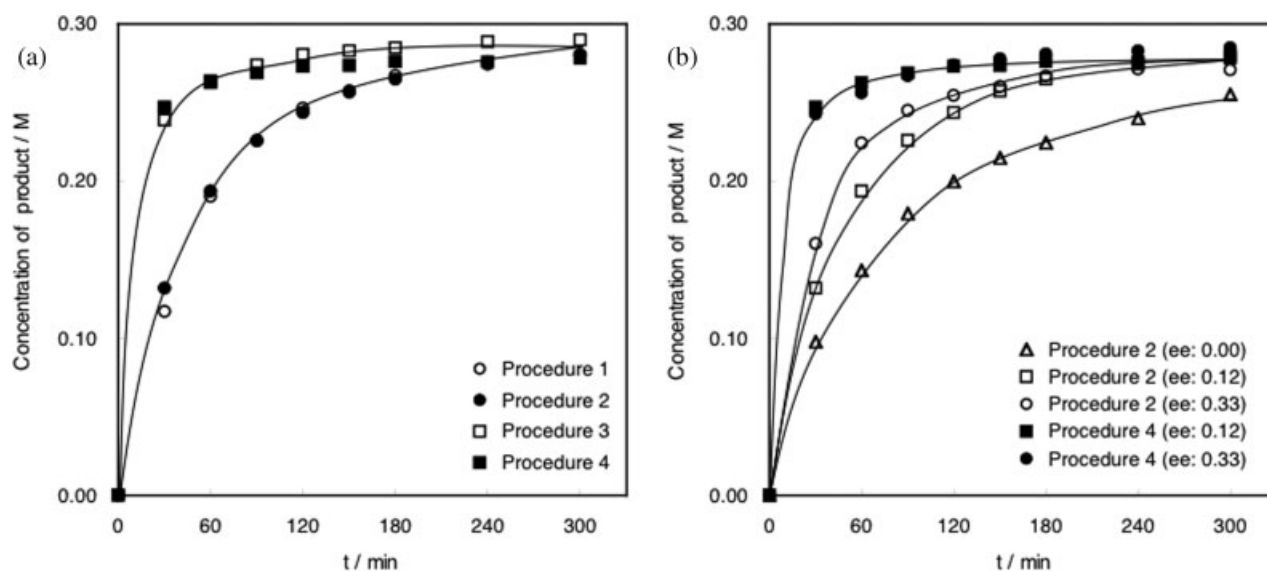


Fig. 2. Time evolution of the concentration of the product observed during the reaction. (a) Experiments were performed by four procedures setting the ee of DCBF at 0.12. (b) Experiments were performed by Procedure 2 and 4 varying the ee of DCBF.

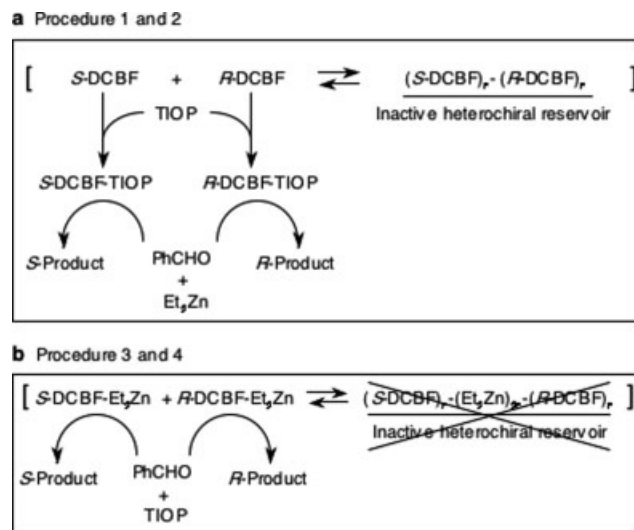


Fig. 3. Mechanism of asymmetric amplification in the reaction catalyzed by DCBF and TIOP. (a) Generation of asymmetric amplification by Procedure 1 and 2. (b) Disappearance of asymmetric amplification by Procedure 3 and 4.

rate of reaction was not influenced by ee of DCBF when Procedure 4 was employed, while the reaction proceeded slower as decreasing the ee of DCBF when Procedure 2 was employed.

From all our experimental observations, we propose the mechanism for the asymmetric amplification shown in Figure 3. In this model, both enantiomers of DCBF form heterochiral oligomeric complex, $(S\text{-DCBF})_n\text{-}(R\text{-DCBF})_n$, that does not possess catalytic activity, and the remaining enantiomerically enriched monomeric DCBF and TIOP forms complexes, $S\text{-DCBF-TIOP}$ and $R\text{-DCBF-TIOP}$, to act as chiral catalysts for the addition of Et_2Zn to PhCHO when Procedures 1 and 2 were employed. Kagan et al. reported that almost racemic precipitate was generated from the toluene and hexane solution of optically active DCBF.¹⁹ The generation of precipitate by mixing DCBF and TIOP was also observed in our experiments by Procedure 1 and 2. The proposed formation of a reservoir of inactive complex in the model is thus based on the phenomena observed in the real chemical experiments. This indicates that the formation of the heterochiral oligomeric precipitate from the corresponding monomeric species reduces the free energy. On the other hand, no precipitation was observed when DCBF was mixed with Et_2Zn by Procedure 3 and 4. In these cases, no inactive heterochiral oligomeric species are formed at the first step, and the monomeric species, $S\text{-DCBF-Et}_2\text{Zn}$ and $R\text{-DCBF-Et}_2\text{Zn}$, react with PhCHO in the presence of TIOP. The formation of heterochiral reservoir, $(S\text{-DCBF})_n\text{-(Et}_2\text{Zn)}_{2n}\text{-(R-DCBF)}_n$, from the corresponding monomeric species, $S\text{-DCBF-Et}_2\text{Zn}$ and $R\text{-DCBF-Et}_2\text{Zn}$, thus increases the free energy of the system.

Although asymmetric amplification was observed by both Procedure 1 and 2, the final ee of the product by the two procedures were different. As shown in Figure 1, the final ee was always higher in Procedure 2 than in Procedure 1. For analyzing a complex behavior of reaction, monitoring the time evolution of ee of the product often gives us important information. As shown in Figure 4, ee of the product was constant throughout the reaction when Procedure 3 and 4 were employed. On the other hand, slight decrease in ee by Procedure 1 and relatively large decrease in ee by Procedure 2 were observed.

There are two stable states in isolated systems: a thermodynamically stable state and a kinetically stable state. If the dissociation of heterochiral reservoir, $(S\text{-DCBF})_n\text{-(TIOP)}_{2n}\text{-(R-DCBF)}_n$, by its reaction with Et_2Zn to form chiral catalysts, $S\text{-DCBF-Et}_2\text{Zn-TIOP}$ and $R\text{-DCBF-Et}_2\text{Zn-TIOP}$, reduces the free energy but has relatively large energy of activation, the ee of the active catalyst is the highest at the initial condition and decreases as the dissociation of the heterochiral reservoir proceeds. In Procedure 1, before the onset of the reaction by the addition of PhCHO into the reaction mixture, Et_2Zn was mixed for 15 min. Dissociation of heterochiral reservoir may proceed during this 15 min to decrease the ee of the catalyst that is active. On the other hand, the dissociation of heterochiral reservoir and the reaction starts at the same time when Procedure 2 was employed. The initial ee of the product is thus the highest in Procedure 2 and decreases as the reaction proceeded.

In order to verify this assumption, experiments extending the time before the addition of PhCHO after the addition of Et_2Zn in Procedure 1 were performed. Results by this modified Procedure 1, i.e., Procedure 1', shown in Figure 5 are clearly consistent with our assumption. In this case, experiments were performed by extending the time before the addition of PhCHO after the addition of Et_2Zn from 15 min to 12 h. The time evolution of ee of the product by Procedure 1' was different from that seen in Procedure 1, but was the same as the one seen in Procedure 3. No asymmetric amplification and variation in ee during

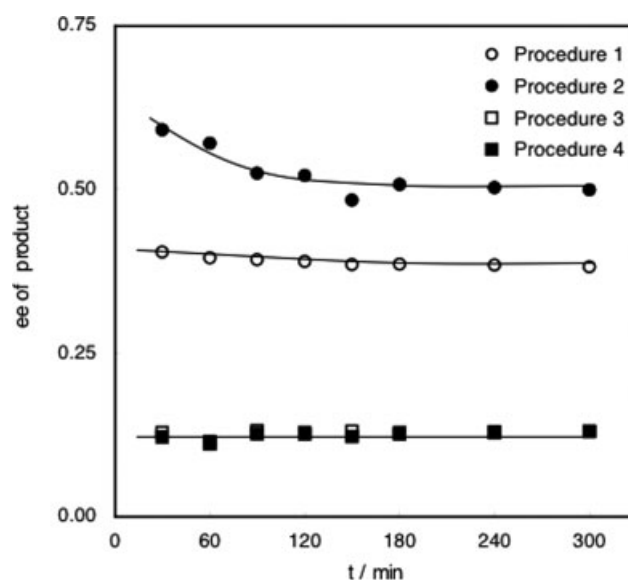


Fig. 4. Time evolution of ee of the product observed during the reaction in four different procedures when the ee of DCBF was set at 0.12.

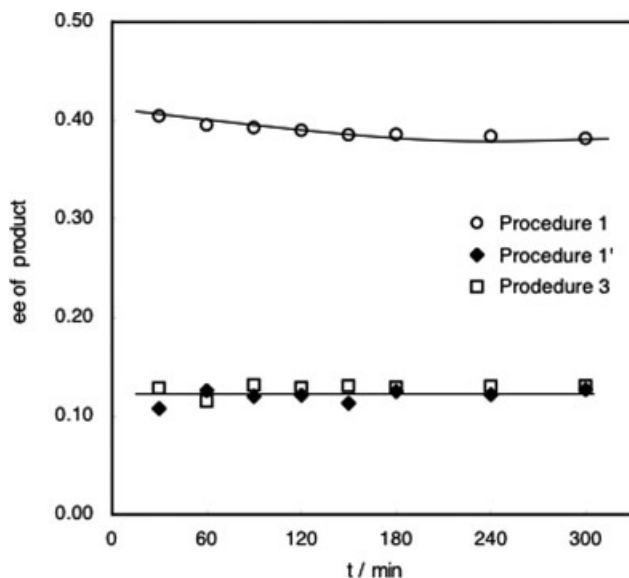


Fig. 5. Variations in ee of the product observed during the reaction by Procedures 1, 1', and 3.

the reaction was observed by Procedure 1'. In this case, dissociation of heterochiral reservoir by Et_2Zn was completed during 12 h of stirring.

CONCLUSION

The asymmetric amplification introduced in this report was known to be influenced by the order of reagents addition.^{11,19} In our previous report, we have shown that the PDB catalyzed asymmetric amplification was also influenced by the order of reagents addition, and clarified the mechanism by monitoring the variation in the product ee during the reaction and the rate of the reaction.¹² In this report, we have succeeded in probing into the mechanism of the asymmetric amplification catalyzed by DCBF and TIOP by the same approach, though the mechanisms of the two asymmetric amplifications were different from each other. Here, we again would like to emphasize the importance of systematic studies for analyzing the mechanism of asymmetric amplification, such as monitoring the variation in the product ee during the reaction and rate of the reaction.

LITERATURE CITED

- Fenwick DR, Kagan HB. Asymmetric amplification. *Top Stereochem* 1999;22:257–296.
- Kagan HB. Nonlinear effects in asymmetric catalysts: a personal account. *Syn Lett* 2001;2001:888–899.
- Puchot C, Dunach E, Zhao S, Agami C, Kagan HB. Nonlinear effects in asymmetric-synthesis. Examples in asymmetric oxidations and aldolization reactions. *J Am Chem Soc* 1986;108:2353–2357.
- Guillaneux D, Zhao SH, Samuel O, Rainford D, Kagan HB. Nonlinear effects in asymmetric catalysis. *J Am Chem Soc* 1994;116:9430–9439.
- Oguni N, Matsuda Y, Kaneko T. Asymmetric amplifying phenomena in enantioselective addition of diethylzinc to benzaldehyde. *J Am Chem Soc* 1988;110:7877–7878.
- Kitamura M, Okada S, Suga S, Noyori R. Enantioselective addition of dialkylzincs to aldehydes promoted by chiral amino-alcohols. Mechanism and nonlinear effect. *J Am Chem Soc* 1989;111:4028–4036.
- Bolm C, Schlingloff G, Harms K. Catalyzed enantioselective alkylation of aldehydes. *Chem Ber* 1992;125:1191–1203.
- Bolm C, Muller J, Schlingloff G, Zehnder M, Neuburger M. β -hydroxy sulfoximines as catalyst for the enantioselective alkylation of aldehydes. *J Chem Soc Chem Commun* 1993;182–183.
- Fitzpatrick K, Hulst R, Kellogg RM. Thiol and disulfide derivatives of ephedra alkaloids 2: a mechanistic study of their effect on the addition of diethyl zinc to benzaldehyde. *Tetrahedron: Asymmetry* 1995;6:1861–1864.
- Rijnberg E, Hovestad NJ, Kleij AW, Jastrzebski JTBH, Boersma J, Janssen MD, Spek AL, van Koten G. Application of S,N-chelating chiral zinc bis(aminoarenethiolates) as new precursor catalysts in the enantioselective addition of dialkylzincs to aldehydes. *Organometallics* 1997;16:2847–2857.
- Luukas TO, Fenwick DR, Kagan HB. Presence or absence of a nonlinear effect according to the asymmetric catalyst preparation in the alkylation of benzaldehyde. *C R Chim* 2002;5:487–491.
- Asakura K, Yamamoto T, Inoue S, Osanai S, Kondepudi DK, Yamaguchi T. A new perspective on the mechanism of asymmetric amplification. *Chem Phys Lett* 2005;406:312–317.
- Kitamura M, Suga S, Oka H, Noyori R. *J Am Chem Soc* 1998;120:9800–9809.
- Takahashi H, Kawakita T, Yoshioka M, Kobayashi S, Ohno M. Enantioselective alkylation of aldehyde catalyzed by disulfonamide-Ti(O-*i*-Pr)₄-dialkyl zinc system. *Tetrahedron Lett* 1989;30:7095–7098.
- Takahashi H, Kawakita T, Ohno M, Yoshioka M, Kobayashi S. A catalytic enantioselective reaction using a C₂-symmetrical disulfonamide as a chiral ligand: alkylation of aldehydes catalyzed by disulfonamide-Ti(O-*i*-Pr)₄-dialkyl zinc system. *Tetrahedron* 1992;48:5691–5700.
- Guo C, Qiu J, Zhang XM, Verdugo D, Larter ML, Christie R, Kenney P, Walsh PJ. Enantioselective addition of diethylzinc to benzaldehyde catalyzed by chiral titanate complexes with helical ligands. *Tetrahedron* 1997;53:4145–4158.
- Pritchett S, Woodmansee DH, Gantzel P, Walsh PJ. Synthesis and crystal structures of bis(sulfonamido) titanium bis(alkoxide) complexes: mechanistic implications in the bis(sulfonamide) catalyzed asymmetric addition of dialkylzinc reagents to aldehydes. *J Am Chem Soc* 1998;120:6423–6424.
- Pritchett S, Woodmansee DH, Davis TJ, Walsh PJ. Improved methodology for the asymmetric alkylation of aldehydes employing bis(sulfonamide) complexes. *Tetrahedron Lett* 1998;39:5941–5942.
- Satyanarayana T, Ferber B, Kagan HB. Asymmetric amplification in catalysis by trans-1,2-diaminocyclohexane bistriflamide. *Org Lett* 2007;9:251–253.

1,3-Bis[*N*-sulfonyl-(1*R*,2*S*)-1,3-diphenyl-2-aminopropanol]benzene: An Excellent Ligand for Titanium-Catalyzed Asymmetric $\text{AlPh}_3(\text{THF})$ Additions to Aldehydes

SHENG-HSIANG HSIEH, CHIEN-AN CHEN, DA-WEI CHUANG, MAO-CHIH YANG, HSU-TANG YANG, AND HAN-MOU GAU*

Department of Chemistry, National Chung Hsing University, Taichung 402, Taiwan, Republic of China

ABSTRACT Asymmetric $\text{AlPh}_3(\text{THF})$ additions to a wide variety of aldehydes catalyzed by a titanium catalyst of 20 mol % 1,3-bis[*N*-sulfonyl-(1*R*,2*S*)-1,3-diphenyl-2-aminopropanol]benzene (**1**) are reported. The catalytic system works excellently for aromatic aldehydes bearing either an electron-donating or an electron-withdrawing substituent on the aromatic ring to afford secondary diaryl alcohols in excellent isolated yields of $\geq 95\%$ and excellent enantioselectivities of $\geq 94\%$ ee. The phenyl addition to cinnamaldehyde or 2-furylaldehyde gave corresponding secondary alcohols in 85% and 95% ee, respectively. For aliphatic aldehydes, increasing enantioselectivities of the addition products in terms of increasing steric sizes of aldehydes are observed, and this trend goes from the linear 1-pentanal (87% ee), the secondary cyclohexylaldehyde (95% ee) or the 2-methylpropanal (97% ee), to the tertiary 2,2-dimethylpropanal (99% ee). *Chirality* 20:924–929, 2008. © 2008 Wiley-Liss, Inc.

KEY WORDS: asymmetric catalysis; phenyl addition; *N*-sulfonylated amino alcohol; triphenyl(tetrahydrofuran)aluminum; titanium tetraisopropoxide

INTRODUCTION

Organozinc compounds have been widely used as reagents in asymmetric C—C bond formation reactions, and numerous catalytic systems have been developed to induce excellent stereoselectivities.^{1,2} In recent years, syntheses of enantiomerically pure diarylmethanols^{3,4} have attracted considerable attentions because of great values of diarylmethanols leading to bioactive compounds.^{5–9} The catalytic synthesis of chiral diarylmethanols can be achieved by asymmetric reductions of ketones employing a catecholborane reagent,¹⁰ asymmetric hydrogenations of ketones,¹¹ or asymmetric aryl additions to aldehydes. The first asymmetric phenyl addition reaction was reported by Seebach and coworkers, employing the titanium catalyst of TADDOLate ligand and the highly reactive $\text{PhTi}(\text{O}-i\text{-Pr})_3$ reagent.¹² After the work of direct ZnPh_2 additions by Fu et al.,¹³ various zinc catalytic systems employing ZnPh_2 ,^{14–17} phenylzinc reagents^{18–21} from reactions of dialkylzinc compounds and ZnPh_2 , or arylzinc compounds^{9,22–26} have been reported to afford diarylmethanols in high enantioselectivities. Though arylzinc reagents are not available commercially, they can be prepared in situ from reactions of excess ZnEt_2 with arylboronic acid at elevated temperatures for 12 h²² or from reactions of aryllithiums with ZnCl_2 and *n*-butyllithium.²⁶ In addition to the aforementioned addition reagents, a few examples of direct asymmetric additions of arylboronic reagents to aldehydes catalyzed by nickel²⁷ or rhodium^{28,29} catalytic systems have also been established. Recently, we discovered that triarylaluminum(tetrahydrofuran) compounds, $\text{AlAr}_3(\text{THF})$, are efficient reagents in asymmetric aryl addi-

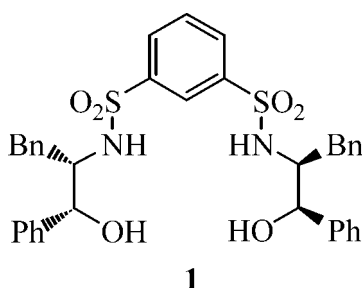
tions to aldehydes³⁰ or ketones.³¹ Furthermore, the $\text{AlAr}_3(\text{THF})$ compounds are also effective coupling reagents with aryl bromides or chlorides catalyzed by the economic $\text{Pd}(\text{OAc})_2/\text{PCy}_3$ catalyst under relative mild reaction conditions.³² Organoaluminum compounds are more reactive than organozinc or organoboron reagents and have been applied to diversified organic syntheses^{33–41} and to asymmetric catalytic reactions.^{42–46}

To continue our effort to develop amino alcohol ligands^{47–50} for asymmetric catalytic reactions and also to demonstrate the application of $\text{AlAr}_3(\text{THF})$ compounds, we herein report asymmetric $\text{AlPh}_3(\text{THF})$ additions to a variety of aldehydes catalyzed by an in situ formed titanium(IV) catalyst of 1,3-bis[*N*-sulfonyl-(1*R*,2*S*)-1,3-diphenyl-2-aminopropanol]benzene (**1**). Compound **1** has been reported to be an excellent ligand in titanium-catalyzed ZnEt_2 additions to aldehydes.⁵¹ In this study, $\text{AlPh}_3(\text{THF})$ additions to diversified aldehydes, such as aromatic, α,β -unsaturated, furyl, and aliphatic aldehydes, catalyzed by 20 mol % titanium(IV) catalyst of ligand **1** at 0°C afford diarylmethanols and other secondary alcohols in excellent enantioselectivities up to 99% ee.

*Correspondence to: Han-Mou Gau, Department of Chemistry, National Chung Hsing University, Taichung 402, Taiwan, Republic of China. E-mail: hmgau@dragon.nchu.edu.tw
Contract grant sponsor: National Science Council, Republic of China; Contract grant number: NSC-96-2113-M-005-007-MY3
Received for publication 27 November 2007; Accepted 29 February 2008
DOI: 10.1002/chir.20572
Published online 6 June 2008 in Wiley InterScience (www.interscience.wiley.com).

TABLE 1. Optimizations of asymmetric $\text{AlPh}_3(\text{THF})$ additions to 4-methoxybenzaldehyde catalyzed by in situ formed titanium catalysts of **1**^a

Entry	1 (mol %)	$\text{Ti}(\text{O-}i\text{-Pr})_4$ (equiv)	$\text{AlPh}_3(\text{THF})$ (equiv)	Time (h)	Yield ^b (%)	ee ^c (%)
1	10	0.95	1.2	12	100	75
2	10	1.15	1.2	12	100	77
3	10	1.35	1.2	12	100	66
4	10	1.15	1.1	12	97	75
5	10	1.15	1.3	12	98	81
6	10	1.15	1.4	12	100	88
7	10	1.15	1.5	12	100	81
8	20	2.3	2.8	12	100	95
9	20	2.3	2.8	6	100	95
10	20	2.3	2.8	3	100	95
11	20	2.3	2.8	1.5	90	90

^a4-Methoxybenzaldehyde = 0.50 mmol; THF, 5.0 ml.^bYields were determined by ^1H NMR.^cee values were determined by HPLC analysis of the alcohol using a Chiralcel OJ column from Daicel.

Experimental Section

1,3-Bis[*N*-sulfonyl-(1*R*,2*S*)-1,3-diphenyl-2-aminopropanol] benzene (**1**)^{51,52} and $\text{AlPh}_3(\text{THF})$ ³⁰ were prepared according to literature procedures. $\text{Ti}(\text{O-}i\text{-Pr})_4$ was freshly distilled prior to use. Aldehydes were purified by distillation or recrystallization from appropriate solvents. THF was dried by refluxing for at least 24 h over sodium/benzophenone and freshly distilled prior to use. All syntheses and manipulations were carried out under a dry nitrogen atmosphere. ^1H NMR spectra at 400 MHz and ^{13}C NMR spectra at 100.70 MHz were recorded on a 400 MHz NMR spectrometer. ^1H and ^{13}C chemical shifts were measured relative to tetramethylsilane at 0.0 ppm as an internal reference. Enantiomeric excesses of secondary alcohol products were measured on HPLC systems using appropriate chiral columns.

General Procedure for the Addition of $\text{AlPh}_3(\text{THF})$ to Aldehydes

A solution of **1** (65.6 mg, 0.100 mmol) and $\text{Ti}(\text{O-}i\text{-Pr})_4$ (0.345 ml, 1.15 mmol) in 2 ml THF was stirred for 1 h under a nitrogen atmosphere at room temperature. The solution was cooled to 0°C and $\text{AlPh}_3(\text{THF})$ (0.462 g, 1.40 mmol) in 3 ml THF was added. The mixture was stirred at 0°C for 0.5 h followed by an addition of an aldehyde (0.50 mmol). The solution was stirred at 0°C for 3 h and quenched by an addition of 1 M HCl (2 ml). The aqueous layer was extracted with AcOEt (2 × 20 ml). The com-

bined organic phase was washed with brine and dried with anhydrous MgSO_4 . After filtration, the volatile material was removed under reduced pressures to afford crude products which were purified by column chromatography (silica gel; eluent: hexane/AcOEt = 4/1) to give secondary alcohols. The enantiomeric excesses of products were determined by HPLC analysis.

RESULTS AND DISCUSSION

Chiral ligand **1** was prepared in high yield according to procedures of our previous work,⁵¹ and in that study, the titanium catalyst of ligand **1** catalyzed asymmetric ZnEt_2 additions to aldehydes affording secondary alcohols in excellent stereoselectivities. In this study, asymmetric phenyl additions of $\text{AlPh}_3(\text{THF})$ to aldehydes employing in situ formed titanium catalytic systems of the same ligand **1** were examined (eq. 1) and results are summarized in Table 1. Under a reaction condition of 10 mol % **1**, 0.95 equiv $\text{Ti}(\text{O-}i\text{-Pr})_4$, 1.2 equiv $\text{AlPh}_3(\text{THF})$ in THF, and a reaction time of 12 h at 0°C, the phenyl addition afforded the desired diarylmethanol in 100% yield and 75% ee (entry 1). When $\text{AlPh}_3(\text{THF})$ was kept at 1.2 equiv but tuning $\text{Ti}(\text{O-}i\text{-Pr})_4$ to 1.15 and 1.35 equiv (entries 2 and 3), the reactions furnished the product in quantitative yield and enantioselectivities of 77% and 66% ee, respectively. The reactions were then examined on reaction conditions of keeping $\text{Ti}(\text{O-}i\text{-Pr})_4$ at 1.15 equiv while tuning $\text{AlPh}_3(\text{THF})$ to 1.1, 1.3, 1.4, and 1.5 equiv (entries 4–7). It was found that the catalytic reaction employing 1.4 equiv $\text{AlPh}_3(\text{THF})$ gave the product in the best 88% ee (entry 6). To further improve the enantioselectivity, the reaction was conducted under a reaction condition of doubling ligand loading to 20 mol % **1**, $\text{Ti}(\text{O-}i\text{-Pr})_4$ to 2.3 equiv, and $\text{AlPh}_3(\text{THF})$ to 2.8 equiv, affording the product in a quantitative yield and an excellent 95% ee (entry 8). It had been established that the arylaluminum compounds are highly efficient reagents. Thus catalytic reactions at shorter reaction times were then examined, and in reaction times of 6 and 3 h, yields of the addition product remained 100% based on the

TABLE 2. Asymmetric $\text{AlPh}_3(\text{THF})$ addition to aldehydes catalyzed by the best performing titanium catalyst of **1**^a

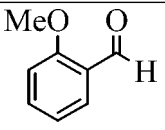
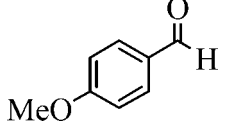
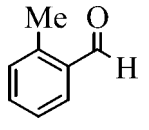
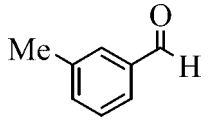
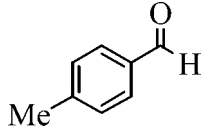
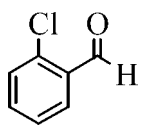
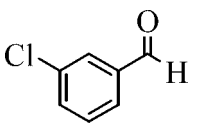
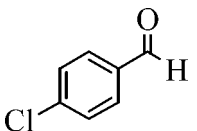
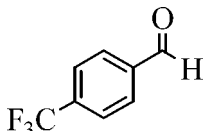
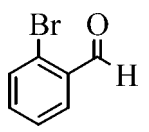
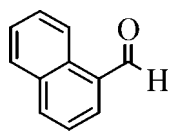
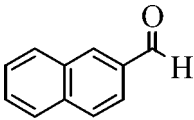
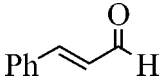
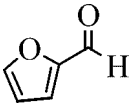
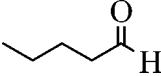
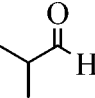
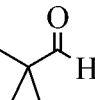
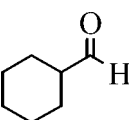
Entry	Aldehyde	Yield ^b (%)	ee ^c (%)
1		95	96 (<i>R</i>)
2		98	95 (<i>R</i>)
3		97	94 (<i>R</i>)
4		97	98 (<i>R</i>)
5		97	98 (<i>R</i>)
6		95	95 (<i>R</i>)
7		97	97 (<i>R</i>)
8		96	96 (<i>R</i>)
9		97	96 (<i>R</i>)
10		97	95 (<i>R</i>)
11		96	95 (<i>R</i>)

TABLE 2. Continued

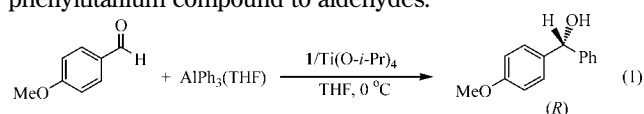
Entry	Aldehyde	Yield ^b (%)	ee ^c (%)
12		97	96 (<i>R</i>)
13		93	85 (<i>S</i>)
14		97	95 (<i>R</i>)
15		90	87 (<i>S</i>)
16		90	97 (<i>S</i>)
17		95	99 (<i>S</i>)
18		85	95 (<i>S</i>)

^aAldehyde/**1**/ $\text{AlPh}_3(\text{THF})/\text{Ti}(\text{O}-i\text{-Pr})_4 = 0.50/0.10/1.15/1.4$ mmol; THF, 5.0 ml; reaction temperature, 0°C; reaction time, 3 h.

^bIsolated yield.

^cee values were determined by HPLC analysis using chiral columns from Daicel.

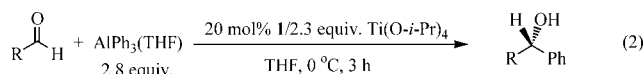
^1H NMR spectra and enantioselectivities are the same 95% ee (entries 9–10). If the reaction time was further reduced to 1.5 h, the product in a lower 90% yield and a lower enantioselectivity of 90% ee was obtained (entry 11). This study demonstrates that the system of 20 mol % **1**, 2.3 equiv $\text{Ti}(\text{O}-i\text{-Pr})_4$, and 2.8 equiv $\text{AlPh}_3(\text{THF})$ in THF is the best performing catalyst in asymmetric $\text{AlPh}_3(\text{THF})$ addition to the 4-methoxybenzaldehyde. In titanium-catalyzed asymmetric dialkylzinc additions to aldehydes, additions through alkyltitanium compounds were suggested.⁵³ Since the same titanium catalyst of **1** catalyzes diethylzinc and triphenylaluminum additions to afford corresponding secondary alcohols in excellent enantioselectivities, the $\text{AlPh}_3(\text{THF})$ addition reactions are proposed to proceed through addition of the phenyltitanium compound to aldehydes.³⁰



To demonstrate generalities of $\text{AlPh}_3(\text{THF})$ additions to aldehydes, asymmetric phenyl additions to a wide variety

of aldehydes, including aromatic aldehydes with an electron-donating or an electron-withdrawing substituent at 2-, 3-, or 4-position on the aromatic ring, were investigated. In addition, phenyl additions to an α,β -unsaturated cinnamaldehyde, 2-furaldehyde and aliphatic aldehydes were also studied. Under the best performing catalytic reaction condition (eq. 2), results of asymmetric phenyl additions are listed in Table 2. Asymmetric phenyl additions to aromatic aldehydes bearing an electron-donating group such as a methoxy or a methyl substituent furnished diarylmethanols in high isolated yields from 95% to 98% with excellent enantioselectivities of 94% to 98% ee (entries 1–5). This catalyst shows no steric effect in terms of the substituted position at the aromatic ring. For examples, phenyl additions to 2- and 4-methoxybenzaldehydes afforded diarylmethanols in similar enantioselectivities of 96% and 95% ee (entries 1–2). Similarly, phenyl additions to 2-, 3-, and 4-methylbenzaldehydes gave corresponding diarylmethanols in comparable enantioselectivities of 94%–98% ee (entries 3–5). For aromatic aldehydes bearing a weak electron-withdrawing Cl substituent (entries 6–8) or a strong

electron-withdrawing 4-CF₃ group (entries 9), the catalytic reactions also gave corresponding products in high yields and excellent enantioselectivities of 95% to 97% ee, respectively. The phenyl addition to the more steric hindered 2-bromobenzaldehyde afforded the chiral diarylmethanol in 97% yield and 95% ee (entry 10). Phenyl additions to 1- and 2-naphthylaldehydes were also investigated and products in excellent 95% and 96% ee (entries 11 and 12) were obtained. In addition to substrates of aromatic aldehydes, the phenyl addition to the α,β -unsaturated *trans*-(*E*)-cinnamaldehyde was studied to furnish the secondary alcohol in 93% yield but in a lower enantioselectivity of 85% ee (entry 13). In contrast, the phenyl addition to the heterocyclic 2-furylaldehyde gave the addition product in an excellent 97% yield and 95% ee (entry 14). Finally, phenyl additions to aliphatic aldehydes were examined and it was found that enantioselectivities of resulted chiral secondary alcohols increase with increasing steric bulk of aliphatic groups from *n*-butyl (87% ee, entry 15), *i*-propyl (97% ee, entry 16), to *t*-butyl (99% ee, entry 17). For cyclohexylaldehyde, the chiral alcohol was obtained in 95% ee (entry 18).



CONCLUSION

In summary, this study demonstrates the second titanium catalytic system employing AlPh₃(THF) as the addition reagent to aldehydes in addition to our previously reported Ti-H₈-BINOLate system. The titanium catalyst of **1** is still efficient in asymmetric phenyl additions to aldehydes in a reaction time of only 3 h compared with longer reaction times required for catalytic systems using addition reagents other than the AlAr₃(THF) compounds. In this study, the catalytic system works excellently for both aromatic and aliphatic aldehydes to afford chiral secondary alcohols with enantioselectivities of $\geq 94\%$ ee except substrates of *n*-butanal (87% ee) and *trans*-(*E*)-cinnamaldehyde (85% ee). The catalyst applies equally well to aromatic aldehydes with an electron-donating substituent or an electron-withdrawing substituent on the aromatic ring. Furthermore, the catalyst gave comparable enantioselectivities for additions to aromatic aldehydes with a substituent at 2-, 3-, or 4-position on the ring. Based on the fact that the same titanium systems^{30,42,51} catalyze both ZnR₂ and AlAr₃(THF) additions to aldehydes to afford products in excellent stereocontrol, it is strongly suggested that arylaluminum compounds would be efficient aryl addition reagents to organic carbonyls employing the same titanium catalysts used for dialkylzinc addition reactions. Further mechanistic study employing arylaluminum reagents is underway and will be published in the future.

LITERATURE CITED

1. Pu L, Yu HB. Catalytic asymmetric organozinc additions to carbonyl compounds. *Chem Rev* 2001;101:757–824.

Chirality DOI 10.1002/chir

2. Ramón DJ, Yus M. In the arena of enantioselective synthesis, titanium complexes wear the laurel wreath. *Chem Rev* 2006;106:2126–2208.
3. Bolm C, Hildebrand JP, Muñiz K, Hermanns N. Catalyzed asymmetric arylation reactions. *Angew Chem Int Ed* 2001;40:3284–3308.
4. Schmidt F, Stemmler RT, Rudolph J, Bolm C. Catalytic asymmetric approaches towards enantiomerically enriched diarylmethanols and diarylmethylamines. *Chem Soc Rev* 2006;35:454–470.
5. Drutu I, Krygowski ES, Wood JL. Reactive enols in synthesis 2. Synthesis of (+)-latifolic acid and (+)-latifoline. *J Org Chem* 2001;66:7025–7029.
6. Scheidt KA, Bannister TD, Tasaka A, Wendt MD, Savall BM, Fegley GJ, Roush WR. Total synthesis of (–)-bafilomycin A1. *J Am Chem Soc* 2002;124:6981–6990.
7. Pu L. Asymmetric alkynylzinc additions to aldehydes and ketones. *Tetrahedron* 2003;59:9873–9886.
8. Roethle PA, Trauner D. Expedient synthesis of (±)-bipinnatin J. *Org Lett* 2006;8:345–347.
9. Wu PY, Wu HL, Uang BJ. Asymmetric synthesis of functionalized diarylmethanols catalyzed by a new γ -amino thiol. *J Org Chem* 2006;71:833–835.
10. Corey EJ, Helal CJ. Catalytic enantioselective synthesis of the second generation histamine antagonist cetirizine hydrochloride. *Tetrahedron Lett* 1996;37:4837–4840.
11. Ohkuma T, Koizumi M, Ikehira H, Yokozawa T, Noyori R. Selective hydrogenation of benzophenones to benzhydrols. Asymmetric synthesis of unsymmetrical diarylmethanols. *Org Lett* 2000;2:659–662.
12. Weber B, Seebach D. Ti-TADDOLate-catalyzed, highly enantioselective addition of alkyl- and aryl-titanium derivatives to aldehydes. *Tetrahedron* 1994;50:7473–7484.
13. Dosa PI, Ruble JC, Fu GC. Planar-chiral heterocycles as ligands in metal-catalyzed processes: enantioselective addition of organozinc reagents to aldehydes. *J Org Chem* 1997;62:444–445.
14. Bolm C, Muñiz K. Catalytic enantioselective aryl transfer: asymmetric addition of diphenylzinc to aldehydes. *Chem Commun* 1999;1295–1296.
15. Zhao G, Li XG, Wang XR. Enantioselective additions of diphenylzinc to aldehydes using chiral pyrrolidinylmethanol derivatives as catalysts. *Tetrahedron: Asymmetry* 2001;12:399–403.
16. Ko DH, Kim KH, Ha DC. Enantioselective additions of diethylzinc and diphenylzinc to aldehydes using 2-dialkyl-aminomethyl-2'-hydroxy-1,1'-binaphthyls. *Org Lett* 2002;4:3759–3762.
17. Qin YC, Pu L. Highly enantioselective addition of diphenylzinc to aliphatic and aromatic aldehydes catalyzed by a readily available H₈-Binol derivative. *Angew Chem Int Ed* 2006;45:273–277.
18. Huang WS, Pu L. The first highly enantioselective catalytic diphenylzinc additions to aldehydes: synthesis of chiral diarylcarbinols by asymmetric catalysis. *J Org Chem* 1999;64:4222–4223.
19. Bolm C, Kesselgruber M, Hermanns N, Hildebrand JP, Raabe G. Application of a planar chiral η^5 -cyclopentadienylrhodium(I)tricarbonyl complex in asymmetric catalysis: highly enantioselective phenyl transfer to aldehydes. *Angew Chem Int Ed* 2001;40:1488–1490.
20. Fontes M, Verdager X, Solà L, Pericàs MA, Riera A. 2-Piperidino-1,1,2-triphenylethanol: a highly effective catalyst for the enantioselective arylation of aldehydes. *J Org Chem* 2004;69:2532–2543.
21. Bastero A, Font D, Pericàs MA. Assessing the suitability of 1,2,3-triazole linkers for covalent immobilization of chiral ligands: application to enantioselective phenylation of aldehydes. *J Org Chem* 2007;72:2460–2468.
22. Bolm C, Rudolph J. Catalyzed asymmetric aryl transfer reactions to aldehydes with boronic acids as aryl source. *J Am Chem Soc* 2002;124:14850–14851.
23. Braga AL, Lüdtkke DS, Vargas F, Paixão MW. Catalytic enantioselective arylation of aldehydes: boronic acids as a suitable source of transferable aryl groups. *Chem Commun* 2005;2512–2514.
24. Dahmen S, Lormann M. Triarylborane ammonia complexes as ideal precursors for arylzinc reagents in asymmetric catalysis. *Org Lett* 2005;7:4597–4600.
25. Lu G, Kwong FY, Ruan JW, Li YM, Chan ASC. Highly enantioselective addition of in situ prepared arylzinc to aldehydes catalyzed by a series

- of atropisomeric binaphthyl-derived amino alcohols. *Chem Eur J* 2006;12:4115–4120.
26. Kim JG, Walsh PJ. From aryl bromides to enantioenriched benzylic alcohols in a single flask: catalytic asymmetric arylation of aldehydes. *Angew Chem Int Ed* 2006;45:4175–4178.
27. Arao T, Kondo K, Aoyama T. Asymmetric Ni-catalyzed arylation of aromatic aldehydes with arylboroxines. *Tetrahedron* 2007;63:5261–5264.
28. Sakai M, Ueda M, Miyaura N. Rhodium-catalyzed addition of organoboronic acids to aldehydes. *Angew Chem Int Ed* 1998;37:3279–3281.
29. Jagt RBC, Toullec PY, Schudde EP, de Vries JG, Feringa BL, Minnaard AJ. Synthesis of solution-phase phosphoramidite and phosphite ligand libraries and their in situ screening in the rhodium-catalyzed asymmetric addition of arylboronic acids. *J Comb Chem* 2007;9:407–414.
30. Wu KH, Gau HM. Remarkably efficient enantioselective titanium(IV)-(*R*)- $\text{H}_8\text{-BINOLate}$ catalyst for arylations to aldehydes by triaryl(tetrahydrofuran)aluminum reagents. *J Am Chem Soc* 2006;128:14808–14809.
31. Chen CA, Wu KH, Gau HM. Highly enantioselective aryl additions of $[\text{AlAr}_3(\text{thf})]$ to ketones catalyzed by a titanium(IV) catalyst of (*S*)-BINOL. *Angew Chem Int Ed* 2007;46:5373–5376.
32. Ku SL, Hui XP, Chen CA, Kuo YY, Gau HM. $\text{AlAr}_3(\text{THF})$: highly efficient reagents for cross-couplings with aryl bromides and chlorides catalyzed by the economic palladium complex of PCy_3 . *Chem Commun* 2007;3847–3849.
33. Negishi EI, Kondakov DY. An odyssey from stoichiometric carbotitanation of alkynes to zirconium-catalyzed enantioselective carboalumination of alkenes. *Chem Soc Rev* 1996;25:417–426.
34. Uchiyama M, Naka H, Matsumoto Y, Ohwada T. Regio- and chemoselective direct generation of functionalized aromatic aluminum compounds using aluminum ate base. *J Am Chem Soc* 126:10526–10527, Soc 2004.
35. Ooi T, Takahashi M, Maruoka K. Rate acceleration in nucleophilic alkylation of carbonyl compounds with a new template containing two metallic centers. *Angew Chem Int Ed* 1998;37:835–837.
36. Ishikawa T, Ogawa A, Hirao T. A novel oxovanadium(V)-induced oxidation of organoaluminum compounds. Highly selective coupling of organic substituents on aluminum. *J Am Chem Soc* 120:5124–5125, Soc 1998.
37. Spino C, Beaulieu C. A novel method to generate chiral quaternary carbon centers of high enantiomeric purity using a highly stereoselective addition of vinylalanes to a chiral aldehyde. *Angew Chem Int Ed* 2000;39:1930–1932.
38. Rainier JD, Cox JM. Aluminum- and boron-mediated C-glycoside synthesis from 1,2-anhydroglycosides. *Org Lett* 2000;2:2707–2709.
39. Haraguchi K, Kubota Y, Tanaka H. Ring opening of nucleoside 1',2'-epoxides with organoaluminum reagents: stereoselective entry to ribonucleosides branched at the anomeric position. *J Org Chem* 2004;69:1831–1836.
40. Wang B, Bonin M, Micouin L. Palladium-catalyzed cross-coupling of aryl electrophiles with dimethylalkynylaluminum reagents. *Org Lett* 2004;6:3481–3484.
41. Kojima K, Kimura M, Tamaru Y. Nickel-catalyzed four-component connection of organoaluminum (organozinc), isoprene, aldehydes and amines: stereo- and regioselective synthesis of trisubstituted (*E*)-homoallylamines. *Chem Commun* 2005;4717–4719.
42. Chan ASC, Zhang FY, Yip CW. Novel asymmetric alkylation of aromatic aldehydes with triethylaluminum catalyzed by titanium (1,1'-bi-2-naphthol) and titanium-(5,5',6,6',7,7',8,8'-octahydro-1,1'-bi-2-naphthol) complexes. *J Am Chem Soc* 1997;119:4080–4081.
43. Pagenkopf BL, Carreira EM. Titanium fluoride complexes as catalysts for the enantioselective addition of Me_3Al to aldehydes. *Tetrahedron Lett* 1998;39:9593–9596.
44. Kwak YS, Corey EJ. Catalytic enantioselective conjugate addition of trimethylsilylacetylene to 2-cyclohexen-1-one. *Org Lett* 2004;6:3385–3388.
45. Biswas K, Prieto O, Goldsmith PJ, Woodward S. Remarkably stable $(\text{Me}_3\text{Al})_2\text{-DABCO}$ and stereoselective nickel-catalyzed AlR_3 ($\text{R}=\text{Me}$, Et) additions to aldehydes. *Angew Chem Int Ed* 2005;44:2232–2234.
46. d'Augustin M, Palais L, Alexakis A. Enantioselective copper-catalyzed conjugate addition to trisubstituted cyclohexenones: construction of stereogenic quaternary centers. *Angew Chem Int Ed* 2005;44:1376–1378.
47. Hui XP, Chen CA, Gau HM. Synthesis of new *N*-sulfonylated amino alcohols and application to the enantioselective addition of diethylzinc to aldehydes. *Chirality* 2005;17:51–56.
48. Hsieh SH, Gau HM. Asymmetric alkynyl additions to aldehydes catalyzed by tunable oxovanadium(V) complexes of Schiff bases of β -amino alcohols. *Synlett* 2006;1871–1874.
49. Hui XP, Chen CA, Wu KH, Gau HM. Polystyrene-supported *N*-sulfonylated amino alcohols and their applications to titanium(IV) complexes catalyzed enantioselective diethylzinc additions to aldehydes. *Chirality* 2007;19:10–15.
50. Hsieh SH, Kuo YP, Gau HM. Synthesis, characterization, and structures of oxovanadium(V) complexes of Schiff bases of β -amino alcohols as tunable catalysts for the asymmetric oxidation of organic sulfides and asymmetric alkynylation of aldehydes. *Dalton Trans* 2007; 97–106.
51. Hsieh SH, Gau HM. Enantioselective addition of diethylzinc to aldehydes catalyzed by titanium(IV) complexes of *N*-sulfonylated β -amino alcohols with four stereogenic centers. *Chirality* 2006;18:569–574.
52. Reetz MT, Drewes MW, Schmitz A. Stereoselective synthesis of β -amino alcohols from optically active α -amino acids. *Angew Chem Int Ed* 1987;26:1141–1143.
53. Balsells J, Davis TJ, Carroll P, Walsh PJ. Insight into the mechanism of the asymmetric addition of alkyl groups to aldehydes catalyzed by titanium-BINOLate species. *J Am Chem Soc* 2002;124:10336–10348.